

NUMERICAL MODELING OF CONCRETE UNDER BLAST LOADING

A

Thesis

Submitted in partial fulfilment of the requirements for the award of the degree

of

MASTER OF TECHNOLOGY

IN

CIVIL ENGINEERING

With specialization in

STRUCTURAL ENGINEERING

*Under the
supervision*

of

Mr. Abhilash Shukla
Assistant Professor

by

Monika Chaudhary

(162653)

to



JAYPEE UNIVERSITY OF INFORMATION TECHNOLOGY

WAKNAGHAT, SOLAN – 173234

HIMACHAL PRADESH, INDIA

May-2018

CERTIFICATE

This is to certify that the Project Report entitled "**Numerical Modeling of Concrete Under Blast Loading**" submitted by **Monika Chaudhary**, enrolled as **162653**, in the partial fulfilment of the requirement for the award of the degree **Master of Technology** at **Jaypee University of Information Technology, Wagnaghat** is an authentic work carried out by her under my supervision and guidance.

To the best of my knowledge, the matter embodied in the Project Report has not been submitted to any other University/ Institute for the award of any Degree.

Dr. Ashok Gupta
Head of Department
Department of Civil Engg
JUIT, Wagnaghat

Mr. Abhilash Shukla
Assistant Professor
Department of Civil Engg.
JUIT, Wagnaghat

External Examiner

DECLARATION

This is to certify that Project Report entitled "**Numerical Modeling of Concrete Under Blast Loading**" which is submitted by **Monika Chaudhary**, student of **Civil Engineering Department**, for the requirement of the award of degree **M.Tech in Civil Engineering at JUIT Wagnaghat (HP)** under the guidance of **Mr. Abhilash Shukla, Assistant Professor, Department of Civil Engineering, JUIT Wagnaghat (HP)**, comprise only original work and due acknowledgement has been made in the text to all other material used.

Monika Chaudhary

Roll No. 162653

TABLE OF CONTENTS

Certificate	i
Declaration	ii
Acknowledgement	v
Abstract	vi
List of Figures	vii
List of Tables	x
List of Symbols	xi
Chapters	
1. Introduction	
1.1 General Introduction	1
1.2 General Definitions	2
2. Literature Review	
2.1 General Introduction	5
2.2 Studies on Concrete subjected to Blast Loading	5
2.3 Goal of Study	23
2.4 Objective of Study	23
3. Methodology	
3.1 SHPB test	24
3.2 Finite Element Analysis (FEA)	25
3.3 ABAQUS FEA software	26
4. Results	
4.1 Results for the SFRC cube sample	36
4.2 Results for the SFRC Brazilian Disc Sample	50

5. Conclusions

5.1 Conclusions 76

5.2 Future scope 77

References

Appendix A

Appendix B

ACKNOWLEDGMENT

As the professional courses not only require theoretical knowledge but practical knowledge too, that's why university conducts projects for the students, so that they can get ample view of practical problems and can be innovative in their work. I find it a matter of honour in showing the feeling of indebtedness and thankfulness to **Mr. Abhilash Shukla, Assistant Professor, Civil Engineering Department, Jaypee University of Information Technology Wagnaghat**. His constant guidance and encouragement received have been a great help in carrying out the project work.

Apart from this I would like to express my sincere gratitude to **Prof. Dr. Ashok Kumar Gupta, Professor and Head of Department, Civil Engineering Department, Jaypee University of Information Technology Wagnaghat**, for providing me an opportunity to do the project. This project bears on imprints of many people. I am also very thankful to my friends and family members who encouraged me all the time to go through this project work.

Monika Chaudhary

Roll No. 162653

ABSTRACT

The blast phenomenon is a complex phenomenon. For analysing and designing of the structures which involves the blast loading conditions requires a detailed understanding of blast waves and also the structural dynamic responses pertaining to these blast conditions. Brittle materials generally involves a non linear behaviour under blast or impact loading, resulting on a complex analysis. In the present scenario the risk of terrorist attacks has increased thus require the protection strategies against the Blast. Thus structural engineers are considering it as an important factor for designing and analysis purpose. With the advancement in the technology it becomes possible to perform the numerical simulations of concrete under dynamic loadings such as blast, impact, earthquake loadings etc. The reliability and accuracy of the results of numerical simulations is influenced by many factors such as velocity of impact, material properties, initial boundary conditions etc. The important factor to be considered among these factors is the material model as it should be universally true to give accurate results under different conditions (i.e. loading conditions, boundary conditions, initial predefined conditions etc.). These models are already included in the software like ABAQUS, LS-DYNA, ANSYS etc. In the present study ABAQUS FEA software has been used. The main aim is to model the concrete under blast loading and numerically simulate the dynamic response using ABAQUS to improve these responses by altering the properties of concrete. The effects of dynamic loads on the materials can be studied with the help of the Split Hopkinson Pressure Bar. It is generally used for testing the material under high strain rates generally between 10^2 to 10^4 s^{-1} . The stress v/s time graph has been plotted to know the effect of stress on the samples relative to the time. Two samples have been taken for modeling, cube sample and disc sample. Results showed that the deformation in the disc starts along the diameter of the disc. For this sample firstly the elements from the edges starts to deform then proceeds to the middle portion along the diameter in which the waves propagate. The lower edge elements deform first then the effect propagates to upper portions. The results of the numerical simulations of the SFRC (Steel Fibre Reinforced Concrete) samples can be used to compare the results of the conventional concrete under blast impacts.

Keywords: High strain rate, Split Hopkinson Pressure Bar, SFRC, Velocity.

LIST OF FIGURES

S.No.	Figure No.	Name of Figure	Page No.
1.	1.1(a)	Frequency of different dynamic loads	4
2.	1.1(b)	Colliding and reflecting blast waves	4
3.	2.1	Variation of blast pressure with distance	8
4.	2.2	Pressure time profile of explosion waves	9
5.	2.3	Refracted waves of the explosion near the ground	9
6.	2.4	Attenuation of peak overpressure with distance from source	11
7.	3.1	Schematic of SHPB	25
8.	3.2	ABAQUS/CAE window	28
9.	3.3	Parts of the geometry	29
10.	3.4	Assembly of the cube sample	31
11.	3.5	Assembly of Disc sample	31
12.	3.6	Interactions of the contact faces	32
13.	3.7	Velocity in striker bar	33
14.	3.8	Meshing of disc sample	34
15.	3.9	Meshing of the cube sample	34
16.	4.1	Contours for Displacement	36
17.	4.2	Contours for Maximum principal stress	37
18.	4.3	Time history curve for stress of cube sample	38
19.	4.4	Time history curve for Strain of cube sample	39
20.	4.5	Time history curve for maximum principal stress of cube sample	40
21.	4.6	Time history curve for stress in element number 1	41

22.	4.7	Time history curve for stress in element number 2500	42
23.	4.8	Time history curve for stress in element number 1325	43
24.	4.9	Time history curve for strain in element number 1	44
25.	4.10	Time history curve for strain in element number 2500	45
26.	4.11	Time history curve for strain in element number 3500	46
27.	4.12	Time history curve for maximum principal stress in element number 1	47
28.	4.13	Time history curve for maximum principal stress in element number 2500	48
29.	4.14	Time history curve for maximum principal stress in element number 1325	49
30.	4.15	Stress generation along diameter	50
31.	4.16	Time history curve for stress of disc sample	51
32.	4.17	Time history curve for strain of disc sample	52
33.	4.18	Time history curve for maximum principal stress of disc sample	53
34.	4.19	Time history curve for stress in element number 1845	54
35.	4.20	Time history curve for stress in element number 1771	55
36.	4.21	Time history curve for stress of cube sample in element number 562	56
37.	4.22	Time history curve for stress in element number 1845	57
38.	4.23	Time history curve for stress in element number 1771	58
39.	4.24	Time history curve for stress in element number 719	59
40.	4.25	Time history curve for stress in element number 4236	60
41.	4.26	Time history curve for stress in element number 1667	61
42.	4.27	Time history curve for stress in element number 482	62
43.	4.28	Time history curve for strain in element number 2500	63

44.	4.29	Time history curve for strain in element number 1771	64
45.	4.30	Time history curve for strain in element number 4400	65
46.	4.31	Time history curve for strain in element number 1771	66
47.	4.32	Time history curve for strain in element number 4236	67
48.	4.33	Time history curve for strain in element number 1667	68
49.	4.34	Time history curve for strain in element number 482	69
50.	4.35	Time history curve for maximum principal stress in element number 1845	70
51.	4.36	Time history curve for maximum principal stress in element number 1771	71
52.	4.37	Time history curve for maximum principal stress in element number 4400	72
53.	4.38	Time history curve for maximum principal stress in element number 1771	73
54.	4.39	Time history curve for maximum principal stress in element number 4236	74
55.	4.40	Time history curve for maximum principal stress in element number 482	75

LIST OF TABLES

S. No.	Table No.	Name of Table	Page No.
1.	3.1	Geometric Properties	28
2.	3.2	Material properties for SFRC	30

LIST OF SYMBOLS

S. No.	Term	Symbol
1.	Ammonium Nitrate	ANFO
2.	Computer Aided Design	CAD
3.	Computational Fluid Dynamics	CFD
4.	Castlegado Sandstone	CG
5.	Computational Structural Mechanics	CSM
6.	Dynamic Increase Factor	DIF
7.	Degree Of Penetration	DOP
8.	Two Dimensional	2D
9.	Three Dimensional	3D
10.	Engineer Research And Development Centre	ERDC
11.	et alia (Neuter Plural)	et al.
12.	Finite Element Analysis	FEA
13.	Finite Element Method	FEM
14.	Fibre Reinforced Concrete	FRC
15.	Holmquist Johnson Cook	HJC
16.	High Strength Concrete	HSC
17.	Indian Standards	IS
18.	Lattice Discrete Particle Method	LDPM
19.	Mons Chalk	MG
20.	Modified Holmquist Johnson Cook	MHJC
21.	Normal Strength Concrete	NSC
22.	Reinforced Concrete	RC
23.	Reproducing Kernel Particle Method	RKPM
24.	Reactive Powder Concrete	RPC
25.	Steel Fibre Reinforced Concrete	SFRC
26.	Split Hopkinson Pressure Bar	SHPB
27.	Timoshenko Beam Theory	TBT
28.	Ternary Complex Kinetic	TCK
29.	Trinitrotoluene	TNT

CHAPTER 1

INTRODUCTION

1.1 INTRODUCTION

Blast is a destructive wave of highly compressed air which spreads outwards resulting from an explosion. Blast near or inside the building can cause huge devastation and catastrophic damage. This can harm the building both externally and internally vis-a-vis structural frames, collapsing of walls, shutting down of life safety systems, fire damage, breaking of glass windows, or complete failure of the structure [1]. This can cause loss of life and injuries to occupants due to direct blast effects, fire, smoke, debris impact, or structural collapse. Sometimes timely evacuation is not possible contributing to additional casualties.

Buildings, bridges, pipelines, dams, power-plants, cultural and heritage structures, historical monuments, industries etc. are the structures are of an immense importance to the economy and prosperity of the country and thus must be protected from the devastating effects of the dynamic loadings. These are the structures which are most prone to terrorist attacks [1]. Explosions create a large dynamic load on the structure, much more than the design loads. Efforts have been made in the past to avoid such threats of extreme loading on the structures. Studies were conducted to know the behaviour of structure during blast loading, for resisting such blast loads the structural analysis and designing methods were developed and it is still current research topic. For analysing and designing of the structures which involves the blast loading conditions require a detailed understanding of blast waves and also the structural dynamic responses pertaining to these blast conditions. Brittle materials such as concrete generally involves a non linear behaviour under blast or impact loading, resulting on a complex analysis.

In the present scenario the risk of terrorist attacks has increased thus require the protection strategies against the Blast. Thus structural engineers are considering it as an important factor for designing and analysis purpose. However every civilian building cannot be made blast resistant. The conventional structures are designed for lower loading conditions as compared to the explosion conditions thus such structures are more prone to blast damage. The potential threats and protective measures can be better

understood by the Building owners and occupants thus the design professionals can take steps to implement such protective measures. With the advancement in the technology it becomes possible to perform the numerical simulations of concrete under dynamic loadings such as blast, impact, earthquake loadings etc. The reliability and accuracy of the results of numerical simulations is influenced by many factors. The important factor to be considered among these factors is the material model as it should be universally true to give accurate results under different conditions (i.e. loading conditions, boundary conditions, initial predefined conditions, environmental conditions etc.). These models are included in software like ABAQUS, LS DYNA, ANSYS etc.

1.2 GENERAL DEFINITION

1.2.1 Meaning of blast

A blast is a destructive wave of highly compressed air spreading outwards from an explosion. According to IS 4991.1968:- Blast wind is the moving air mass along with the overpressures resulting from pressure difference behind the shock wave front. The blast wind movement during the positive phase of the overpressures is in the direction of shock front propagation [19].

1.2.2 Shock wave

Explosion results into a shock wave. This wave travels in the air, moving outward in all the directions. It moves at a very high speed which cause a time-dependent pressure and suction effects at all points in its way. The shock wave has both a positive pressure phase and a negative suction phase. The blast wind which accompanies the shock wave is the cause of dynamic pressures. This is the reason for the drag effects on any obstacle coming in its way. Reflected pressure is caused at the obstacle's surface as a result of the diffraction of the wave at the surface. However this pressure vanishes with time depending on the size of the obstacle's surface.

1.2.3 Types of structures in view of blast

There are mainly the following two types of structures

- (a) Diffraction Type Structures: The closed structures not having any openings, and having the total area which oppose the blast. The shock wave over pressures and the dynamic pressures caused by blast wind act on such structures [19].

(b) Drag Type Structures: The open structures having small projected area which oppose the shock wave. Mainly the dynamic pressures act on such structures.

1.2.4 Dynamic strength and stress

The Plastic deformation of the structural elements such as beams, columns, slabs etc. should be permitted wherever the functioning of the structure would not be adversely affected by their permanent displacements. The materials develop the higher strength than in the statically loaded members under the high strain rates (such as the straining effects associated with the blast loading). The average dynamic yield stress of structural carbon, mild, weld able or rivet steels may be assumed to exceed the minimum specified static yield stress by 25 percent and that of high strength alloy steels by 10 percent [19]. The brick and the stone masonry have the same dynamic flexural strength as corresponding to the static strength. The compressive strength shall be taken 25 percent higher than the corresponding static strength. For unreinforced brick work the ductility ratio may be limited to 1.5. For reinforced brickwork, with not less than 0.05 percent steel on each face and not more than balanced percentage, the ductility factors as for reinforced concrete may be used [19].

1.2.5 Load combinations for design

The wind load and the earthquake load must be neglected while considering the blast loading on the structures. The temperature and shrinkage effects must also be neglected.

(a) Live load on floors are taken as per IS : 875-I 1967 depending upon the class of building. Roof live load is taken as zero at the time of blast [20].

1.2.6 Explosions

Explosion is the result of increase in the volume in a rapid manner and thus energy is released in an extreme manner. Explosions results into the increased temperatures and release of gases.

1.2.7 Types of blast

The blast do not have any particular classification but can be classified on the basis of the explosive material used, the method of attack as Moving vehicle attack, Stationary vehicle bomb, exterior attack, arsons, ballistic attack.

1.2.8 Range of frequencies of different loads

Although the seismic loads also cause the dynamic responses but the dynamic responses produced by the blast load are much more devastating. The frequency range of the wind load, sound waves, mechanical vibrations, earthquake waves and blast load are depicted in the following Fig 1.1(a). From the Figure it is clear that the blast load intensity is much more than the other dynamic loads at low to high frequency range. At the low frequencies also the loading intensity falls in the high ranges for the blast waves. However for the very low to medium frequency range of the wind and earthquake waves, the load intensity falls in a high range but much lesser than the load intensity for blast waves.

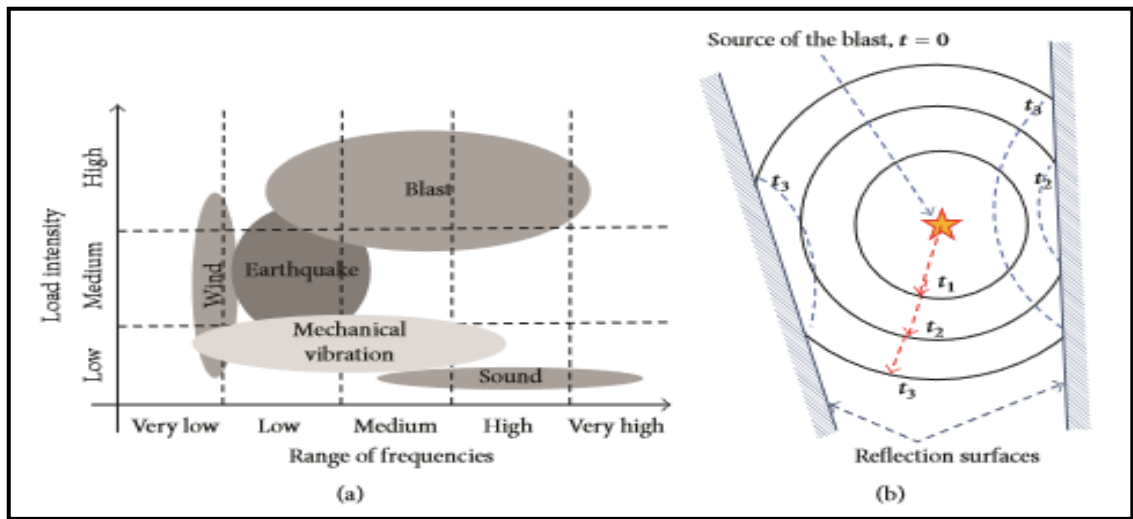


Fig 1.1: (a) Frequency range of different dynamic loads (b) Colliding and reflecting blast waves
[Andreou M. et al 2016]

During blast the blast waves originating from the source spread out in all the directions. The source point lying in the middle spreading waves in all the directions. As and when the blast wave comes in contact with any obstructing surface in its path, it collides with the obstructing surface. After this collision of waves at the obstructing surface these waves immediately gets reflected back. This is depicted in the Fig 1.1(b). This figure shows the explosion point at the middle ($t=0$) and the transmitted and reflected waves are shown with respect to different points of time. The reflecting waves are shown with dashed blue coloured lines, which are reflecting back at the obstructing surface while the transmitted waves are shown with the solid black coloured lines.

CHAPTER 2

LITERATURE REVIEW

2.1 GENERAL INTRODUCTION

In the last 5 decades the concrete under blast loads has gained importance as a matter of research due to increase in terrorist attacks. Much research is done, but it is difficult to access complex state of stress acting inside the brittle material like concrete, which is subjected to blast loading. Many studies are of empirical nature which are given for the concrete which is subjected to dynamic loads such as blast loads. Experimental studies also focuses only on the derivation and accuracy of the empirical formulae. The base model taken in account for most of the studies is Holmquist model. Original Holmquist Johnson Cook model is for computing the impact on the material experiencing the large strains, the high strain rates, & the high pressures. It is the elastic visco plastic model coupled with isotropic damage where response is separated into hydrostatic and deviatoric contributions. Theoretical model is relatively simple and takes into account the important characteristics of concrete behaviour such as pressure dependencies, rate dependencies, damage patterns and the properties such as compaction, strength etc. But due to certain limitations in the HJC model, modified form of HJC was developed. These limitations are the non linear behaviour before the peak load, the stiffness degradation, the stiffness recovery, induced anisotropy, shear reduction influenced by state of stress. HJC model can be improved by introduction of third stress invariant as only two stress invariants are included in it.

2.2 STUDIES ON THE CONCRETE SUBJECTED TO BLAST LOADING

2.2.1 Numerical Predictions of Ballistic Limits for Concrete using Modified Version of HJC model

M. Polanco-Loria et al.(2007), observed the need to study the Modified HJC model, which is designed to overcome the limitations of original HJC model. The original model contains the discontinuous description and disobey the identification of the cohesion parameter. Thus MHJC model is developed which is based on a continuous function for normalized equivalent stress depending on pressure. Tri-axial experiments on concrete resulted into the substantial difference of shear strength between the compressive meridian and tensile meridian [15]. The strain rate influence is defined as a

linear function on the logarithmic scale of the strain rate. It is characterized by the slope. In MHJC, care has been taken to avoid the negative values for relative strain rates. Pressure-volume response is considered in 3 stages, as given in the original Holmquist model. The three basic damage mechanisms i.e. tensile, shear and compaction damage are treated separately and for this reason 3 variables for internal damage are taken separately.

Fracture criteria that are taken are Rankine, St. Venant, and critical hydrostatic tensile strain criteria. Shear is more important in tensile cracking in RCC. Cumulative damage of HJC model is adopted but separately take from volumetric and shear strain damage. Compaction damage is considered due to plastic volumetric strain. The material model must be proper and accurate for the numerical simulations. In this literature the numerical simulations of the concrete slab is done. Initial and residual velocities curves are obtained for the slab from where ballistic limits are calculated. The main conclusion is that with the increase in the unconfined compressive strength by a factor of three, the ballistic limit velocity increases by 20% only [15].

The third deviatoric stress invariant is considered for the new pressure shear function. Also a new strain-rate sensitivity formulation is included and three damage variables are introduced separately for the tensile cracking, shear cracking and pore compaction mechanisms. Comparing with the experiments, with the ballistic limits within 8% the MHJC model proves to be the best choice for the simplicity and the accuracy for large scale computations of concrete under impact loadings.

2.2.2 Penetration of concrete targets using a MHJC material model

M. J. Islam et al.(2012), found that in MHJC model of concrete is used here, which contains the simplified and improved strain rate expression and P-V relationships. The compressive strength of the High strength concrete is three times more than that of the normal concrete. However the residual velocities get reduced by only 20% for high strength concrete. The compressive strength and the impact resistance of concrete slab are not directly related to each other. The robust material model is used. Fibre reinforced concrete are more resistant to cracking. thus improvise the impact resistance of the concrete, as proposed by Clifton and Knab 1983 and Tai 2009 models of concrete[10]. At the same displacement values the dynamic cracking causes less stress

intensity than the static cracking. DIF is the short for Dynamic Strength Increase factor. It is defined as the ratio of dynamic strength to static strength. And the critical stress is given as cube root of strain rate. Its value differs for the compression and tension. Thermal diffusion distance is an important parameter to be considered while dealing with the blast. The distance to which the heat gets transferred during certain period of time is called the Thermal diffusion distance. During low thermal diffusion distance of concrete and high strain rate, some part of the heat generated in concrete remain within and results in high velocity impact.

Pressure-volume relationship adopted is a multi linear function. For the same loading and unloading paths the fully compacted concrete follows a non elastic behaviour. Pressure volume relation is determined and compared with the experiments. For numerical simulations ogive nose steel projectile is used. Residual projectile velocities are recorded. Residual velocity versus initial velocity curves are plotted for determining the ballistic performance of concrete. The number of layers used are 3 for the concrete specimen. Axis-symmetrical 2D FEM element is adopted [10]. Element distortion problem occurred during the FEM analysis process due to large deformations and larger depth of crack propagation during the projectile penetration. Propagation pattern in the concrete is from the impact face to the rear face. But the damage at the rear face is small as compared to the entry surface. Numerical simulations describes its failure with reasonable success.

2.2.3 Numerical simulations of oblique penetration into reinforcement concrete targets

Yan Liu et al.(2010), developed a dynamic constitutive model with the tensile and compressive damage models as basic models to be referred to and its implemented into 3D finite element code, ABAQUS. Oblique penetration causes the tensile and compressive damages hence the damage to reinforcing bars are obtained. Obliquity angles are changed and thus the penetration depths are obtained. Dynamic response of concrete is described by a constitutive elastic perfectly plastic equation. The compression or tension loads are complicated for oblique penetrations. Generally dynamic damage models take into account the TCK and HJC models as base models. During oblique penetration process tensile behaviour is generated by TCK model and compressive behaviour is generated by HJC model. Concluded that the tensile damage

region which is near the free surface is due to the circumferential tensile stress [12]. The tensile waves gets reflected from the free surfaces, while the compression forces gets accumulated and thus forming the compression damage region. Compression damage is concentrated to a small region than tensile damage. The steel near ballistic trajectory gets deformed. The depth of penetration (DOP) decreases with angle. This model gives the idea of material dynamic behaviour such as tensile damage, compressive damage, micro cracking growth.

2.2.4 Blast loading on structures

Mrvoje Dragani et al.(2012), defined the problems associated with blast loads and risk mitigation strategies are found with standard structural analysis software. Although the software has limited non-linear capabilities. The basic feature of the explosion is presented here as the spread out waves of high intensity from the initiation point to near environment. The speed of the waves gets reduced further reducing the strength with the propagation of the waves.

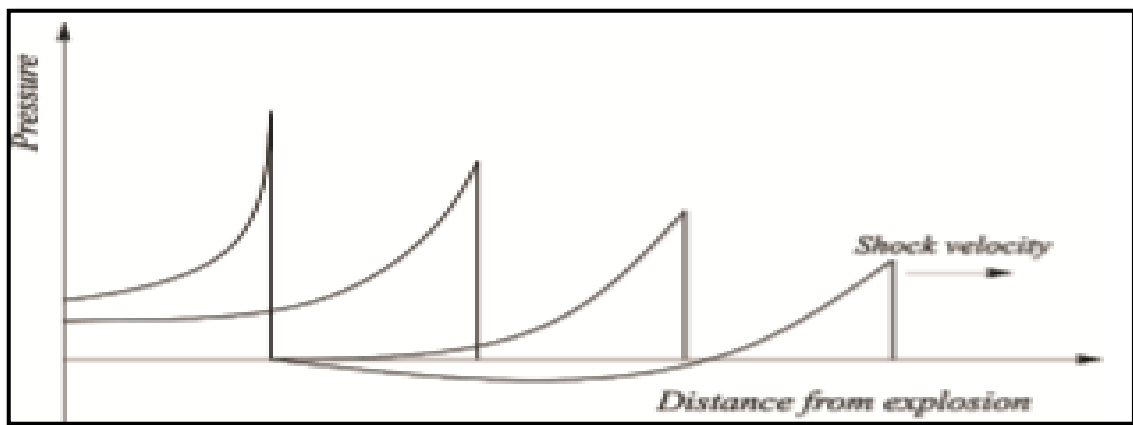


Fig 2.1: Varying Blast pressure with distance [Dragani H. et al. 2012].

The other important factor on which propagation of wave depends is the time duration. It is given by a positive phase and a negative phase. Positive phase predominates for small durations as compared to negative phase. However the damage is more in the positive phase than that of negative phase. The change of pressure with time is shown in the Fig. 2.2.

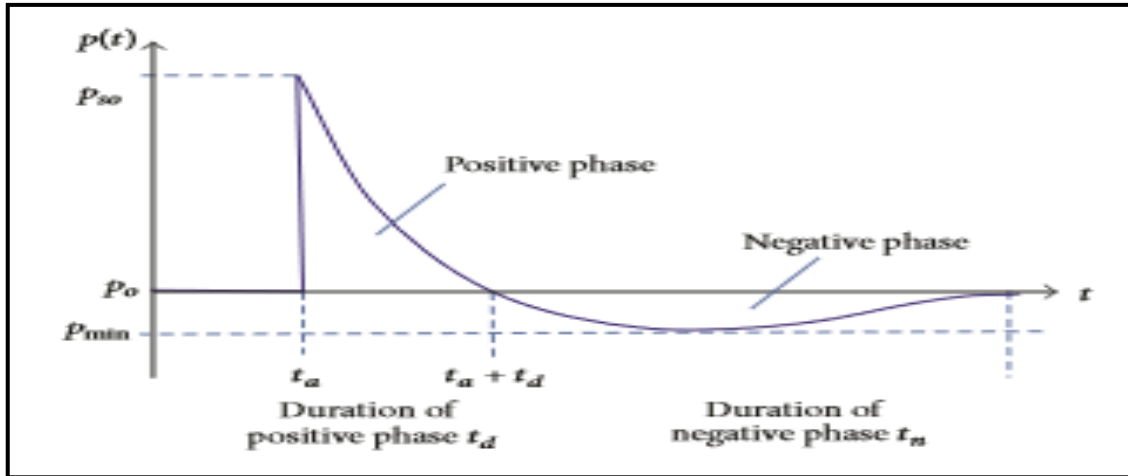


Fig 2.2 Pressure time profile of explosion wave [Dragani H. et al. 2012].

Reflection from ground gives rise to the increased refracted wave. At the detonation point refracted wave is mingled with the initial wave to form a single wave (Fig. 2.3).

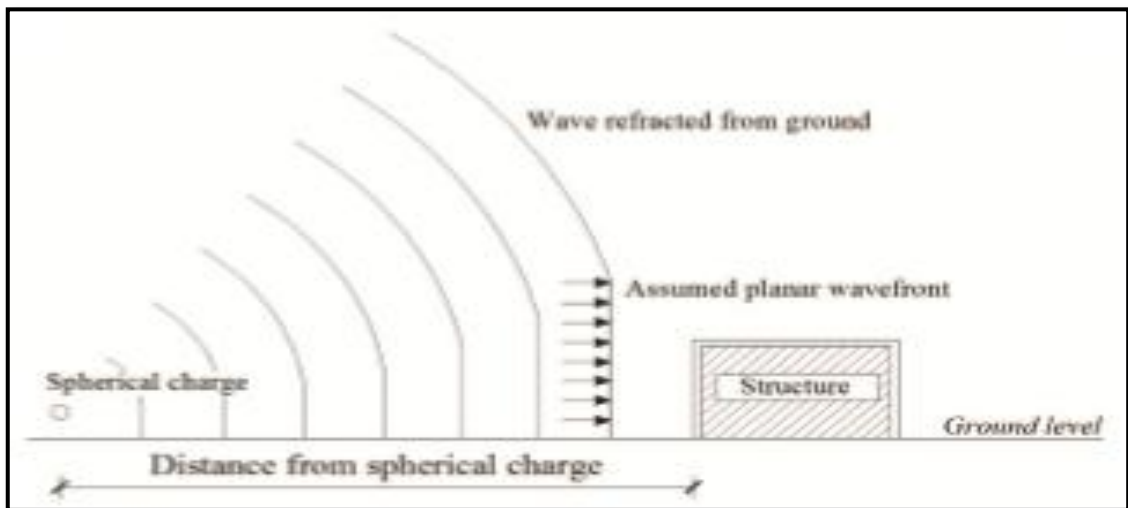


Fig 2.3: Refracted wave of the explosion near the ground [Dragani H. et al. 2012].

The explosion in or near the structure can cause catastrophic damage to the structure. Here the blast load for close explosion was determined and simulated on a model building using SAP2000. SAP2000 is used for structural analysis. Initial load defined as pressure over time. As the source point is in close proximity to the ground so the load on surface need not to be determined [9]. The loading for each point is to be analysed. Deformation history was calculated. Check applied within the deformation limits to know post-blast state of the element.

2.2.5 Modeling blast effects on a reinforced concrete bridge

Markellos Andreou et al.(2016), Blasts are very short duration phenomenon. Dynamic pressure waves are generated during the blast which spread out in all directions. This gives rise to excitation of dynamic response. Here in this paper, the blast phenomenon, it's devastating effects on structures are investigated. Elastic finite element simulations gives the idea of the deformed shapes. Than structural response is calculated. Two span bridge is considered and damage pattern and localization is studied.

It is proposed that the pressure acting on the surfaces of the structure due to blast waves. This pressure is the impulsive load. Vibrations in structure is caused due to increased potential energy damage. Reflected waves effects the surfaces which are perpendicular to the blast waves. Incidental waves effect the sides and back of the structure. A two step procedure is adopted for this study [1], which reduces the complicated blast phenomenon problem to a simplified two step procedure. The deformed shape is estimated using finite element analysis and then a displacement based pushover analysis is conducted.

The pressure and time are plotted against time. This plot shows the primary effect in the positive phase and negligible effect from negative phase. The mass participating in dynamic response gets involved at later time owing to short duration of blast. This happens when the impulse delivers its potential energy to surroundings. This results into the difficulty in resonance due to mobilisation of mass. During explosion time the main pressure wave is transmitted uniformly to all directions. With time the pressure waves gets transmitted. The peak pressure point depends on the distance from the source and amount of explosive material.

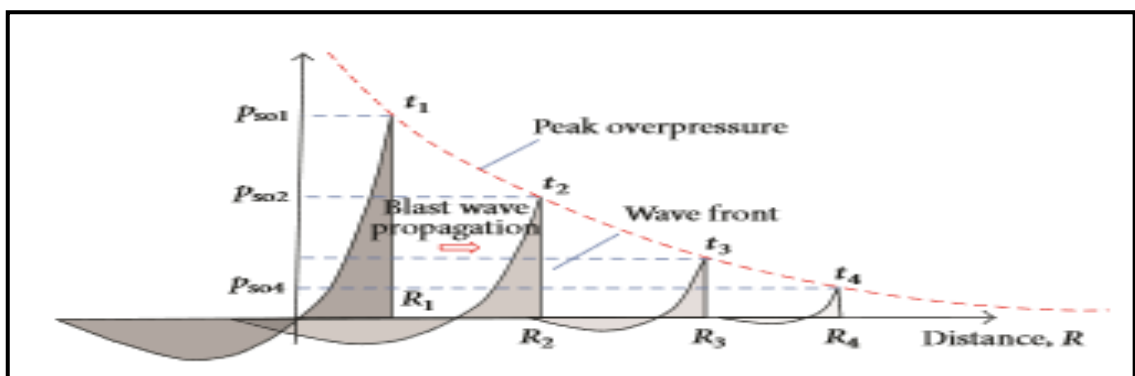


Fig 2.4: Attenuation of peak overpressure with distance from source [Andreou M. et al 2016]

For each explosion the same values are obtained for each point located at a specific distance from the source. The results shows that local yielding is rare while the brittle failure is dominant. This methodology is a versatile tool for first-order estimation of the effects of blast explosions on structures, which would otherwise require an extensive and complicated nonlinear time history analysis [1]. Thus it makes the nonlinear static analysis possible at a much reduced computational cost as compared to 3D solid nonlinear finite element modeling. The schematic representation of the blast wave contact with the bridge is shown in the Fig 2.5.

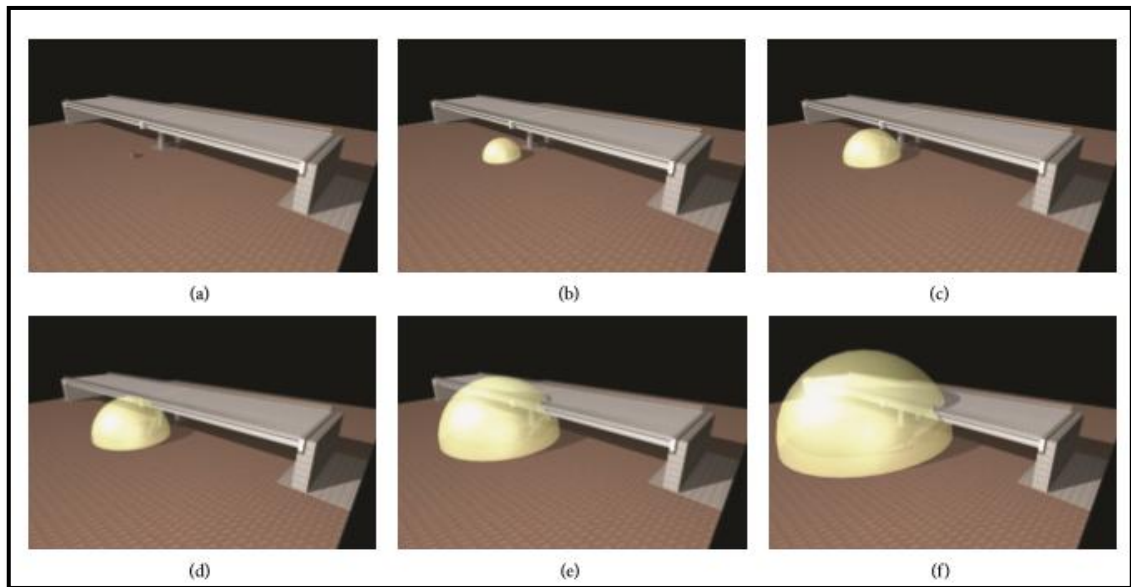


Fig 2.5: Schematic representation of contact of the blast wave with the bridge [Andreou M. et al 2016]

2.2.6 Modeling of dynamic behaviour of concrete material under blast loading

Yong Lu et al. (2004), This model depicts dynamic strength and other strain rate dependent characteristics of concrete. Model for damage of concrete subjected to blast loading is developed. To formulate evolution of damage, continuum fracture mechanics of micro cracking nucleation growth and coalescence are also studied. Concrete has an enigmatic behaviour of increased resistance when subjected to loads with very high strain rate. Earlier studies suggests that micro crack initiates and grow immediately at tensile strains. But recent studies suggests that concrete do not fail at tensile stress up to a certain limit. Complete failure needs a few moments in case of brittle material under stress higher than its static strength. More unstable behaviour is noticed for post peak response. Mechanism of pre peak and post peak differs.

The energy barrier during propagation of the waves delay the fracture of the material. Homogeneity affects shape of softening zone [18]. A cohesion crack model is developed. Crack size is the measure of damage. Initial dynamic Young's modulus is at a stress value immediately below the quasi static state, where the damage is considered nil under dynamic load. Material constants are evaluated by measured dynamic strength and static strength. Then dynamic stress strain relationship for obtaining relation between different strain rates, different element sizes and fracture strain energies is applied to theoretical model. Concluded that compression results in cracks and coalescence. Dynamic tensile strength increases by three to four times the static strength. For strain rate of 100 per second the dynamic compressive strength is 1.5 times greater than the static strength. While tensile strength is 7 times greater at same strain rate [18]. The results are consistent to the experimental data. Young's modulus is to the strain rate is also taken into view in this model of concrete. This model is applicable for all strain rates.

2.2.7 Recent ERDC Developments In Computationally Modeling Concrete Under High Rate Events

J O'Daniel (2010), FRC is the fiber reinforced concrete, which is being used more recently in the structures subjected to impact loadings such as blasts and penetration events. FRC is defined at multi scales, here in this study its studied at structural level called as macroscale, individual fibre and relative matrix called as mesoscale, and transition zone called the microscale. Quantitative comparison is done for the residual velocity in fragment simulating projectile and qualitative comparison is done for damage to the panel. Several methods have similar characteristics but definition of damage to FRC varies widely. So different methods use different definition of damage but the results are comparable. The simulations are done in different codes. The HJC and AFC models resided within the EPIC code [13]. The K&C model present in LS-DYNA was used for this study. Various numerical method models used in this study are:

- (a) Phenomenological Model and AFC Model.
- (b) Reproducing Kernel Particle Method.
- (c) Lattice Discrete Particle Method.
- (d) Microplane Model for FRC.

Experimental data is collected after the experiments for the measurement of FRC's resistance to ballistic projectile penetration. Experiments are performed with an underground ballistic range. The outside support building is used for housing cartridge preparation area. This area contains proper equipment to handle various varieties of cartridge. Johnson-Cook material model is adopted for simulating steel. Complete perforation of panel was achieved. Damaged concrete matrix have large number of fibres extended out. The macroscopic AFC model is shows excellent results allowing for relatively fast simulating speeds. The precise characteristics can be examined at multiple scales with RKPM and LDPM methods [13].

2.2.8 Blast Loading and Blast Effects on Structures – An Overview

T. Ngo et al.(2007), The basics of explosion are studied in this literature. And categorization of explosions based on their nature is done as physical, nuclear and chemical. Physical explosions, energy required is released from the catastrophic failure of cylinder containing compressed gas, volcanic energy or energy from mixing of two liquids at different temperatures. Redistribution of the protons and neutrons within the interacting nuclei provides the energy to Nuclear explosion. while rapid oxidation of carbon and hydrogen atoms provide the energy for chemical explosion. Another classification based on the physical state is solid, liquid or gas explosives. Blast effects are best known for solid explosives [16]. Another classification is based on their sensitivity to ignition as secondary or primary explosive. These are the outcome of simple ignition from a spark, flame or impact. Examples of primary explosives are mercury fluminate or lead azide and that of secondary explosives are trinitrotoluene (TNT) and ANFO.

From pressure-time curve positive and negative phase of duration are observed. Negative phase extends longer but intensity is low. Increasing stand-off distance increases duration of positive-phase having low amplitude. Distance also plays an important role in intensifying the effects of blast. Thus whole structure is effected by shock wave. Reflection and diffraction effects creates complex patterns around the structure. Additional damage is caused by debris impact during the negative phase. Strain rate effects results into the increase in strength of reinforced concrete. Elastic and inelastic responses can be assessed and monitored easily due to the isotropic properties of metallic materials.

Response of reinforced concrete structures under blast loading is called as membrane/bending failure. Ground shock results from the explosion. A part of this shock energy is directly transmitted through ground in the form of directly-induced ground shock, while part is transmitted through the air as air-induced ground shock. High strain rate effects on ductility of RC structures is known from parametric study. The model adopted is Strain-rate dependent Current Building Regulations and Design Standards should include abnormal load cases and preventions.

2.2.9 Concrete Structures Subjected to Blast Loading, Fracture due to dynamic response

Jonas Ekström (2015), investigated the effect of shock wave on a concrete wall. The failure is generally spalling failure. The gradual increase in inelastic strain of concrete results into the spalling. Simple Bi-axial numerical model is adopted here in the investigation. Thus spalling occurs after a number of loading cycles and does not depend on first reach tensile strength criteria. Extent and position of crack is known by the numerical simulations. In the second study the response of reinforced concrete structures subjected to blast loads was investigated taking a reinforced concrete beam and a one way slab [4]. Numerical simulations are done on these two with a combined damage and plasticity constitutive model for concrete. The fracture tensile energy can be known and corresponding effects on deformations can be known irrespective of strain-rate dependency. It is a well known fact that the meshing size and modeling technique adopted effects the numerical simulation results considerably.

Numerical models are a way to hint about the approximate but accurate real behaviour and hence is a way to know the actual real phenomenon. Numerical models costs much lower than actual experiments. The control of time is within the hands of the user for any numerical simulations. Also provides a way for studying responses for the conditions where actual real experiments are difficult to be performed. On the basis of the time duration loads are basically divided into static load, quasi static load and dynamic load. Dynamic loads takes much more time than the static loads. Different types of responses are yielded from different time frames. Strain rate is the main commonly used measure for the initial predefined loading condition which is dependent on the time interval. Properties of the structure does not affect the responses for a blast wave more or less. Unlike the cluster of fragments, the material properties of elements

plus material properties of the structure will affect the stress wave. Velocity plays an important role for the magnitude of the stress wave. Stiffness of elements and structure also affects stress waves and its duration.

Failure that may occur are spalling, scabbing, flexural and shear failures. Spalling behaviour in specimen due to a blast wave was considered for studying [4]. The assumption that the damage due to the tensile stress from the release wave develops instantaneous within a time singularity was shown to be inaccurate. During the development of the fracture, i.e. the crack propagation, the release wave continued to propagate past the point of first crack initiation. In the studied case where the length of the blast wave was much longer than the studied concrete specimen, the crack did not form until multiple compression and release waves had passed. Convergence occurred in areas of large compression. Convergence also occurred for distortion for the slab analyses, i.e. around the support and at the top of the slab. For a cure elastic elements were used in the outer layer of the slab in these areas.

2.2.10 Effects of Blast Loading on Reinforced Concrete Facade Systems

Indunil Rajith Kumara Galhena et al., (2015), One of the advancements in construction industry is facade systems. Facade systems can take normal service loads and can perform well in severe weather conditions. However these are not designed for blast loadings. The behaviour of reinforced concrete facade panels under blast with flexible support conditions is investigated. The 3-D finite element modeling using LS-DYNA and 1-D analytical modeling using a theoretical development is done. The 3-D finite element model is developed using the LS-DYNA finite element model. 8 different material model for concrete and reinforcing steel are considered for the initial model development. Mesh sensitivity analysis is also performed [5]. The 1D analytical solution is developed using the Timoshenko Beam Theory (TBT), as an alternative to the 3-D finite element tool.

Computational methods in explosive loading and response can be broadly split into two categories; (a) prediction of blast pressure parameters, and (b) prediction of structural response to an explosion. A coupled computational program is a combination of Computational Fluid Dynamics (CFD) module and Computational Structural Mechanics (CSM) module working in tandem. CFD module predicts blast wave parameters while

CSM module predicts response of a structure under blast wave [5]. Explicit time integration is adopted in these. Unlike in uncoupled analysis, the combined analysis process allows the structures to deform and even predicts the failure, resulting in more accurate blast wave parameters. LS-DYNA, ABAQUS, ANSYS, AUTODYN etc. are typical examples of coupled analysis programs.

A number of experimental studies have been conducted on the blast loading of concrete panels. The Hawkins shear slip method was applied with a constant rate enhancement factor (DIF). Boundary conditions are adopted. None of the material models available in LS-DYNA was able to capture localized damage associated with spalling and scabbing accurately. Thus requiring a need for improving the localised damage predictions. For spherical charges it's easy to predict blast pressure-time profiles accurately with inbuilt loading functions. However erroneous results are obtained for different shaped charges.

2.2.11 Development of Geometrical Parameters for Numerical Simulations Using the Holmquist-Johnson-Cook Constitutive Model for Concrete

Christopher S. Meyer (2011), found that the Holmquist-Johnson-Cook (HJC) constitutive model for concrete captures pressure and strain-rate dependent strength behaviour and void crushing damage behaviour of porous materials reasonably well. It is readily available in many software. It is generally used to simulate high-velocity penetration of concrete. This literature describes the basic material parameters for HJC material model. Example is also given in the report. Numerical simulations using the material parameters for brick and mortar were compared with true stress and engineering strain data provided by ERDC. 3 different mechanical tests are simulated. Strain is applied to the cube to produce compression against boundary conditions [11]. Strain was applied in different configurations of the three directions to produce the loading conditions as Uniaxial compression, Hydrostatic compression, Triaxial compression [11].

Determination of Failure strains are done from mechanical test data. However HJC model over predict the penetration rate for high velocity impacts for concrete. Residual velocity is predicted well. HJC model is one among limited number of tools available for use in simulations. Further studies in this regard are needed to be performed. Penetration experiments provides high-pressure and fracture data needed for comparing

simulations of penetrations using these material parameters to penetration events. With the availability of such data further explorations can be made. Development of constitutive material models for brick and for mortar for use in high velocity penetration simulations is ideal but impractical these material parameters provide a near-term solution for modeling brick and mortar masonry in penetration simulations.

2.2.12 Review of the current practices in blast-resistant analysis and design of concrete structures

Hong Hao1 et al. (2016), depicted a state-of-the-art review of the current blast-resistant design and analysis of concrete structures under blast loading. It describes the available materials, approaches and numerical tools under higher values of strain rates. Discussions on the accuracies and advantages of these current approaches and suggestions on possible improvements are given. Level of confining pressure affects concrete strength. Lateral expansions are there for dynamic deformations. But due to certain factors it's not able to expand laterally [2]. One of such factors is include inertial restraint that generates lateral stresses which restricts the expansion. Lateral inertial affecting dynamic strength has been the controversial topic up till general consensus reached. Another factor affecting dynamic strength is friction between test apparatus and sample. This may result into increased strength values. Friction results into the restriction to freedom to deform laterally. This creates a confinement of the sample and results in increased values of dynamic strength. Weaker sections are more prone to cracking under quasi-static load conditions [2]. Propagation of cracks causes the failure. The fast rate of loading results into fast deformation leading to cracking.

Higher dynamic concrete strength results from damage of aggregates. Until the water content reaches a certain specific level the influence of these factors seems nil on the impact strength. It is generally believed that critical strain increases strain rate. This occurs irrespective of the quality, type of material, testing methods and conditions. Field blasting test is important to investigate blast loading but such an approach is practically very difficult to handle and is uneconomical in terms of money, safety. Thus such test responses needs numerical simulations to be done. Single value measurement and time-dependent measurements are applied in the testing. But with the results of field experiments, theoretical and analytical models can be verified. However, field blast testing is expensive, time-consuming costly. Load is to be determined for numerical

procedures of blast responses. There are two types of procedures which can be followed i.e. implicit method or explicit method. One of these solutions are employed to know the solutions or responses of blast effects. Both of these procedures are predefined in the finite element simulating software [2]. Although they have certain positive and negative effects.

2.2.13 Effects of blast loading on seismically detailed reinforced concrete columns

Conrad Kye (2014), worked with the seismically designed structures under blast loading and found that this is a very source of research. Blast resistance has been studied over seismically detailed RC column. Numerical simulations are performed for RC columns. The finite element code LS-DYNA has been used. For different levels of seismicity has been used for simulations. Results showed lateral reinforcement detailing effects significantly the responses of RC column under blast load [7]. It is affected significantly. For designing the column for higher seismicity the lateral reinforcement spacing must be reduced. This has resulted in maximum lateral displacement reduction. It's expected that the plastic hinge forms at mid height of column. Thus lateral displacement gets reduced significantly when the mid height lateral reinforcement spacing has been reduced.

This has shown that small values of spacing of lateral reinforcement have more resistance to blast effects. Numerical study is also conducted to know effect of axial loading. Increasing load ratio resulted in increased blast resistance. However, at high, axial load ratios, the columns suffered concrete crushing in the compression zone. This leads to higher lateral displacements and instability. Increasing axial load ratios resulted in reduced maximum lateral displacements at longer distances. Seismically-detailed columns performs similar to conventional column thus not have any significant advantage for blast load. At lower scaled distances reducing transverse reinforcement spacing resulted in reduced lateral displacements. At high axial load ratios, RC columns suffers scabbing and crushing of concrete [7]. Buckling effects are also seen during the simulations. Longitudinal reinforcement in mid-region buckled at lower load and low scaled distance. Suggesting that a multi-degree freedom system needs to be developed for better results under blast loads.

2.2.14 Laboratory simulation of blast loading on building and bridge structures

M. M. Gram et al. (2006), found that blast simulation system and its capabilities can be known from this study. Pressure transducers are required for field testing of samples under blast loading. Impulse generated by pressure data is calculated. This process faced a challenge of reproducing the impulse suited to a laboratory. The technology used in the Blast Simulator was developed by MTS Systems for production of test equipment requiring high energy impacts: artillery firing simulators, automotive crash simulators, shock testing equipment, and high rate material test systems [17]. The impulse measurement is given below.

Accelerometers mounted on the impacting mass measure the acceleration during the impact. Friction force can be calculated or measured and subtracted. It is very small and is usually ignored. The BG is controlled to provide low acceleration at the point of impact. The pressure transducers measure the internal pressures in the BG actuator, and the force is calculated. The speed of sound in steel and oil causes a delay of about 1 ms between the transducer and accelerometer data [17]. This delay is calculated and the force during impact is recorded and added as a correction to the inertial force. The resulting force, on each impactor, is integrated over the time of the pulse to find the impulse delivered to the specimen.

Comparison of post-test laboratory and field data from similar tests conducted on similar test specimens have revealed excellent correlation of impulse, deformation, and failure mode, thus showing the blast simulator accurately simulates live explosive loads. Example comparisons of laboratory and field impulse and failure mode is done. Finally, it is emphasized that the absence of the fireball associated with the field event allows one to follow the specimen failure-time history.

2.2.15 Fracture of concrete structural members subjected to blast

G. Morales Alonso (2013), worked with the cohesive crack which has been inserted in the finite elements through the Embedded Crack Approach (or Strong Discontinuity Approach). According to the Cohesive Crack Model, or Fictitious Crack Model damage is assumed to concentrate in a discontinuity line, and it is governed by a relationship between the crack opening, and stress transmitted across the crack sides through a certain mathematical function, called softening curve [8]. Crack initiates in a

perpendicular direction when maximum principal stress is beyond the tensile strength. Therefore the crack orientation is computed as the unit eigenvector associated to such maximum principal stress. Normal strength concrete (NSC) and high strength concrete (HSC) were tested. Explosive charge is kept same. LS-DYNA explicit finite element code is used for numerical simulations [8]. Hexahedral elements are used. Constant stress is taken for these elements.

The model is based on the embedded crack approach in conjunction with the cohesive crack concept. Strain rate effects are taken into account following a multiplicative approach by using the Dynamic Increase Factor (DIF) applied to the tensile strength and subsequently to fracture energy. Influence of strain rates on crack patterns and fracture modes are known from simulations as well as experimentally.

2.2.16 Dynamic Brazilian test of concrete using split Hopkinson pressure bar

Xudong Chen et.al (2016), worked with the Split Hopkinson Pressure Bar which is the device used to test the blast effects at the laboratory. Here this test is performed over different sets of loading angles and impact velocities. Strain gauges are attached to the SHPB apparatus to know the strain rate values. Stress equilibrium can be achieved under lower impact velocities. In that case the stress-state of specimen is similar to that of quasi-static condition. In quasi static state [3] initiation of crack is at the centre and propagation along the loading diameter direction. Stress equilibrium is harder to achieve at the higher velocities. At some points multiple cracks and ribbon fracture pattern appear at the centre of specimen. Local stress distribution is affected significantly by the loading angle. While the velocity plays an important role in the fracture pattern. Loading angle can improve the responses effectively.

Results shows that when the impact pressure keeps constant, the mean value of dynamic tensile strength increases with the increase of the loading angles, while the tensile strength obtained from the standard arc loading is close to the results of 20° loading. More impact pressure more will be the tensile strength with same loading angle. Complicated stress distribution is obtained for Brazilian disc under dynamic loading. Stress equilibrium should be evaluated at time and space fields simultaneously. Lower the velocities more chances of stable stress equilibrium. The first crack usually initiates at disc centre and propagates along the loading direction. Higher the velocities more

difficult to reach the stress equilibrium rather impossible [3]. Three primary kinds of failure pattern of concrete were observed in dynamic splitting tensile tests. When stress reached equilibrium, start-split location appeared at the centre of specimen and cracks propagate along the loading diameter direction, and the specimen is split into two pieces completely. As the impact velocity increased, specimen fractured before stress equilibrium. The initial crack location was uncertain and multiple cracks propagated at the same time, with a larger fragment zone at the center of specimen. Impact velocity plays a significant role in the failure pattern of concrete specimens under dynamic loading. Using 15° arc loading can improve the local stress state and reduce the local failure, which approximated to the real failure pattern under dynamic loading [3]. Stress distribution and failure process simulated by software LS-DYNA are coincided with experimental results. LSDYNA code is used for simulations. Stress and failure pattern are coincidental with the test results for this study.

2.2.17 A simple Discrete-Element-Model of Brazilian Test

Sumanta Kundu et.al (2015), presented a statistical model in this for Brazilian test of rock samples. Increasing the force beyond its load capacity results in breakage of elements which is irreversible. Once this breaking gets initiated the nearby elements gets weakened and lose its load carrying capacity. Defected zone expands as more deletion and breakage happens. Stress strain behaviour for Brazilian disc sample has been obtained in this. Numerical simulations are also performed. Some Brazilian tests on Sandstone and Chalk samples are performed to know the responses. Qualitatively agreement is well established with the laboratory testing data. Peak value obtained for stress strain curve is similar to the Brazilian test experiments [6].

The Brazilian test is indirect tensile strength test. Here its performed over two rock types - Castlegate sandstone (CG) and Mons chalk (MC). Both rocks have a fairly homogeneous and isotropic structure. Specimen discs have geometries as 22 mm thickness and 52 mm diameter. Masking tape is used along circumference [6]. This is done smoothen contacting surface between rock and steel curved jaws within which the disc is clamped during the test. This curved jaws is then placed in a loading frame. Load is increased slowly but at constant speed of crosshead, until the failure of the sample occurs. From the load-time plot it is obvious that the tensile strength of CG is greater than that of MC.

2.2.18 A study of constitutive relation and dynamic failure of SFRC in compression

Z.L. Wang et al. (2010), performed SHPB test over steel fibre reinforced concrete and numerical simulations are done with the help of LS DYNA software. A constitutive relation has been developed and dynamic behaviour is found by these simulations. LS DYNA code [14] is one of the widely used software for getting the solutions of many non linear problems. It is an explicit finite element code. Particularly employed for solving dynamic problems associated with large deformations. Mass, momentum and energy conservation are used in this software. For the simulations of SFRC erosion algorithm is to be employed. Erosion algorithm deletes the elements when critical value is reached in that element. Deletion cannot be reversed. Once the critical value is reached elements gets eroded and can't be generated again.

All three bars i.e.. striker, incident, output bars have a diameter equal to 50mm and lengths are 500, 1600, and 1600 mm respectively. Meshing is done generating 7500 and 48000 3-dimensional SOLID164 elements for projectile [14] and the bars respectively. Specimen's elements length is 0.25 cm and meshed elements are 3000 in number. Surface to surface was set between the bar and the specimen. Velocity of striking was 11 m/s. The projectile has mass density= 7800 kg/m³, Young's modulus= 231 GPa, Poisson ratio= 0.30. After the striker strikes the incident bar, stress wave gets generated. These propagates along the z-axis direction [14]. This results in fracture or failure. When the value of principal strain is critical value (0.0035) the failure occurs in the upper portion of the specimen. As the critical value increases, the failure of the element further develops in the upper end and at the same time, it moves down along z axis. This is due to the effect of reflected wave. At t=400 μ s, there is no element failure in the specimen. At t=500 μ s the element in both the upper and lower portions are deleted in terms of the erosion criterion. When t=750 μ s, the rupture near the lower end begins to consolidate closely due to compression of wave [14]. The stress strain curve for SFRC under quasi static condition and the medium strain rate loading are different. Former the damage softening prevails and in the latter case pressure dependent plastic hardening prevails.

After going through the literature its clear that the dynamic response of structures under the blast loading is a vast and emerging topic for research, since the number of terrorist attacks are increasing at an alarming rate. Many software are there for studying the behaviour of concrete under impact or blast loadings viz. ABAQUS, LS-DYNA, AUTODYNE 3D etc. ABAQUS has been used here in this project to numerically simulate the results of concrete subjected to blast loads. Results of dynamic response of blast loading will suggest the properties of composites such as SFRC, RPC to be incorporated in the concrete to improve the resistance to blast effects.

2.3 GOAL OF STUDY

This project deals with the concrete under blast load. The main aim is to model the concrete under blast loading and numerically simulate the dynamic response using ABAQUS, a FEM software and to improve these responses by altering the properties of concrete.

2.4 OBJECTIVE OF STUDY

Concrete is considered to have high blast resistance compared to other materials. However normal strength concrete structures require higher strength to improve their impact and blast resistance. To protect the structures from blast loadings there is a dire need to study, model, and simulate the results of concrete under blast loadings. these objectives leads to goal accomplishment.

This project has been prepared with the basic objective of:

- (a) Modeling of steel fibre reinforced concrete composite for blast loading.
- (b) To numerically simulate the response of concrete under different strain rates.
- (c) To optimize the properties of steel fibre reinforced concrete composite for improved responses.

CHAPTER 3

METHODOLOGY

3.1 SHPB TEST

The Split Hopkinson Pressure Bar device is mostly used to study the mechanical properties of material under dynamic loading. It is generally used for testing the material under high strain rates generally between 10^2 to 10^4 s^{-1} . Conventional SHPB places a short specimen in between a long incident bar and a long output bar. The schematic is shown in the Fig 3.1. By striking the end of one bar, a compressive stress wave shall be generated and will immediately traverse across the stricken bar and reaching at one end of the specimen. The wave shall be partially reflected back and traverse a path back to the impact surface. Rest of the wave passes the specimen. Then reaches the second bar causing the irreversible plastic deformation on the specimen.

These waves are in a proportion to the strain rate and stress of specimen. The reflected wave have proportionality with respect to the strain rate while the transmitted waves have proportionality with respect to the stress. Integrating the strain rates results into specimen's strain. Stress-strain time history can be obtained by monitoring the strains in these two bars. Practicable operation of the apparatus relies on not only the accuracy of the hardware frame manufacturing but also the incorporated instrumentation with excellent capability to intercept, condition and output the measuring data. Moreover, the signals to be captured are in the dynamic status in very short time but with mass data to be filtered and recorded. Generally there are cracks and voids in SFRC. Damage gets effected by these. Hence the fracture failure can be considered as an effect of plastic hardening and damage softening taken together. In the initial loading stage damage is less significant. Damage softening plays an important role when stress is in the vicinity of the peak value. This is true for quasi static situation. However for medium strain rate effect of pressure related plastic hardening is to be considered. Concrete when tested under impact loadings generate a lot of equations and data to be solved, which is difficult to solve manually software makes these calculations easier. The analysis of the concrete under blast loading is a difficult task. So many software have been designed for this type of analysis. With the use of FEM dynamic problems can be solved easily and precisely.

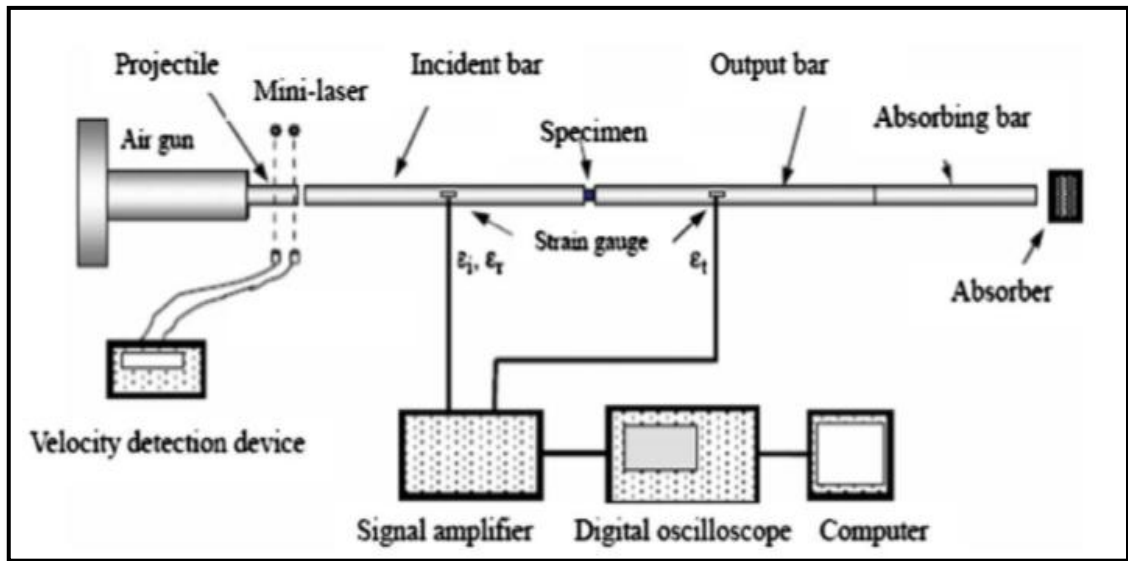


Fig 3.1 Schematic of SHPB [Wang et al. 2010]

3.2 FINITE ELEMENT ANALYSIS (FEA)

FEA is widely applied to engineering problems. It is a computational tool to get the solutions of complex problems. It provides a way to split the whole complex model into a number of small elements. The discretization of the complex models has several advantages as it provides an accurate representation of the complex geometry, local effects can be easily computed, dissimilar material properties can be easily adopted thus providing an opportunity for the new innovations in the field of engineering. It is an easy way of representation of total complex solution. FEA involves a large number of equations and thus a tedious job to handle manually. Thus a dire need of the software is there to study the responses of complex problems. Various software are there for such an analysis such as ABAQUS, ANSYS, LS-DYNA, AUTODYNE-3D etc.

These software which utilises the FEA tool for modeling and analysis discretized the large structure into smaller units. This is achieved by meshing. After that the FEM algorithm coded in software does its part for problem solving. All the structure analysis software generally consists of three parts as Pre-Processor, Analysis Engine and Post-Processor. As the name suggests the Pre-Processor is responsible for the generation of the model, the Analysis engine performs the calculating and analysing part, and the Post Processor displays all the calculated and analysed responses performed in the analysis part.

3.2.1 Pre-Processor

- (a) Generate the model with all the data needed for the analysis.
- (b) It provides all the geometrical tools options to draw, edit, erase, assemble etc.
- (c) It also provides a way to assign the material properties to the modelled parts.
- (d) Initial predefined fields such as boundary conditions, loadings, initial velocities, displacements, accelerations, energies etc. are available with this.

3.2.2 Analysis Engine

- (a) Calculate displacement, forces, stresses, strains, energies etc.
- (b) It is the brain of the software that analyse the model.
- (c) It works on the FEM equations for each element separately.
- (d) It is responsible for performing all the necessary calculations.

3.2.3 Post-Processor

- (a) Displays the results for analysis and design.
- (b) Post-processing procedures are designed for extracting the data of interest from a finite element solution.

3.3 ABAQUS FEA SOFTWARE

ABAQUS has been used in this project for simulating the responses of concrete under blast loading using the SHPB model under high strain rate loadings. ABAQUS is an engineering simulations software. It has made finite element analysis much easier, which was earlier performed by hand. Model can be created for simulating the effects of different attributes such as temperature, pressure, strength etc. on structures, mechanical or electronic models. It is possible with software to know the effects or functioning of any model, without actually performing the destructive tests on structures or machines. For example, ABAQUS software may simulate functioning of a bridge throughout its life, economical design can also be known with simulations for a slide by utilising less while assuring safety also.

Most ABAQUS simulations are performed using the ABAQUS/CAE software, which is one of the main products. In the complex model is divided in parts with meshing operation and then each segmented parts are modelled and tested. More fine meshing means more time for completion of the job. First step is to define the geometry by

providing dimensions and then assigning the physical properties. Finally. Then model meshing is done. At last model is simulated and analysed by ABAQUS software. The results may be known for displacements, forces, resultants, stresses, strain, fracture, energy, electromagnetic efficiencies, temperatures and pressures etc. Time history analysis can be known easily. ABAQUS enable bi-directional CAD connectivity, geometry clean-up tools, automatic meshing, and quick simple definition of initial and boundary conditions.

In this project ABAQUS has been used as it is a user friendly software. The SHPB test has been performed over concrete to get the responses of blast loading over concrete. ABAQUS comes with various solution options such as explicit dynamics, fluid flow fluent, static structural, transient structural etc. Here explicit dynamics has been used for the modeling and analysis of the project. Some of the experiments when performed practically are difficult and uneconomical. To get rid of such a problem software is used. ABAQUS software is a best choice for such simulations. This is a very user-friendly software, easy to operate and easily understandable. Some of the problems are complex in terms of interactions, huge deformations, higher strains, short-duration etc., ABAQUS is the problem solver for these problems. Thus it helps to solve complex explicit problems easily. Minimum inputs and efforts are required in this software even for shorter duration problems. As this software involves the Explicit method of solving so its easy to get the results for high pressure, larger impacts, quick and heavy loading, waves propagating phenomenon etc.

3.3.1 Modeling Steps

1. ABAQUS window

- (a) Start with a click on the ABAQUS CAE icon, ABAQUS/CAE window will be opened.
- (b) Choose one of the options that appear from the options which are "Create Model Database" with Standard & Explicit Model, with CFD Model, With Electromagnetic Model.
- (c) Here the project is revolving around the explicit working model so "Create Model Database with Standard & Explicit Model is selected.
- (d) Screen is opened with the appearance of various toolbars.

(e) Window that appears on the screen is shown in Fig 3.2.

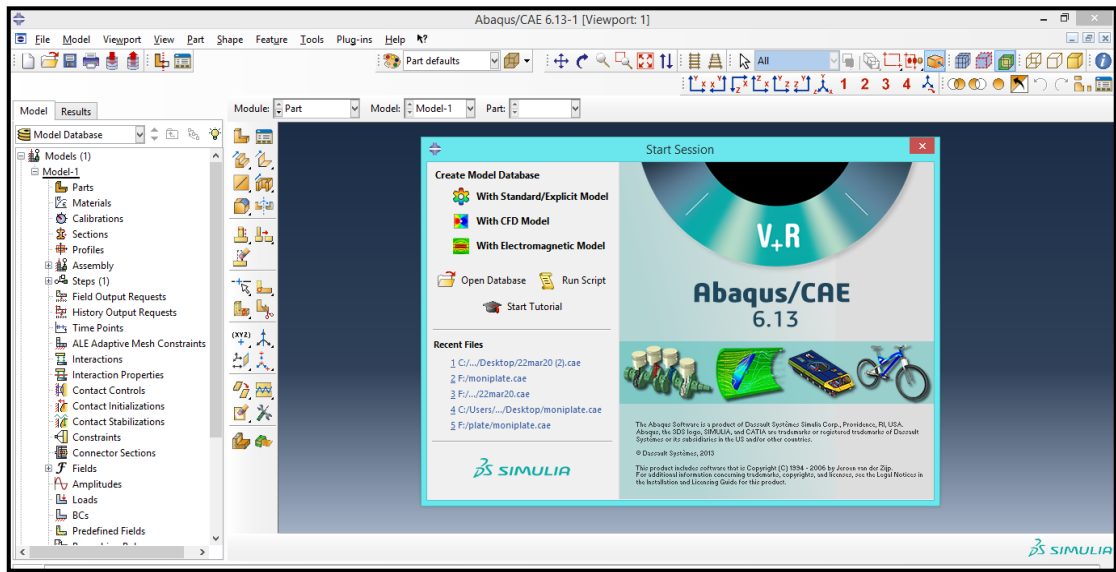


Fig 3.2: ABAQUS/CAE Window

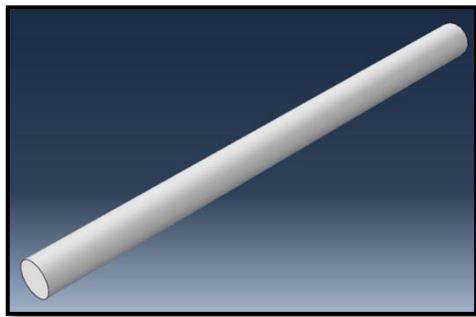
Table 3.1: Geometrical Properties

S.NO.	PROPERTY	VALUE
1.	Diameter of the bars	0.02 m
2.	Length of Incident bar	2.00 m
3.	Length of Transition bar	1.00 m
4.	Length of Striker and Absorber bars	0.30 m
5.	Diameter of the Disc	0.02 m
6.	Thickness of the Disc	0.01 m
7.	Side length of the Cube	0.013 m
8.	Velocity of the Striker bar	14m/s,10m/s,7 m/s

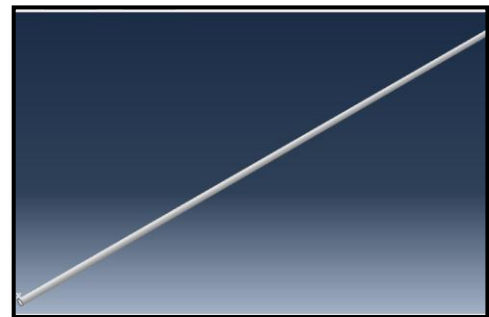
The geometrical properties to be adopted for the modeling purpose are given in the Table 3.1 above. The velocity adopted for the striker bar is 14 m/s, 10 m/s, 7m/s for the three different cases to be taken for simulations. The cube and the disc samples are analysed separately for these three different velocity conditions.

2. Geometry

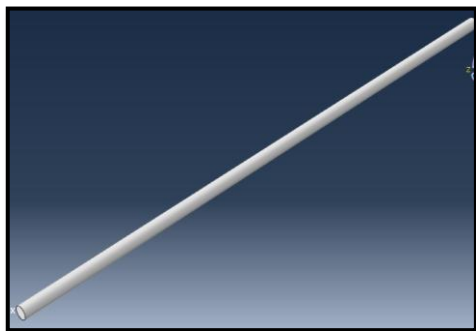
- (a) Start drawing the geometry by drawing it part by part.
- (b) Abacus provides this feature under Module→ Part→ Create Part→ "Name"→ 3D→ Solid→ Extrusion→ Continue.
- (c) One can have other options also for modeling space, type and shape depending upon the geometrical features.



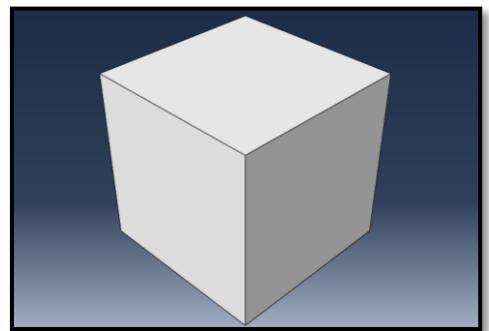
(a)



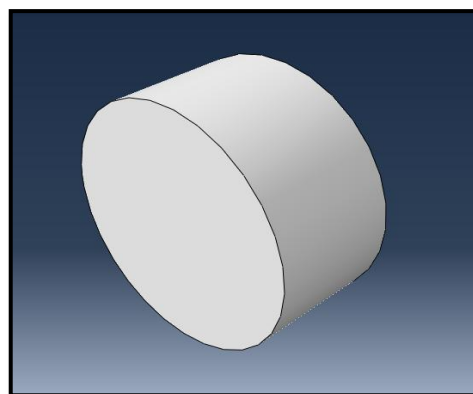
(b)



(c)



(d)



(e)

Fig 3.3: Parts of the geometry in ABAQUS (a) Striker bar (b) Incident bar (c) Output bar (d) Concrete Cube sample (e) Brazilian Disc

3. Property

- (a) Select the Material manager→ Create→ "Name"→ Select the property to be valued.
- (b) Make the sections for the materials by selecting the "section manager option".
- (c) By selecting the "Section Assignment Manager" option, one can assign the section their material properties.
- (d) The material properties used here are listed in the Table 3.2, below.

Table 3.2: Material properties for SFRC

S.NO.	MATERIAL PROPERTY	VALUES	UNITS
1.	Density, ρ	2550	kg/m ³
2.	Elastic Modulus, E	30.00	GPa
3.	Poisson's ratio, ν	0.190	-
6.	Tangent modulus, E_t	08.90	GPa
4.	Compressive strength	179.2	MPa
5.	Initial yielding stress	88.22	MPa

Apart from these properties, initially the Elastic modulus of the concrete is taken equal to 90 GPa and velocity is taken as 14 m/s, for validating the numerical model.

4. Assembly

- (a) Click on Module→ Assembly→ Create instance→ Select Part→ Independent mesh→ Click Ok.
- (b) There are two options to assemble any part that are dependent or independent part instance. One can also edit an instance and change it from dependent to independent or vice-versa. By default it is set to dependent option.
- (c) Dependent part can't be meshed. One must mesh the original part to mesh it automatically get meshed in the assembly.
- (d) However the other mesh attributes can be changed in dependent instance without changing the original mesh controls.
- (e) While the independent instance is a duplicate copy of original instance. The disadvantage of independent instance is that one have to mesh each instance individually and it uses more memory

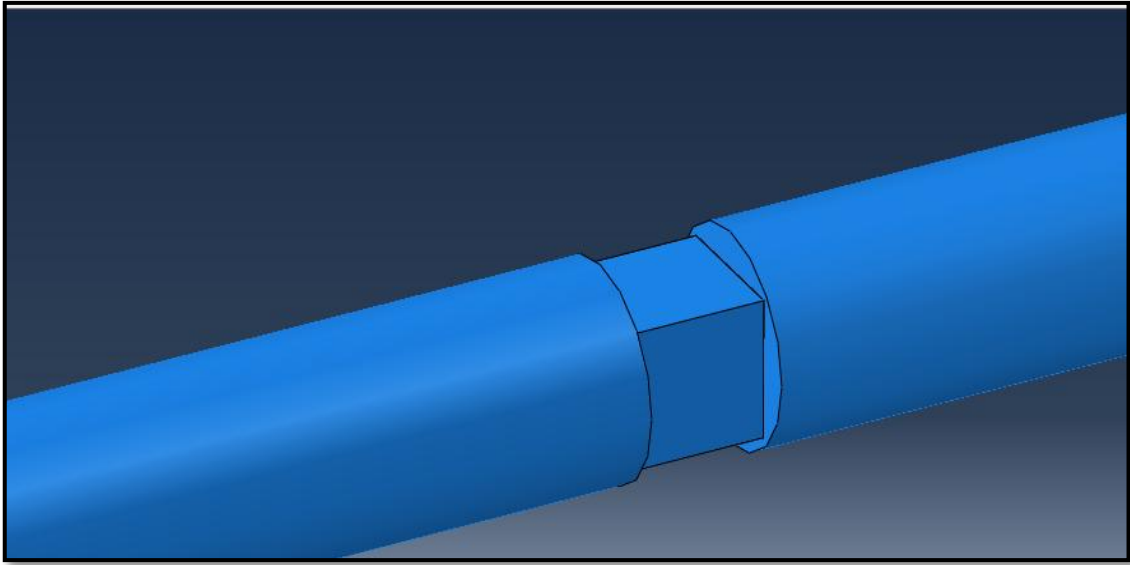


Fig 3.4: Assembly of the cube sample

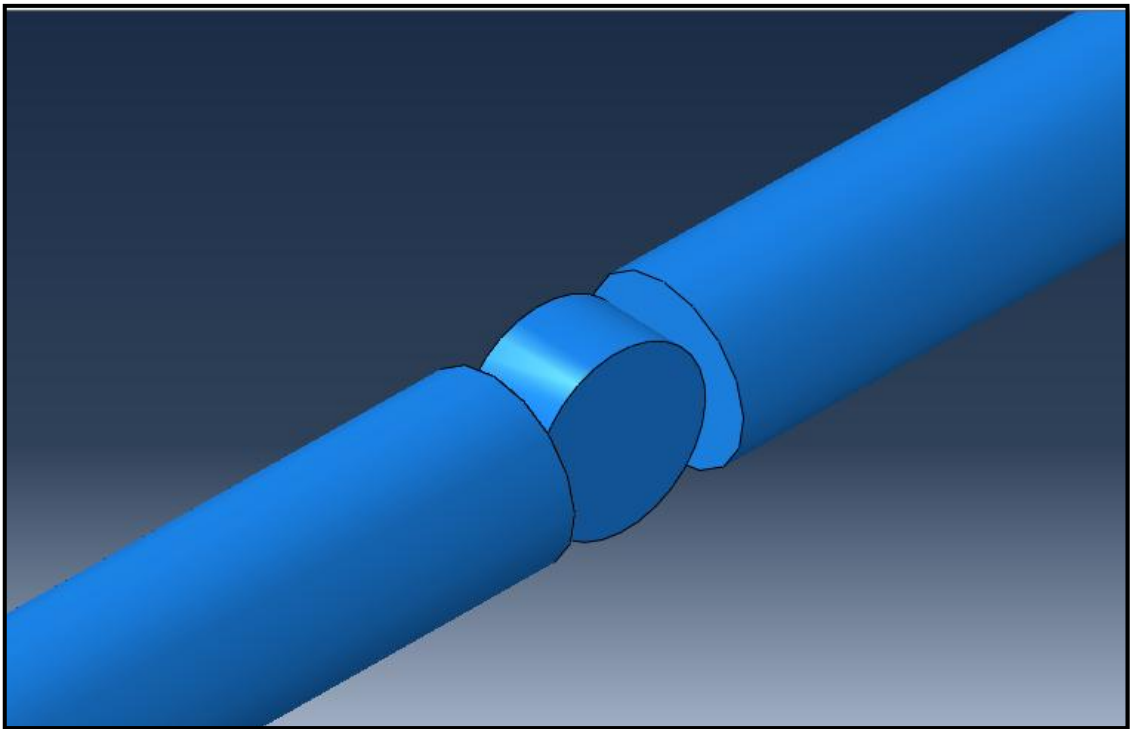


Fig 3.5: Assembly of Disc sample

Fig 3.4 and Fig 3.5 shows the zoomed view of assembly of the cube sample and the disc sample respectively. The incident bar, transition bar and the samples are shown in these Figure while the striker bar and absorber bars are also available in assembly at the same distance as mentioned earlier in Table 3.1.

5. Interactions

- (a) Start with a click on Module→ interactions→ Create interactions→ Choose the Type of the Procedure→ Contact interaction Property→ Choose the contact property option as mechanical, electrical or thermal→ Click ok.
- (b) Surface to surface interaction property has been selected for this project work. And contact property mechanical tangential frictionless has been adopted over here.
- (c) After defining the interaction property, assign the interactions between different surfaces. Fig 3.6 shows the interactions of the contact faces for this project.

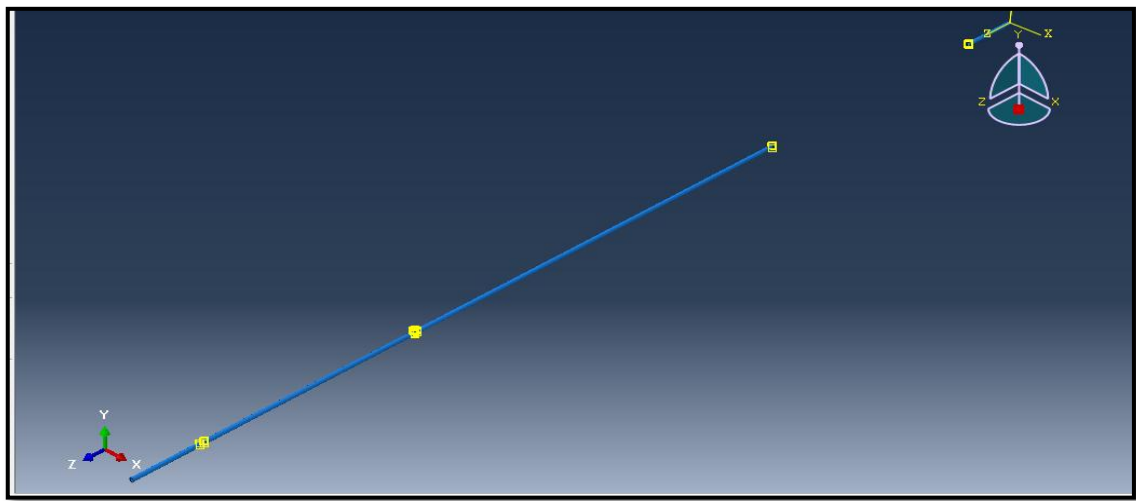


Fig 3.6: Interactions of the contact faces

- (d) The finite sliding and small sliding are the two options provided in this software for interactions.
- (e) For this model the interaction properties defined as kinematic contact with small sliding.
- (f) The slave surface and the master surface are to be defined in the interactions.
- (g) There are four interactions that are to be adopted here in this work. These are surface of the striker bar interacting with the input bar, other end surface of the input bar that is going to interact with one end surface of the sample, other end surface of the sample interacting with the output bar, and last one is the interacting surfaces of the output bar and the absorber bar..
- (h) Providing the erroneous interacting properties will lead to erroneous results at the end, so interactions are to be provided carefully.

6. Boundary Conditions and Loadings

- (a) Go to Module→ Load→ Boundary condition manager→ Create→ Specify the name→ Category→ Type of BC→ Continue.
- (b) For SHPB analysis the initial boundary conditions will be fixed condition for the absorber bar and translation motion for the striker bar in the direction of velocity application.
- (c) Go to Module→ Load→ Predefined field manager→ Create→ Type of selected step→ Continue→ Select the geometry to be assigned→ Done.

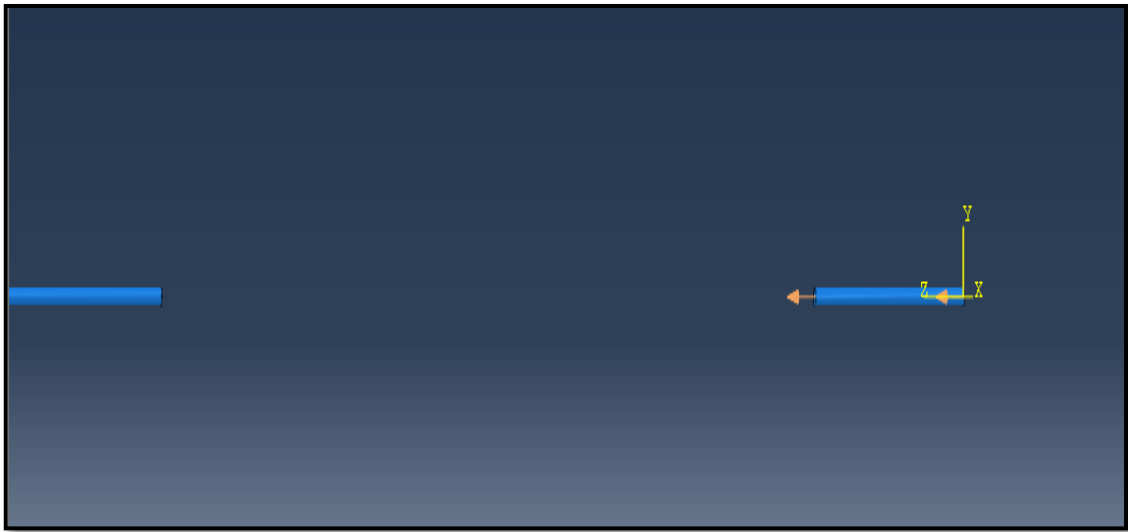


Fig 3.7: Velocity (direction shown by arrows) in striker bar

7. Meshing

- (a) Start by clicking on Module→ Mesh→ click on Assign mesh controls→ Select the element shape, technique, algorithm→ click Ok.
- (b) For creating local seeds for the meshing click on Seed edges or Seed instances, then select the geometry to be assigned local seeds. One can define the seeds by number of elements or by size particularly.
- (c) The number of elements generated for incident and the transition bars are 39984 and 19992 respectively. For the striker and absorber bars this number is equal to 5992. For the cube sample and disc sample number of elements generated are 125000 and 169330 respectively. These elements are Linear Hexahedral Elements of type C3D8R.
- (d) Generated meshes for the two samples are shown in Fig 3.8 and Fig 3.9.

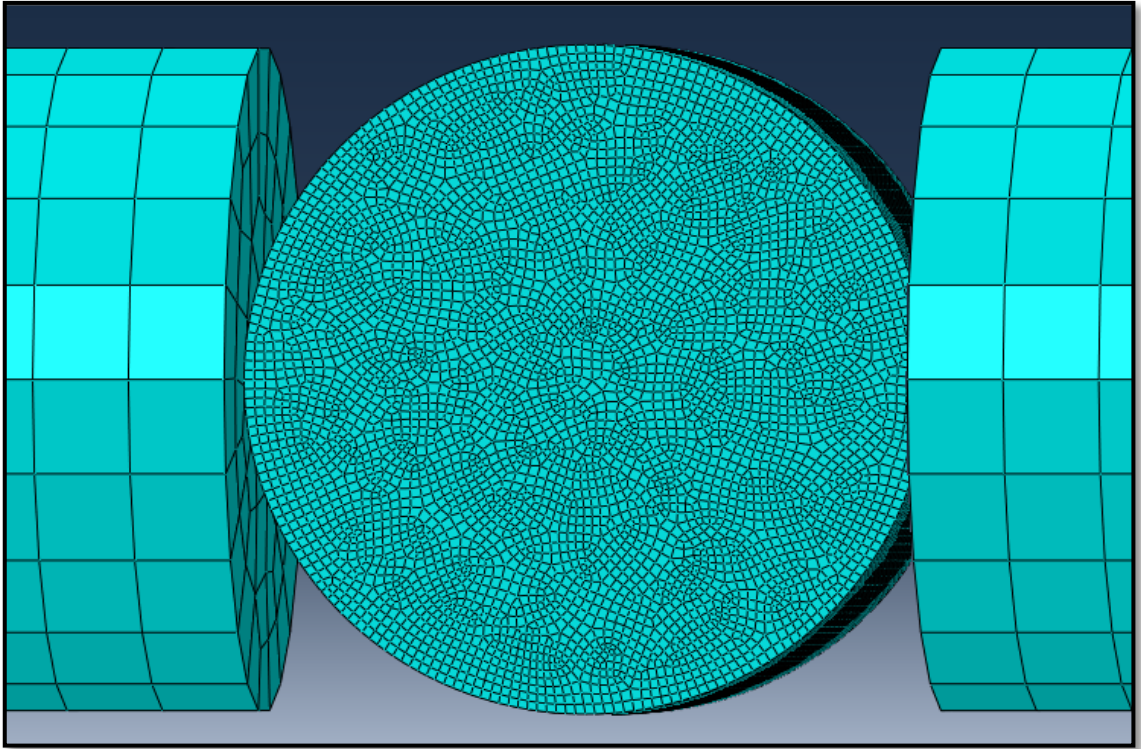


Fig 3.8: Meshing of the Disc sample

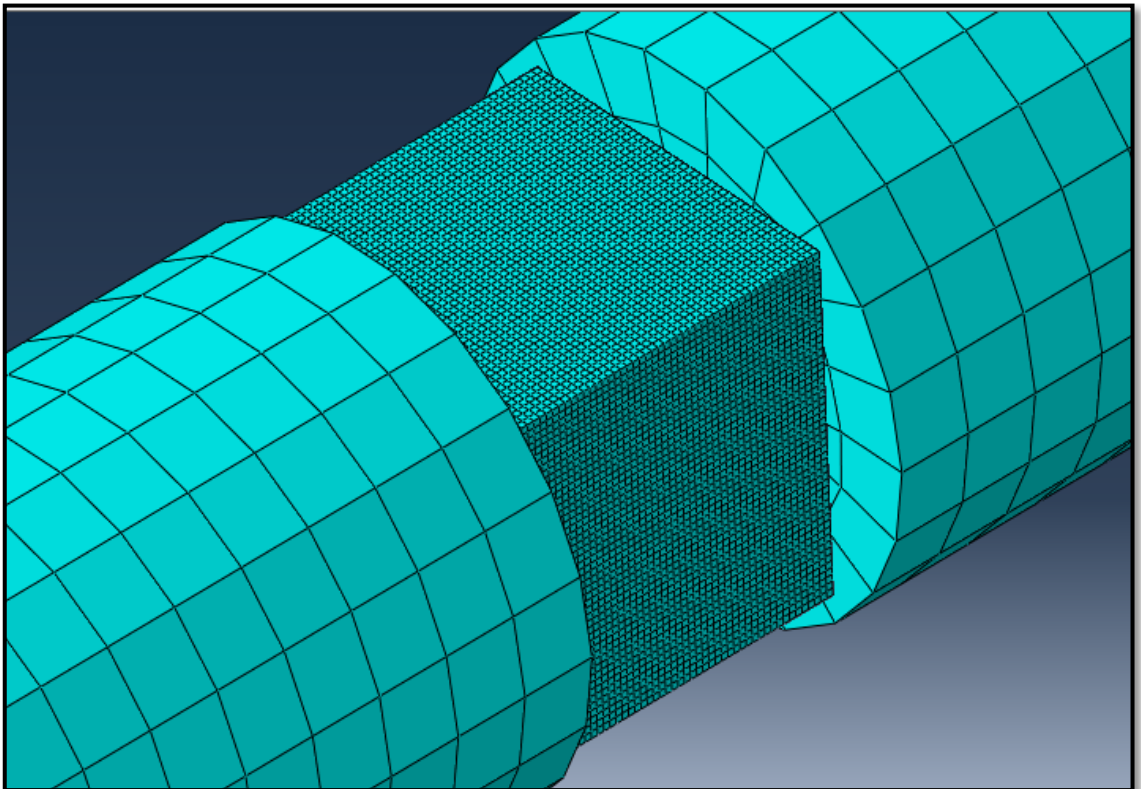


Fig 3.9: Meshing of the Cube sample

8. Output manager

- (a) Click The Module→ Step→ Step Manager→ Create→ Procedure Type→ Continue→ Specify Time Period.
- (b) Module→ Step→ Field Output Manager→ Specify the Output Attributes wanted such as displacement, stress , strain, etc.→ Click OK.
- (c) Also specify the time interval, frequency, and timing in the above mentioned step.
- (d) Module→ Step→ History Output Manager→ Specify the domain, frequency interval→ Specify the fields required such as contact, energy or user defined fields→ OK.

9. Analysis

- (a) Module→ Job→ Create→ specify the Job Type, Run Mode→ OK→ Submit→ now the analysis process gets started→ check for any errors or warnings if any.
- (b) One can also use the schedule option to submit the job at a future time.
- (c) Results will be there after few seconds, minutes, hours or days depending on the meshing size and total time provided by the user in the field output manager and history output manager under the step module option.

10. Visualisations of the results and graphical representations

- (a) After the successful completion of the job click on the visualisation option under the modules.
- (b) From here one can easily check out the results.
- (c) Another way to access the results is to click on the job option, then select the job that has been completed already, there is the results option provided to check out the results.
- (d) For plotting the graphs click on XY data option then choose the option as required then click plot.
- (e) Plot is available in few seconds which can be saved.

Although it is a versatile and user friendly software but with the only disadvantage that that user has to keep track of the units of the variables to be assigned. This is a tedious job and if one will not keep track of the units the results will be erroneous. The results given after the job will be in the same units as initially assigned to the variables by the user but displayed in numbers only.

CHAPTER 4

RESULTS

4.1 RESULTS FOR THE SFRC CUBE SAMPLE

Initially the properties for the cube sample are taken as specified in Table 3.1 except the Elastic Modulus. The Elastic Modulus has been taken as 90 GPa for the cube sample and the velocity of striker bar is taken as 14 m/s. And the results are represented here in this section.

1. Displacement

From the results it is clear that the resultant of the displacement is constant throughout the cube elements. The resultant displacement has a maximum magnitude of 0.11 m. In the x axis direction the magnitude of the displacement ranges from 0.747 mm in negative x direction to 2.33mm in x direction. In the y axis direction the magnitude varies from 1.5 mm in negative y axis direction to 1.2 mm in positive y axis direction. In the direction of the applied velocity i.e. z axis direction or the wave propagation direction the magnitude of displacement is constant. Max magnitude is 110 mm. Fig 4.1 shows the contours for displacement.

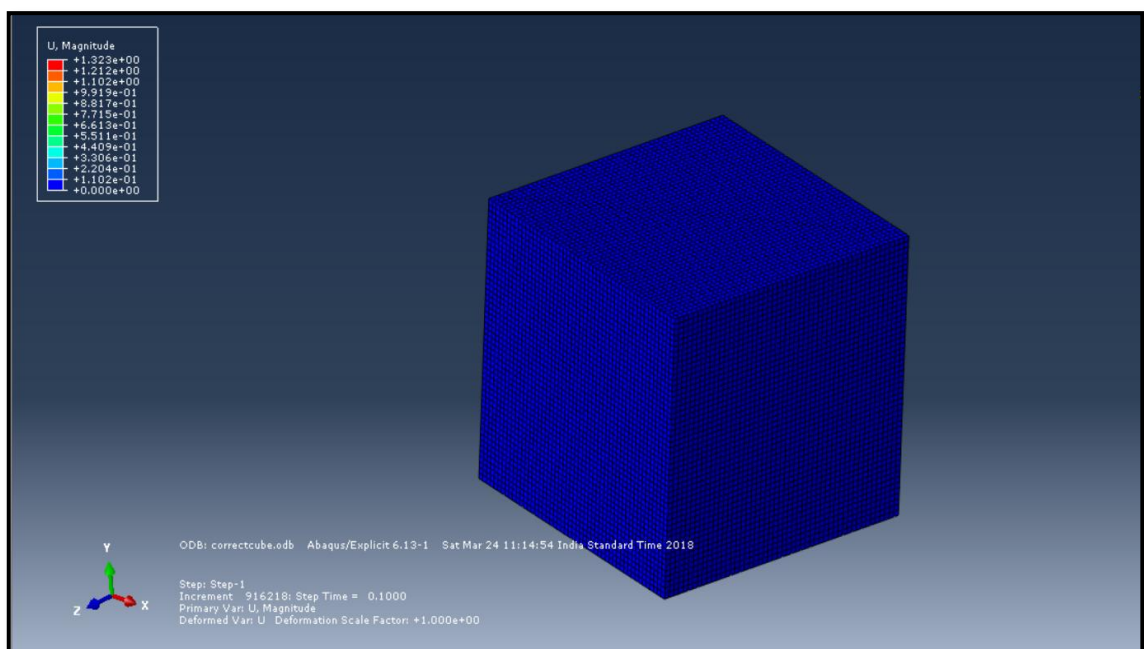


Fig 4.1: Contours for Displacement

Note: Related Figures are provided in Appendix A.

2. Stress

- (a) The analysis results shows that the stresses comes from the corners of the cube to the middle section.
- (b) Firstly the lower edge elements starts to deteriorate then the effect is transferred to the upper portions also.
- (c) The Von Mises stresses are having magnitude ranging from 0 to 32 MPa.
- (d) Maximum principal stresses are from 1.42 to 45 MPa.
- (e) Strain varies from 0 to 0.005.

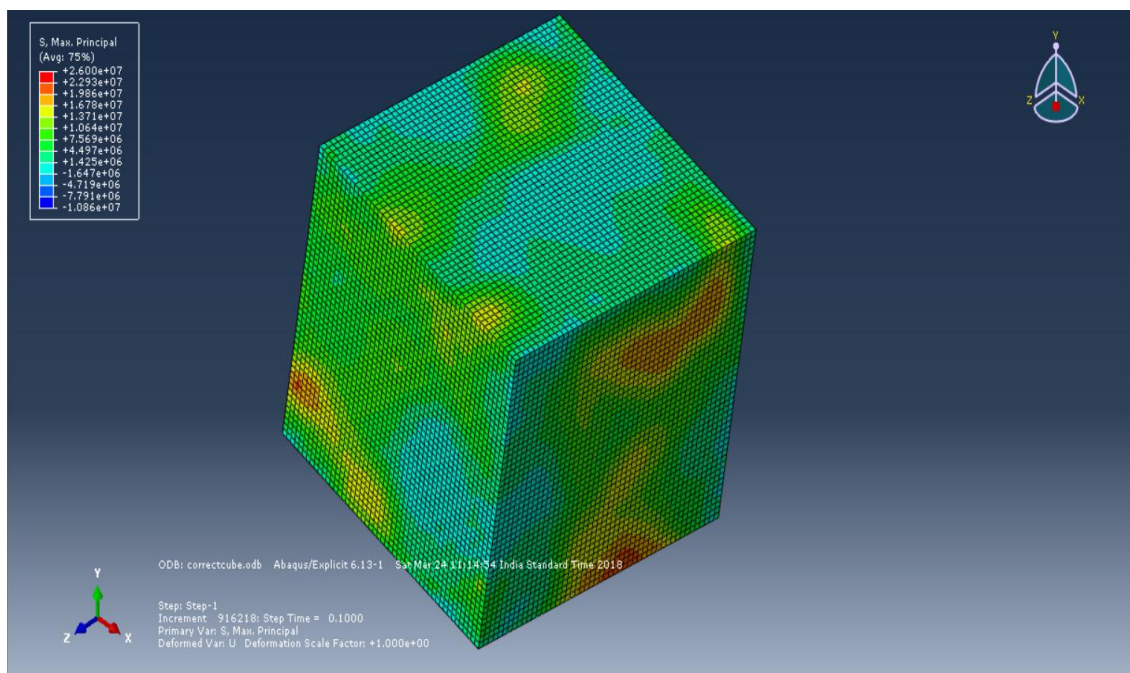


Fig 4.2: Contours for Maximum Principal Stress

Fig 4.2 shows the contours for maximum principal stress for the cube sample. Here the lower value for maximum principal stress is represented by red coloured pattern while the lowest values are represented by blue colour. This figure shows resultant of the maximum principal stress comprising the effects in all the three directions.

Note: Related Figures are provided in Appendix A.

4.1.1 Graphical representation of the analysis results

- (a) The properties adopted for this modeling is same as defined in Table 3.1 and in Table 3.2 except the value Elastic modulus for concrete which is taken as 90 GPa. This has been done to check the validation of the model. The velocity for striker bar is 14 m/s. The results obtained are represented in this section.

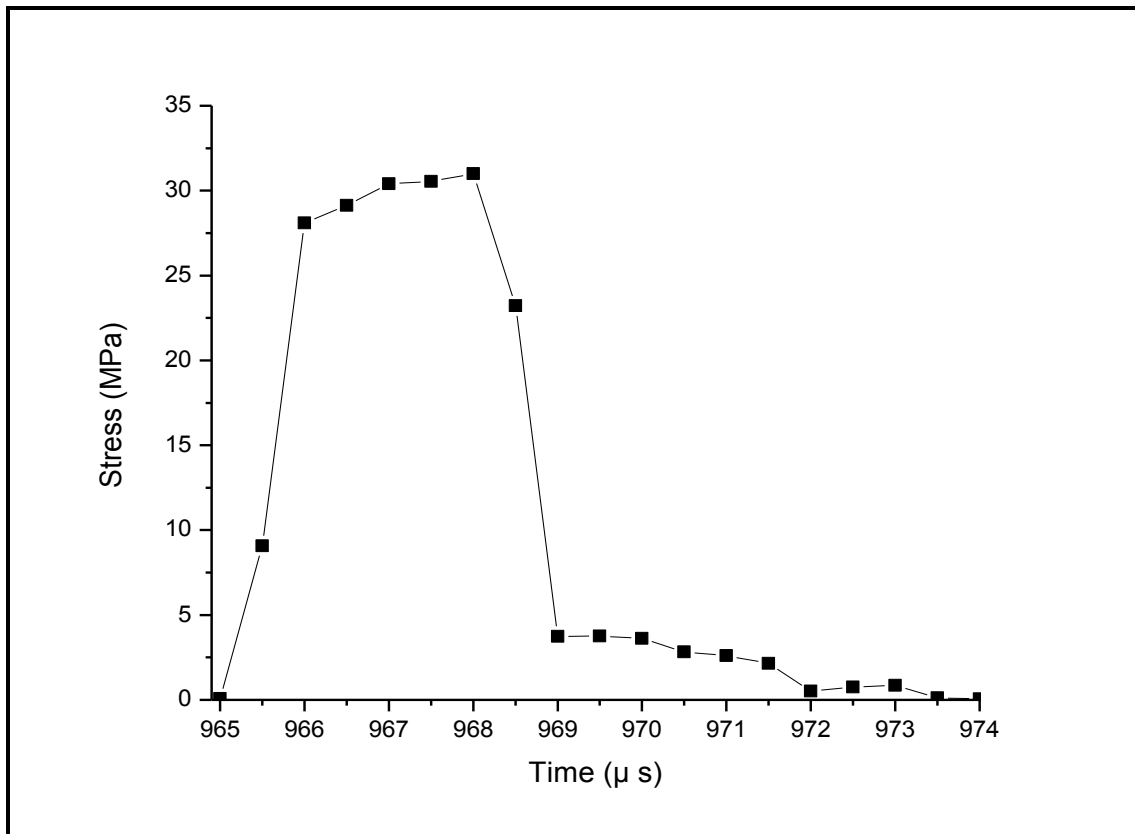


Fig 4.3: Time history curve for stress in cube sample

The stress v/s time graph has been plotted in Fig 4.3 to know the effect of stress on the cube sample relative to the time. This graph reveals that at the time of 965 μs the stresses starts to achieve an increase from the zero value. Then goes to a higher value 26 MPa at 966 μs and then starts to flatten to get a highest peak value of 32 MPa at approximately 968 μs. As most of the waves have passed the sample the stress curve starts to recede. There occurs the plastic hardening. It can be seen that by that time most of the waves have passed the cubical sample and gets transferred to the output bar. Due to this the output bar moves in the direction of waves and the effect of stress starts to recede by that time and attains the zero value at 974 μs.

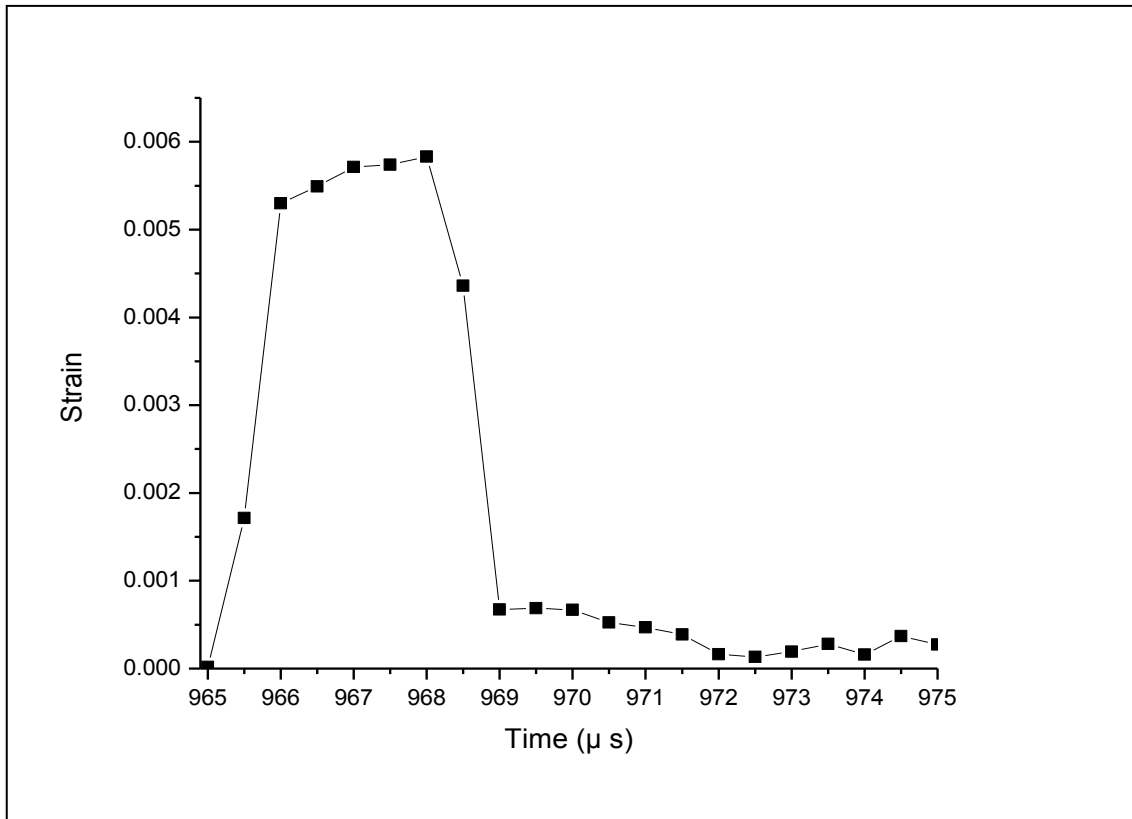


Fig 4.4: Time history curve for Strain of cube sample

Fig 4.4 shows the variation of logarithmic strain versus time curve. Results are observed for the velocity of strike equal to 14 m/s and the geometrical dimensions are the same as in Table 3.1. It can be easily seen from the plot that the strain value starts to increase from zero to maximum value between the time interval 965 μs to 970 μs approximately. It achieves its maximum value of strain approximately equal to 0.005 at 966 μs. Then it flattens down and reach a value in between 0.005 and 0.006. Again another peak is obtained near about 0.006 value and at 968 μs. Afterwards curve starts to recede to a minimum value zero at time 972 μs. Then again starts to increase having lower sharp peaks after 969 μs. Afterwards it reaches a zero value. The abrupt increase or decrease in the values reveals the loading and unloading conditions i.e. when the waves reaches and passes through the sample. When the curve goes beyond 972 μs it has small increase and decrease in values for extremely short durations before it reaches zero value.

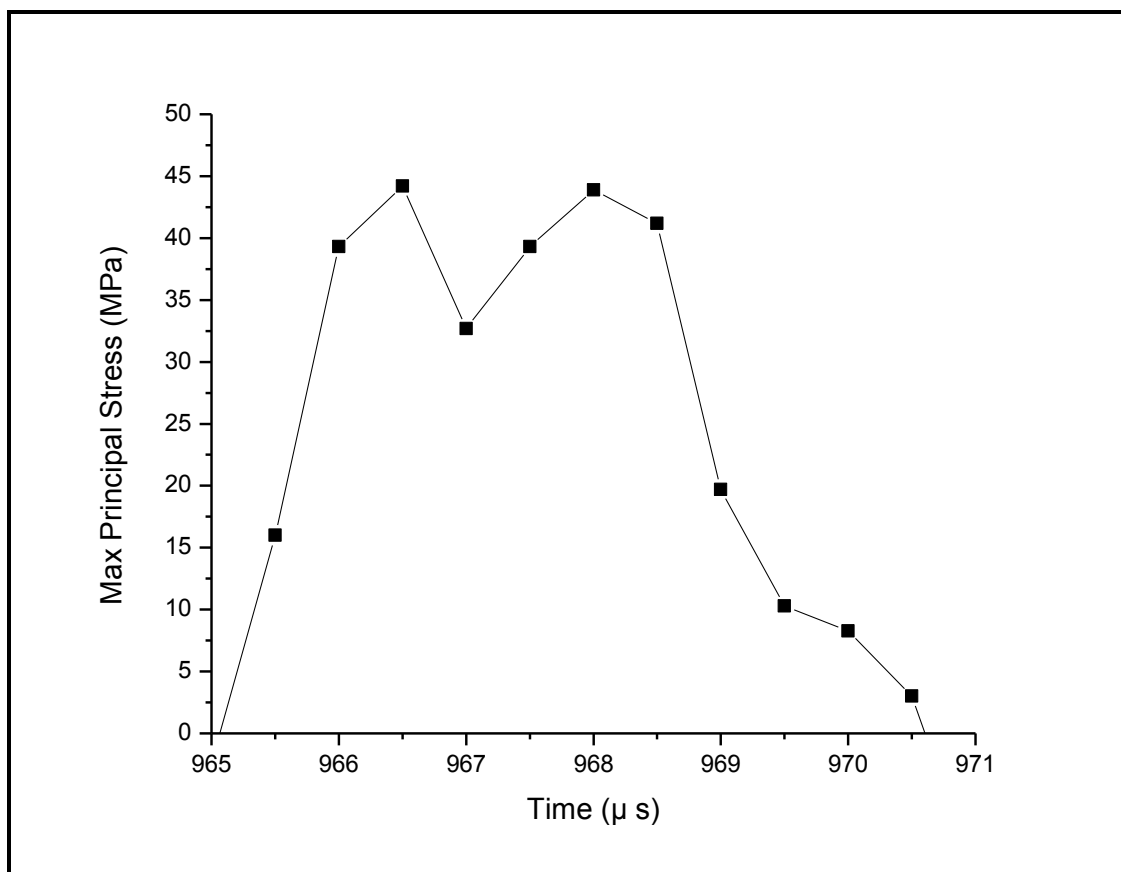


Fig 4.5: Maximum Principal Stress versus Time curve

Fig 4.5 shows the graph between Maximum Principal Stress versus Time. Time is in micro-seconds and stress is in mega-Pascal units. The highest peak portion of the whole graph has been depicted in this graphical representation. It can be inferred from this Figure that the maximum peak point of this graph is between 965.00 μs to 971.00 μs. The peak maximum principal stress is 45 MPa approximately. There are two peaks of this graphical representation, one at about 966.50 μs and other one at 968.00 μs. At initial stages the curve has an abrupt increase in stress values with almost a linear variation. Afterwards the curve reach the maximum value and first peak is obtained. It starts to recede afterwards upto 32 MPa at about 967.00 μs. Then again an increase in the values can be seen upto the second peak at about 968.00 μs. It is approximately of the same value as was the first peak. Than the graph again falls back to zero value at about 970.50 μs. The reason for getting the two peak points is the partial reflection of the waves from the sample. Some part of the waves get reflected back partially thus causing the stress in the sample after the first falling limb of the curve. Hence stress again reaches a peak value and after that falls to zero value.

(b) For this simulation model the geometrical and material properties are same as mentioned in Table 3.1 and Table 3.2. Also the Elastic Modulus is similar as in Table 3.1 i.e. 30 GPa. The velocity of striker bar is taken as 14 m/s. the results are obtained and graphically represented here. It has been observed that the critical elements are located in the corners of the cube sample. So two opposite corner elements and one middle element are compared here.

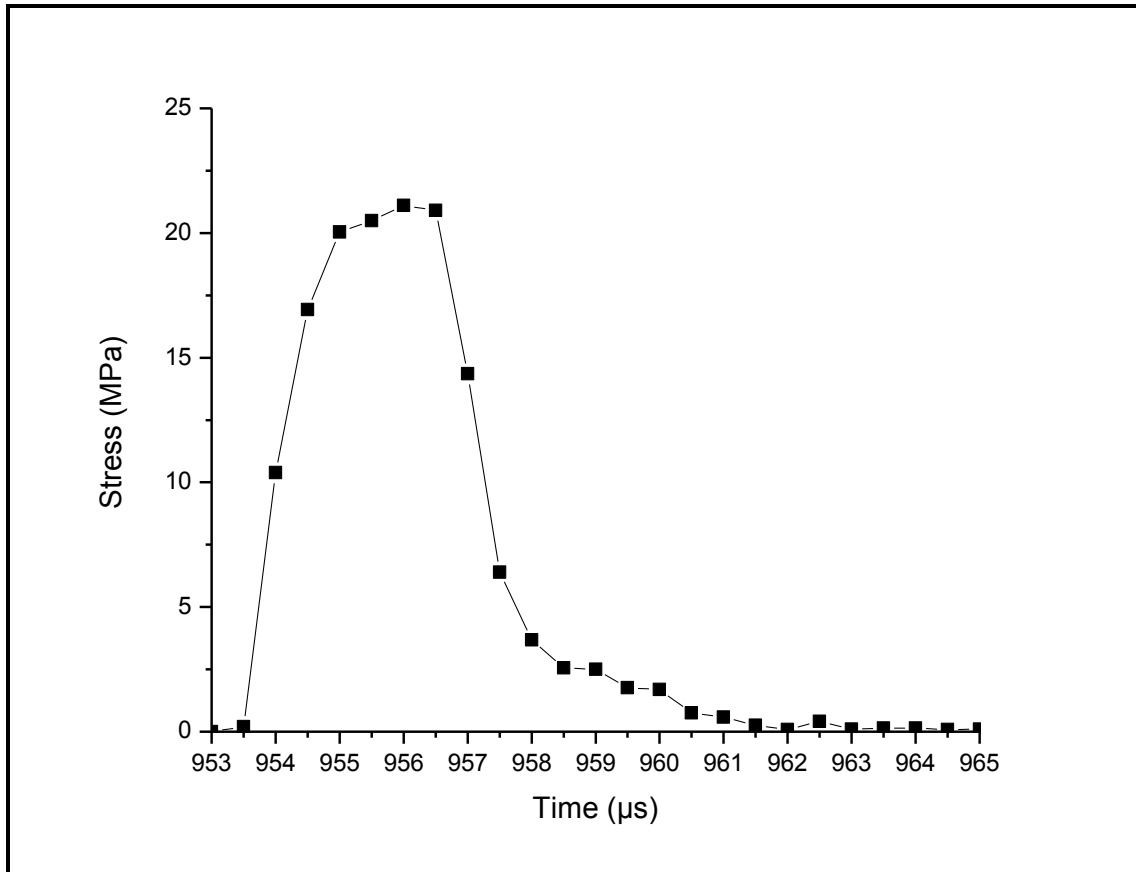


Fig 4.6: Time history curve for stress in element number 1.

The Fig 4.6 represents the time history curve for the cube sample. Element number 1 has been represented here. It is the element situated at the top edge which is adjacent to the incident bar, rather one face of which is in direct contacting surface with the incident bar. From the graph it is clear that the peak value of stress is equal to 21 MPa and at 956 μs. After reaching the peak value curve starts to fall and attains a zero value at 962 μs. Here its clear that the time span of whole process has decreased as compared to the sample with higher Elastic Modulus of 90 GPa. This shows the earlier failure of the sample as compared to the earlier sample.

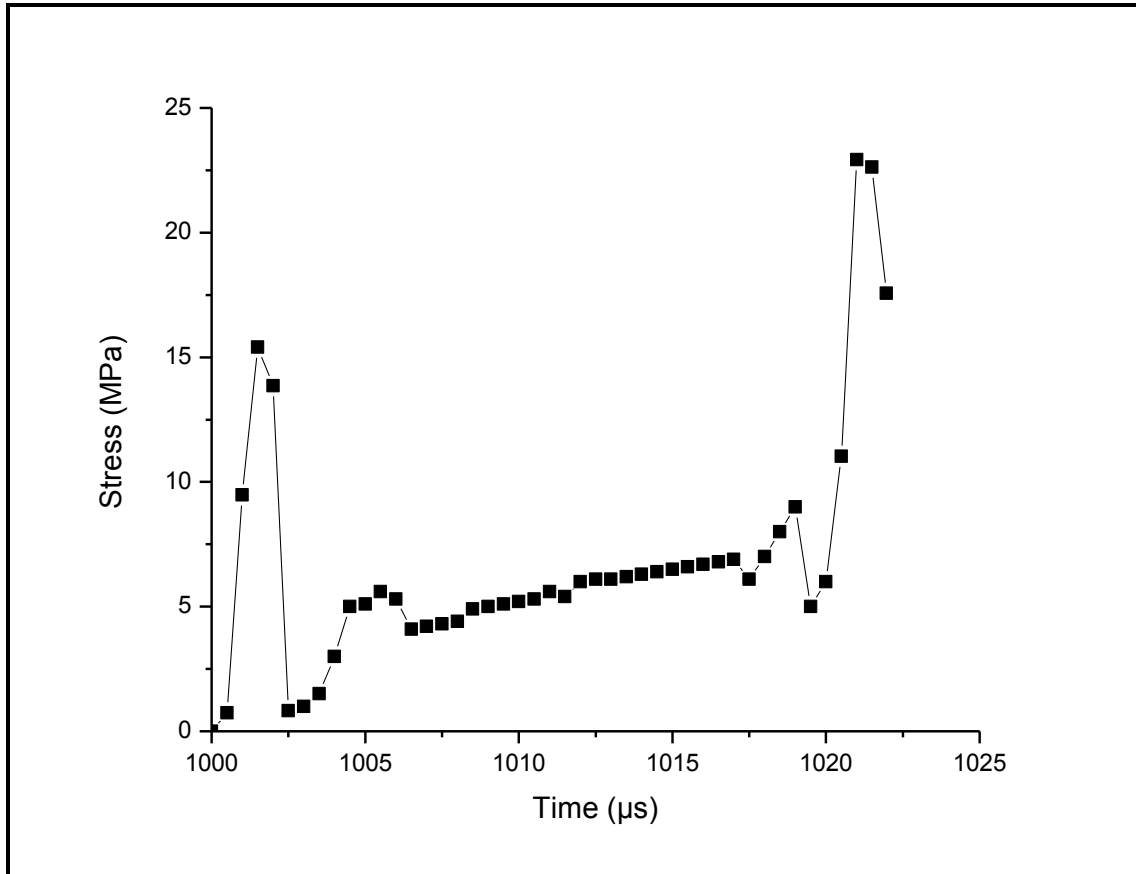


Fig 4.7: Time history curve for stress in element number 2500

Fig 4.7 shows the time history curve for stress in element number 2500. This element is the lowermost element at the bottom edge having contacting surface at right side with the incident bar. Here the graph starts to increase in value from zero to 15 MPa at 1000.20 μs than falls back upto 1MPa. Again an increase in values can be seen at about 1020 μs of time. It attains its highest peak at about 1020.10 μs. After that point it starts to decrease in value and finally it gets a failure beyond 1020 μs. The deformation exceeds the failure value so the curve gets a halt point at 1020.20 μs. It has its maximum peak stress of 23 μs. After getting the failure value for the curve the solution gets to a stop for this element representing the maximum erosion criteria has been reached for this element. Element gets deleted for this situation. This shows that the element is the most critical element and the failure firstly starts from the lower edge element which is in contact with the incident bar.

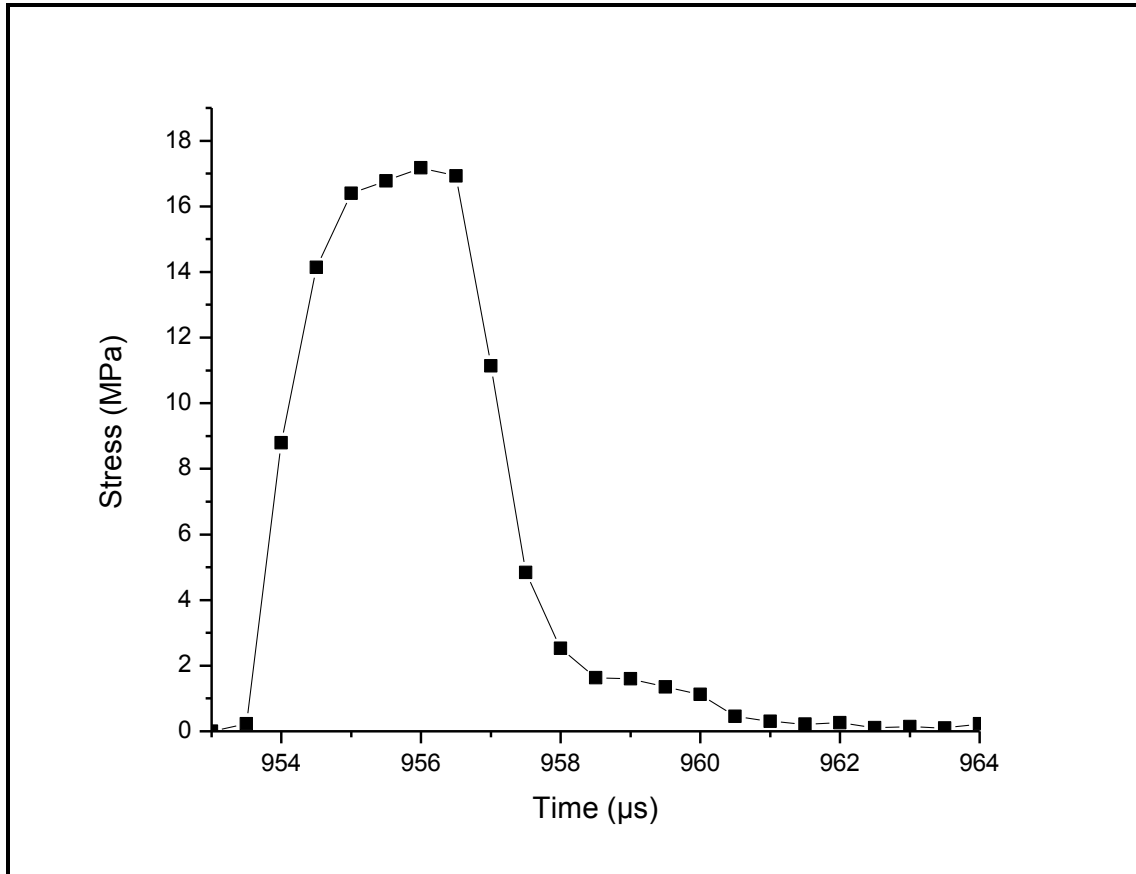


Fig 4.8: Time history curve for stress in element number 1325

Fig 4.8 represents the time history curve for element number 1325. This is the element present in the middle of the face of the cube with incident bar at right side and transition bar at left side. This element is in the middle of the face as the effect of waves is smaller in this portion of the face as compared to the corners or edges of the cube. This can also be seen from the peak stress value which is equal to 17MPa at about 956 μs. The loading and unloading is between 953 μs to 963 μs. At 953 μs the curve starts to increase in values then reaches a peak and afterwards start to decrease to reach the zero value.

(c) Time history for the strain has been found for three elements that are element number 1, 2500 and 1325, which are situated at three different locations viz. corner at top edge, corner at bottom edge and middle position of the face. The model used was same as specified in section 4.1.1 (b).

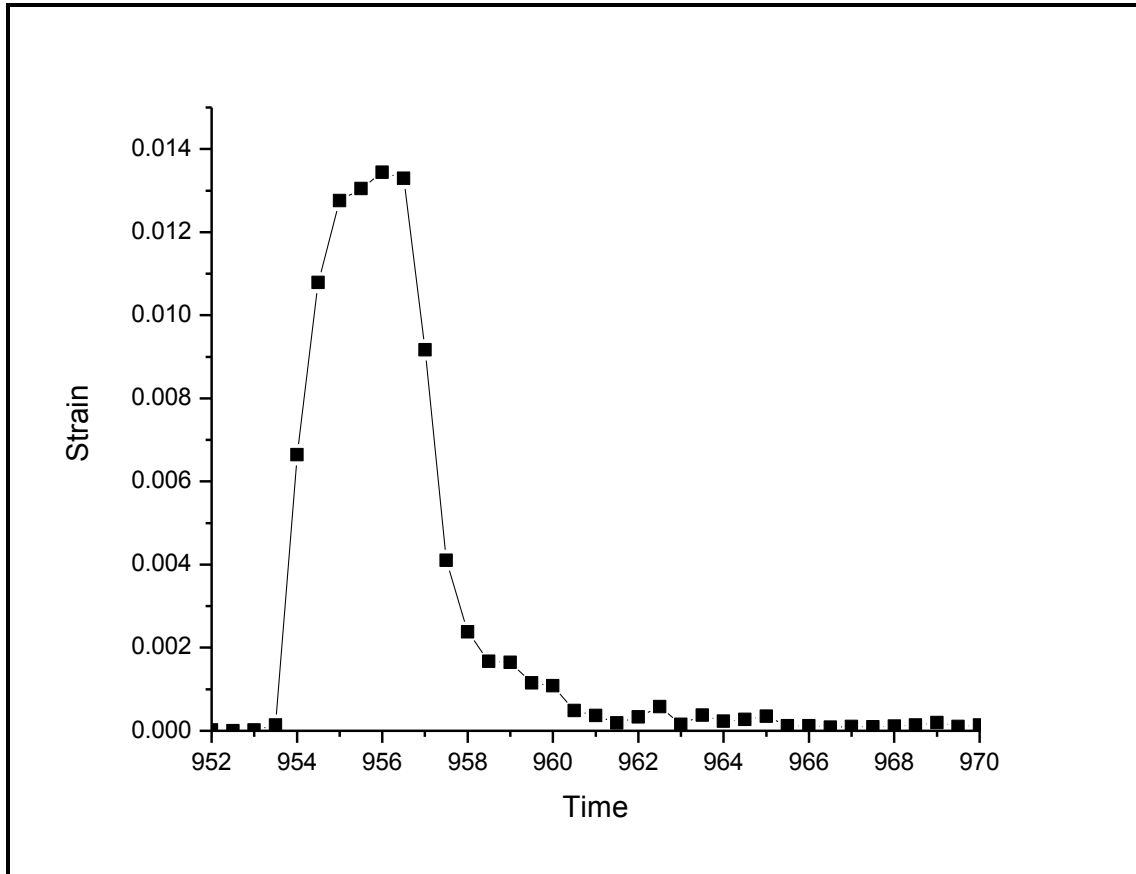


Fig 4.9: Time history curve for strain in element number1

Fig 4.9 shows the time history curve for strain of the element number 1. Here the curve can be seen with a rising limb, peak points and a falling limb. The rising and the falling limbs are due to change in strains due to loading and unloading conditions. The zero values are at 953 μ s and 967 μ s. The peak value is 0.0130 at about 955 μ s. Then another peak is obtained after 1 μ s i.e. at 956 μ s. This peak value is about 0.0135. Beyond this time after 956 μ s. After the receding curve it falls back to zero at about 967 μ s. beyond 968 μ s it has a little hump in the curve upto the next 2 micro seconds. Finally it reached the zero value.

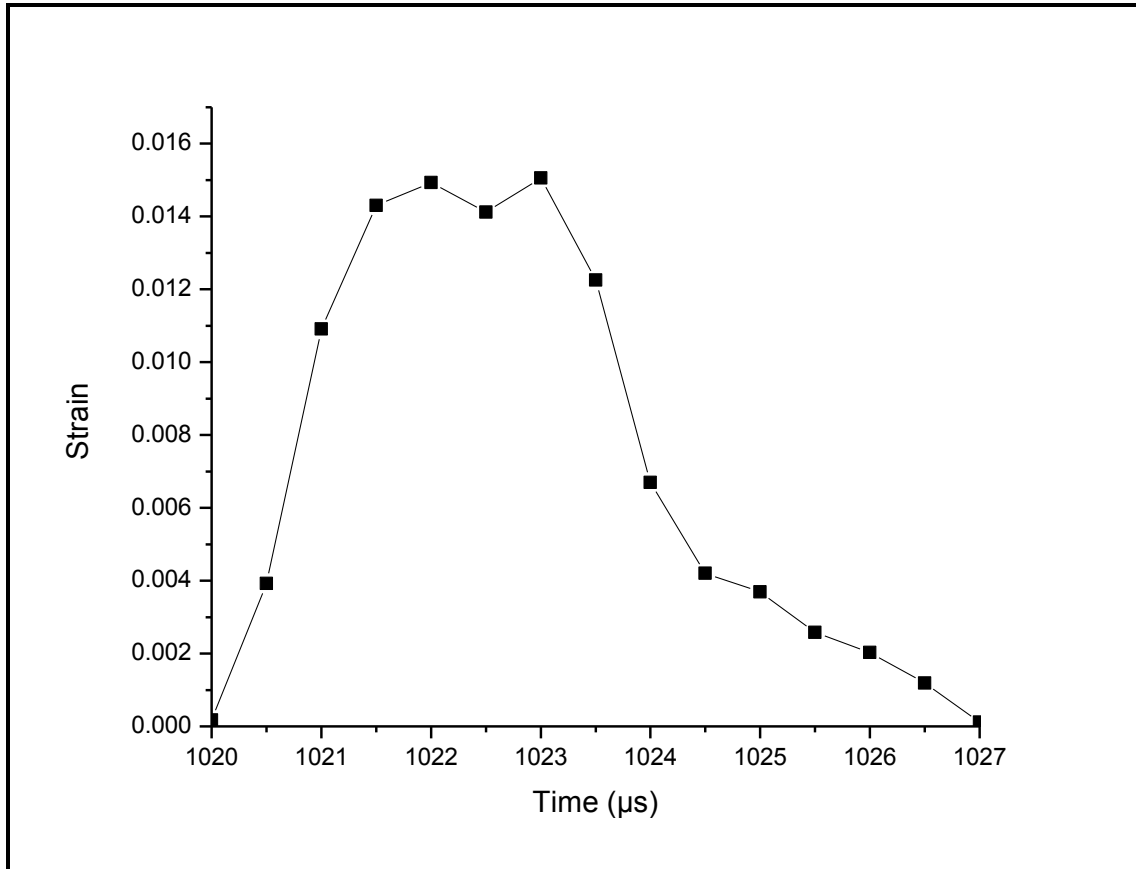


Fig 4.10: Time history curve for strain in element number 2500

This curve Fig 4.10 shows the time history for strain value of the element number 2500, which is the lowermost corner element in the sample. The curve covers a time period from 1020 μs to 1027 μs. At 1020 μs curve increases almost linearly. At 1022 μs it attains its first peak value of 0.015. Then it falls back upto a value of 0.014. Again an increase can be seen in the curve which is equal to the peak value. But now the peak point is obtained at 1023 μs. Zero value is reached at 1027 μs. From the strain values it can be easily inferred that this element reaches a critical value of strain earlier. Thus the failure can be seen in this element first rather than the other elements situated in the top edge or in the middle portion of the sample.

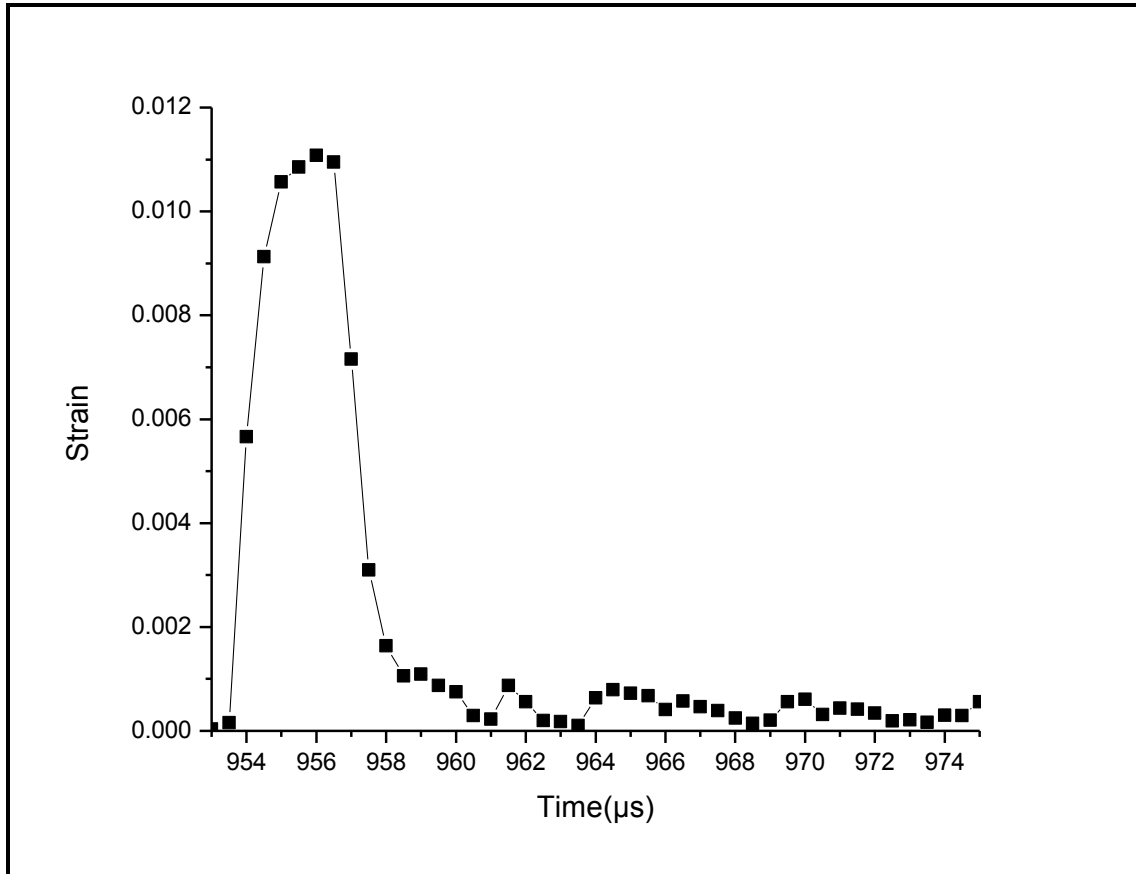


Fig 4.11: Time history curve for strain in element number 3500

The element number 3500 is located in the middle portion of the face of the cube sample. Fig 4.11 shows the variation of this element with respect to time. It can be seen from the graph that at 953 μs the waves travelling from the sample plays its part of deforming the sample. There is an abrupt increase in the curve between the time period from 953 μs to 956 μs . At 956 μs it achieves its peak strain value of 0.011. Then an abrupt decrease in the value can be seen upto 958 μs . A constant value is seen from 958 μs to 959 μs . Then again a recession comes in the graphical value. These ups and downs in the curve continues upto 976 μs . And after 974 μs the value reaches a zero value. Comparing this curve with the other elements curves for strain it can be seen that in the middle portion the value of strain i.e. the ratio of changed dimension to original dimensions is lower. This signifies that the middle portion elements are deformed much lesser than the edge elements. While the lower edge corner elements are deformed more and reaches the failure point much earlier than those in the other portions. And the deformation in the upper corner point is in between these two cases.

(d) Maximum principal stress versus time curve has been plotted for the three elements that are elements with element number as 1, 2500 and 1325. These are the elements located in different locations as already has been discusses in this section (article number 4.1.1(b)).

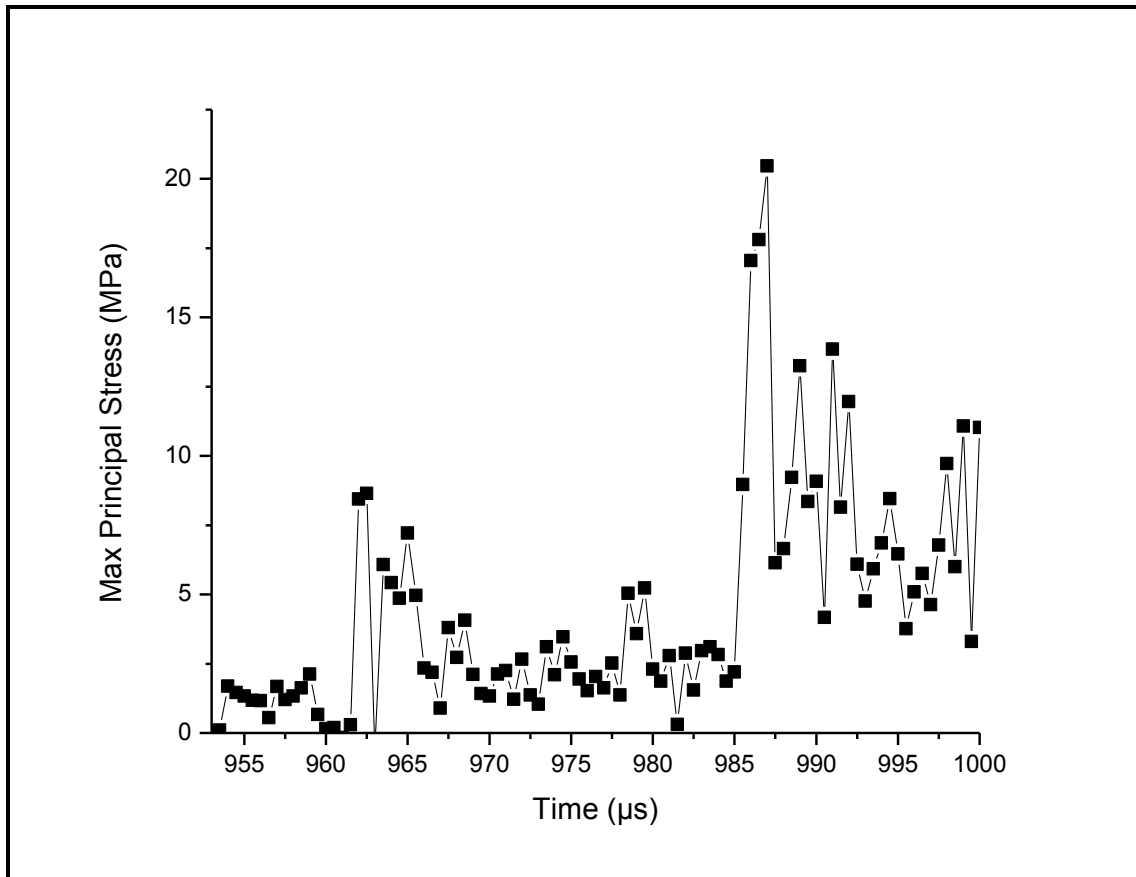


Fig 4.12: Time history curve for maximum principal stress of element number 1

Maximum principal stress versus time curve has been plotted for the element number 1 which is located at the top right corner adjacent to the incident bar. Fig 4.12 shows this variation clearly. A number of peaks are obtained for maximum principal stress of the sample. Peak point for this curve is 20 MPa. There are multiple smaller peaks after the highest point in the curve has been reached. These peaks are the result of residual stresses beyond the highest peak point. After some time these residual stresses also comes to a zero value. The zero value is obtained beyond 1000 μ s of time.

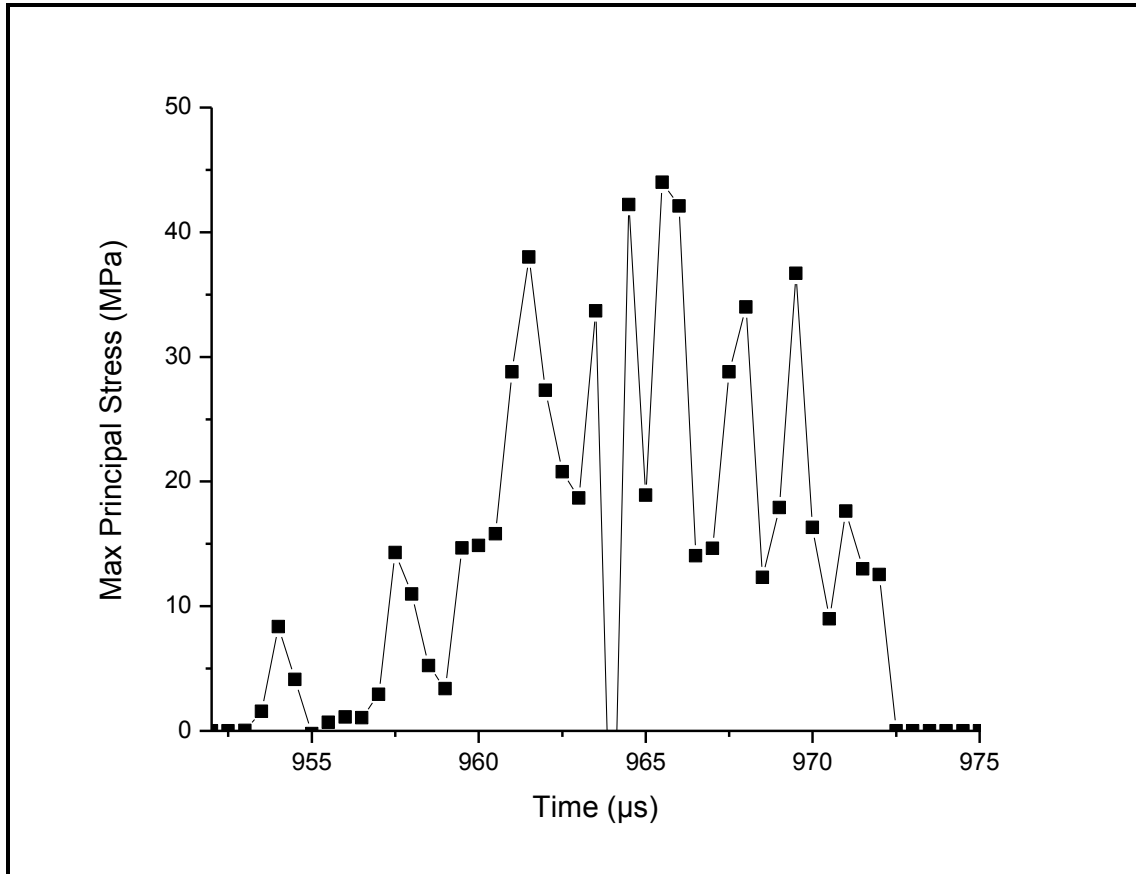


Fig 4.13: Time history curve for maximum principal stress of element number 2500

Time history curve for maximum principal stress of element number 2500 has been shown in the Fig 4.13. Element number 2500 is the element at bottom corner position adjacent to the incident bar. It has been easily inferred from this figure that it is the most critical element as the peak value of maximum principal stress is about 45 MPa, which is much higher than the elements at top edge or at middle portion of sample. This peak is at 965.20 μs of time. After this peak point several other peaks arise but with lower magnitude, and finally these come to an halt at about 973 μs of time. These peak points are the result of residual stresses. These residual stresses occur for an extremely short period of time. Here these residual stress comes at about 967 μs to 973 μs of time. Residual stresses diminishes after this time and becomes zero. And several zero magnitude points can be seen after 973 μs of time showing the removal of all the loads and stresses.

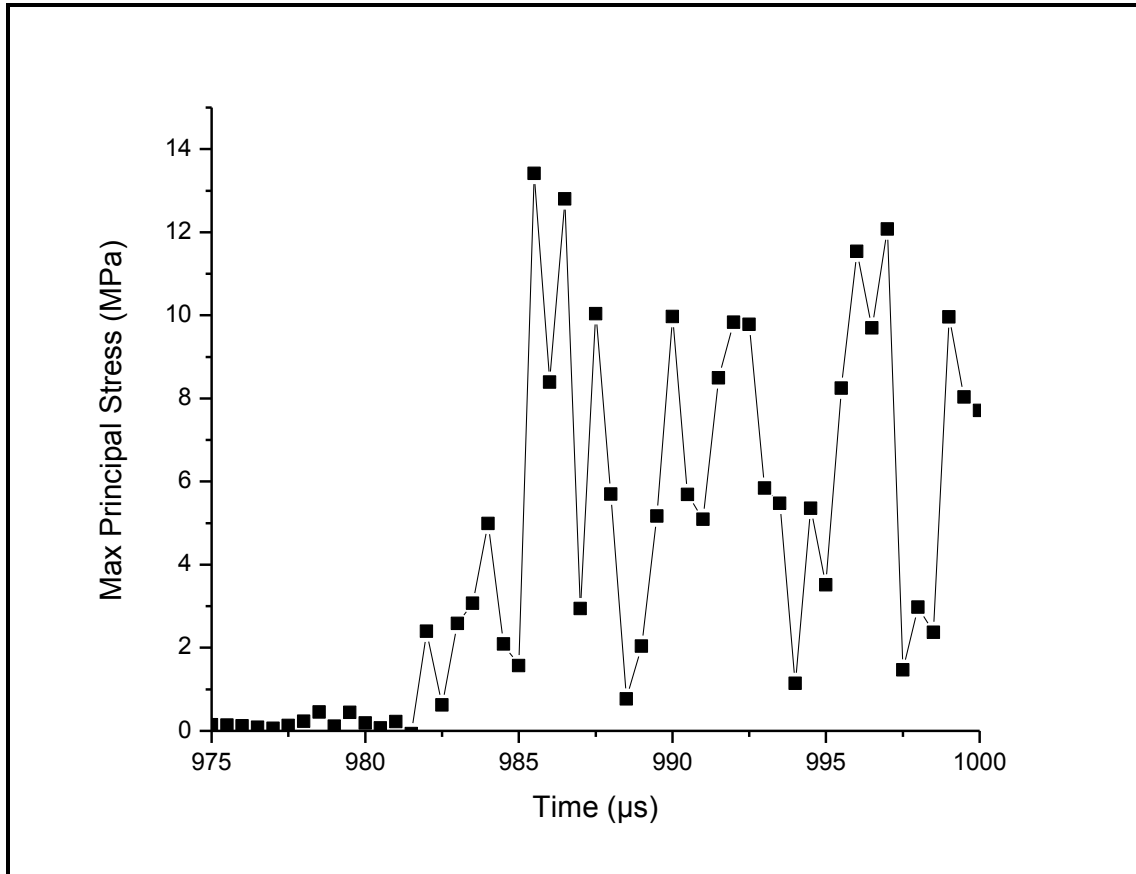


Fig 4.14: Time history curve for maximum principal stress of element number 1325

In the Fig 4.14 time history curve for maximum principal stress has been shown. At about 986 μs the maximum value of the maximum principal stress arises, this value is equal to 13 MPa. This shows that this portion of the sample has developed the stresses at somewhat later moment of time than the other portions. As this element is situated at the middle portion of the sample this behaviour is absolutely accurate. After 986 μs of time there is a sudden decrease in the value for maximum principal stress. Multiple peak behaviour of the curve can be seen in a short span of time. These multiple peaks are the result of residual stresses in the sample. However the maximum principal stress value becomes zero beyond 1000 μs showing the removal of these residual stresses.

4.2 RESULTS FOR THE SFRC BRAZILIAN DISC SAMPLE

1. Displacement

- (a) The deformation in the disc starts along the diameter of the disc.
- (b) Firstly the elements from the edges starts to deform then proceeds to the middle portion along the diameter in which the waves propagate.
- (c) The deformation ranges from the 100 mm to 220.50 mm.
- (d) As the waves propagate further the failure starts to propagate along the diameter first then to other portions of the disc.

2. Stress

- (a) The stresses in the disc initiates from the edges portion which are touching the incident and the output bars.
- (b) Afterwards it moves to the inner middle portions.
- (c) These are generated along the diameter.
- (d) When the stresses are increased the lower elements starts to erode first then the upper elements.
- (e) Fig 4.15 shows the stress generation along the diameter of disc sample at different points of time.
- (f) Here in this figure the stress originates from the corners along the loading diameter. Then these stresses starts to propagate along the loading diameter as shown in the second part of Fig 4.15.

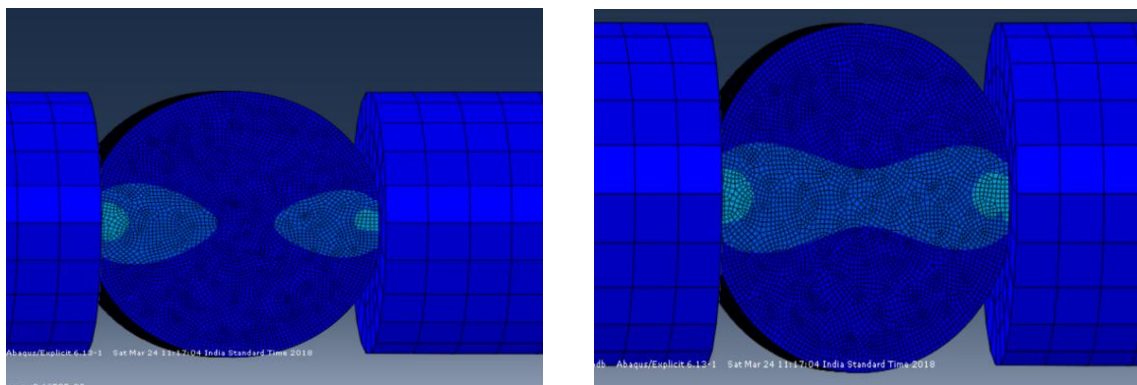


Fig 4.15: Stress generation along diameter

Note: Related Figures are provided in Appendix B.

4.2.1 Graphical representation of results for disc sample

- (a) For the first case all the properties geometrical as well as material properties are taken similar to Table 3.1 and Table 3.2, except the Elastic Modulus of the sample has been taken as 90 GPa instead of 30 GPa.

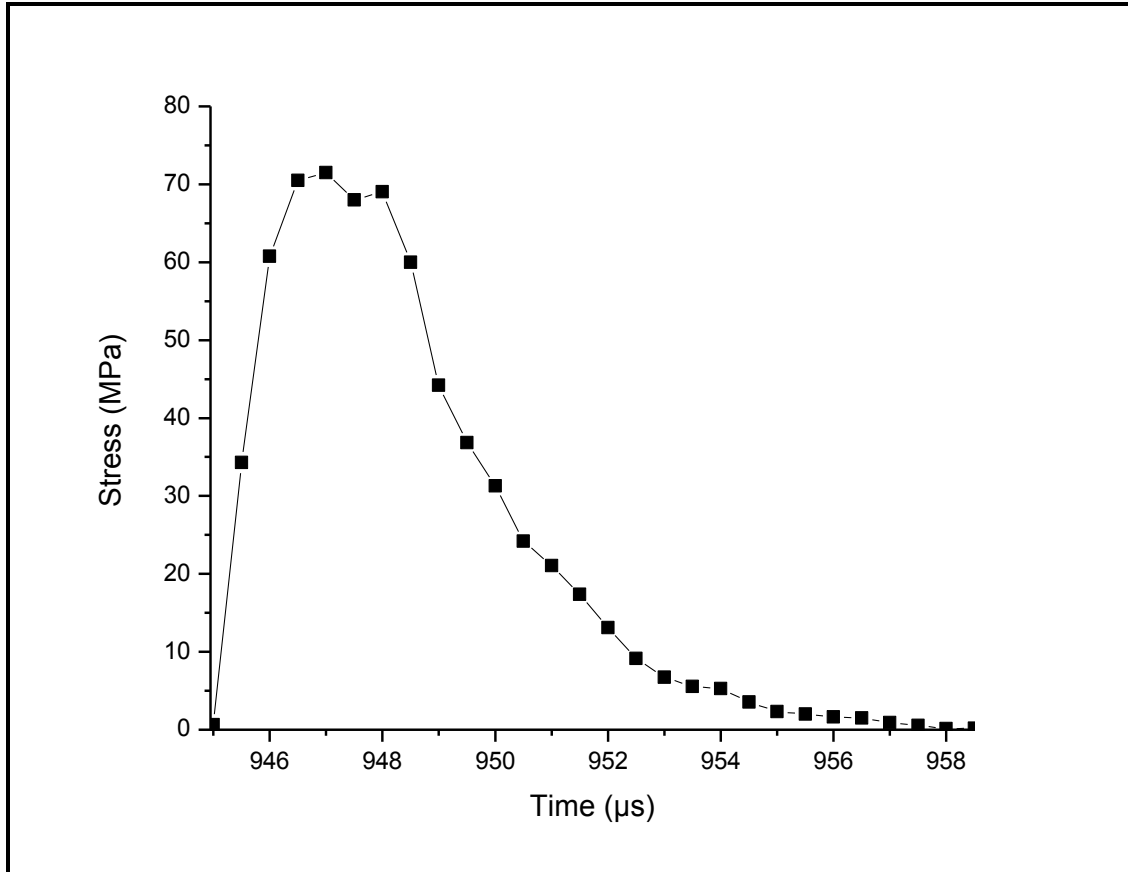


Fig 4.16: Time history curve for Stress of disc sample.

Fig 4.16 represents the time history for stress of disc sample. It can be easily known from the graph that the stress rises from zero value at 945.00 μs. It rises to have the first highest peak at 947.00 μs. The peak value is equal to 71.00 MPa. A small decrease in stress can be seen in the graph from 947.00 μs to 947.50 μs. At 948.00 μs it has its next peak equal to 70 MPa. Then curve decreases to zero at point 958 μs. This whole process has taken just 13 micro seconds.

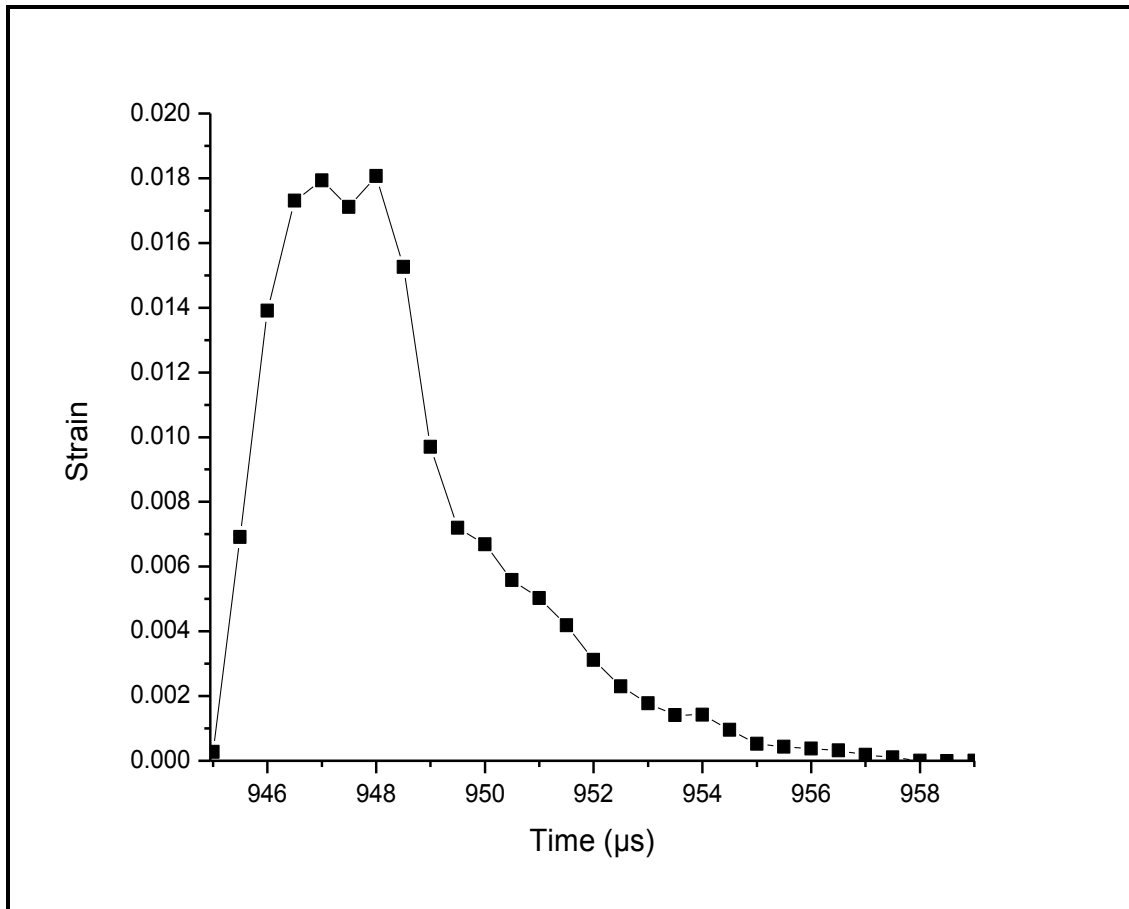


Fig 4.17: Strain versus time curve for disc sample

Time history curve for strain has also been plotted for the same sample. This has been shown in Fig 4.17. Here the graph is plotted for a time interval from 945 μ s to 958 μ s. The strain reaches its peak value at about 947 μ s and attains a peak strain value of 0.018. As the stress value has also been decreased from 947 μ s to the next 0.05 μ s the strain value has also been decreased. However beyond that point it starts to increase to have another peak point of 0.018 value at about 948 μ s. Afterwards the curve decreases and attains a zero value at about 958 μ s. These peaks are the result of plastic strain hardening of the sample.

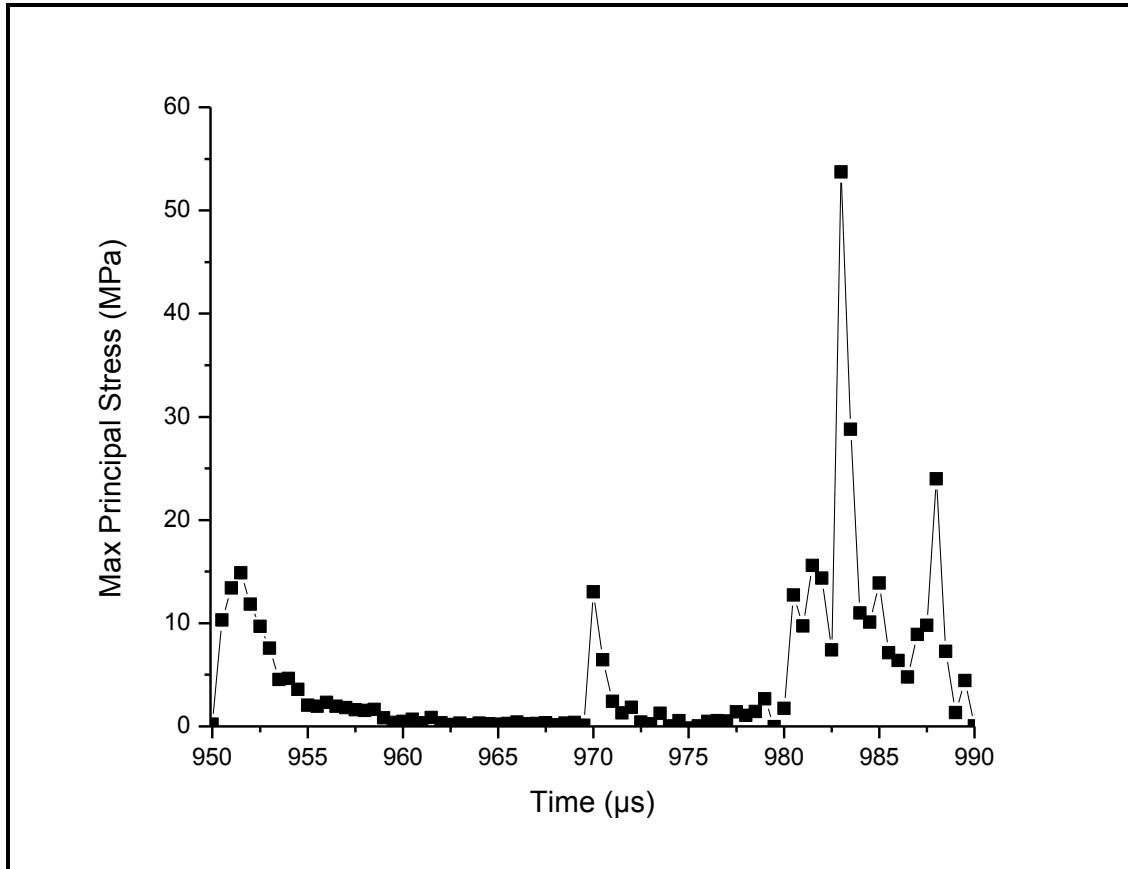


Fig 4.18: Maximum Principal Stress v/s Time for disc sample

Maximum principal stress has been plotted against the time for the disc sample model. The Fig 4.18 clearly shows this plot. The information depicted here is from 950 μs to 990 μs of time. Multiple peak behaviour can be seen for this curve. As the elastic modulus for this sample is very high equal to 90 GPa so the results of maximum principal stress is also high as compared to the another model which will be discussed in this section at latter stages. Here in this Figure the maximum peak arises in the time span of 10 μs , i.e from 980 μs to 990 μs . The maximum principal stress value is about 55 MPa at 985 μs . This value is very high as compared to other results. Beyond the peak point of this curve the curve starts to recede and then several multiple peaks of smaller magnitude arises. These smaller peaks are the result of residual stresses which remain after the peak magnitude has been achieved. Here from this figure it is clear that after small period of time these residual stress peaks has also diminished to become zero.

(b) The next model consists of the properties exactly as mentioned in Table 3.1 and Table 3.2. The velocity has been taken equal to 14 m/s. Various graphs has been plotted for this model and are shown in this section.

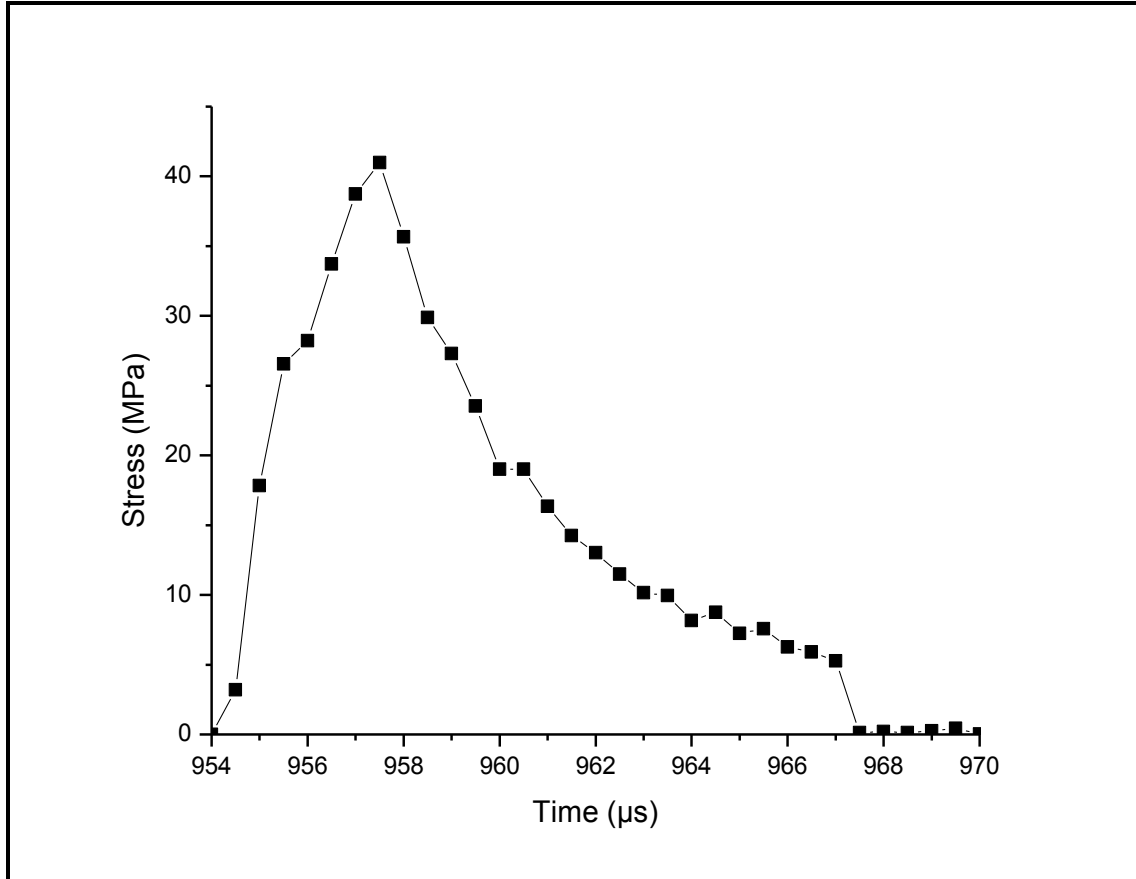


Fig 4.19: Time history curve for stress in element number 1845

Element number 1845 is the element situated at the diameter along the loading direction. Fig 4.19 shows the time history curve for stress in element number 1845. It is situated at the extreme corner position, one face of which is in contact with the incident bar. As the element is in the loading direction this element is the most critical element giving the maximum values for stresses and strains. The curve achieves a rise at 954 μs and reaches a peak point at 41 MPa for stress. Then the curve suddenly falls down to have a zero value at about 968 μs .

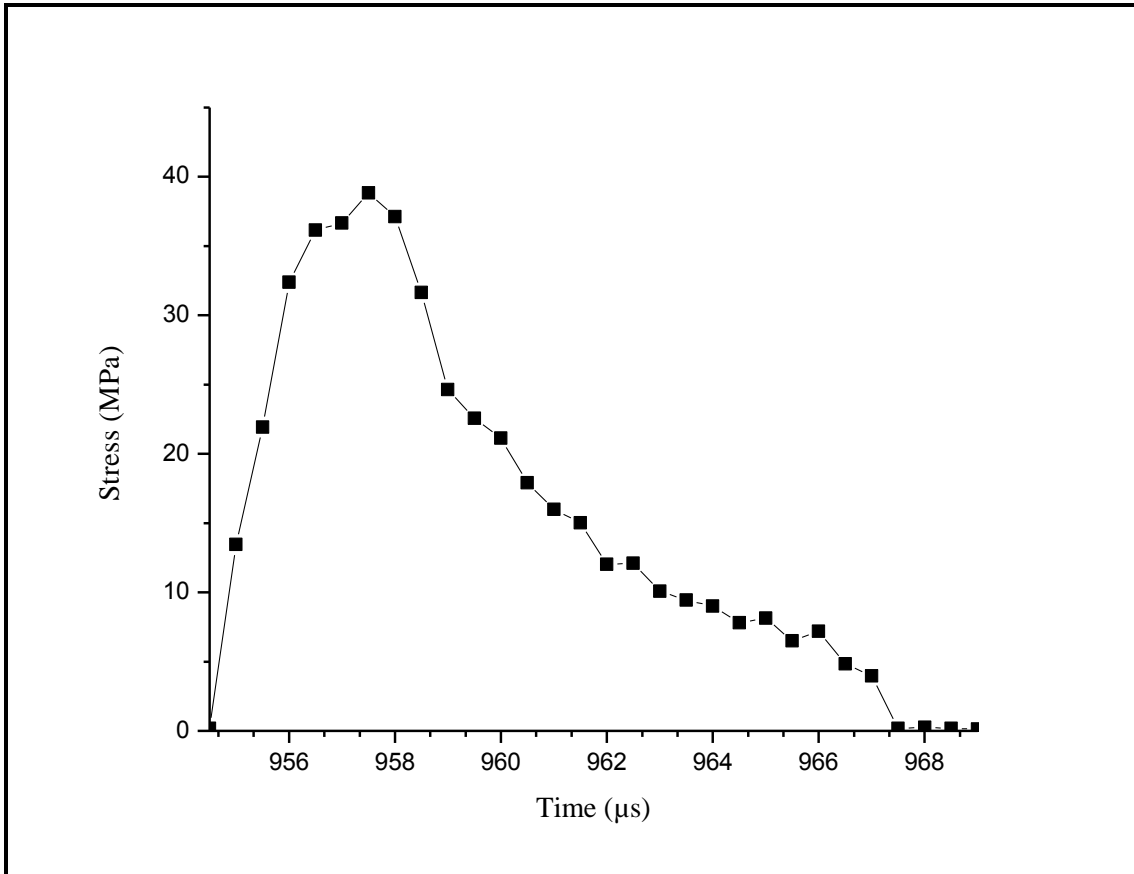


Fig 4.20: Time history curve for stress in element number 1771

The element number 1771 is the element situated at the extreme position along the loading diameter adjacent to the transition bar, one face of which is in contact with the transition bar. At 955 μs of time the curve starts to rise and reaches a peak value at the 38 MPa. Then it falls back to zero at 968 μs of time. The maximum value of stress for this element is lower than that of the opposite portion element which is element number 1845. Thus here the effect of waves is smaller than that of the former element as is shown by Fig 4.19 and Fig 4.20.

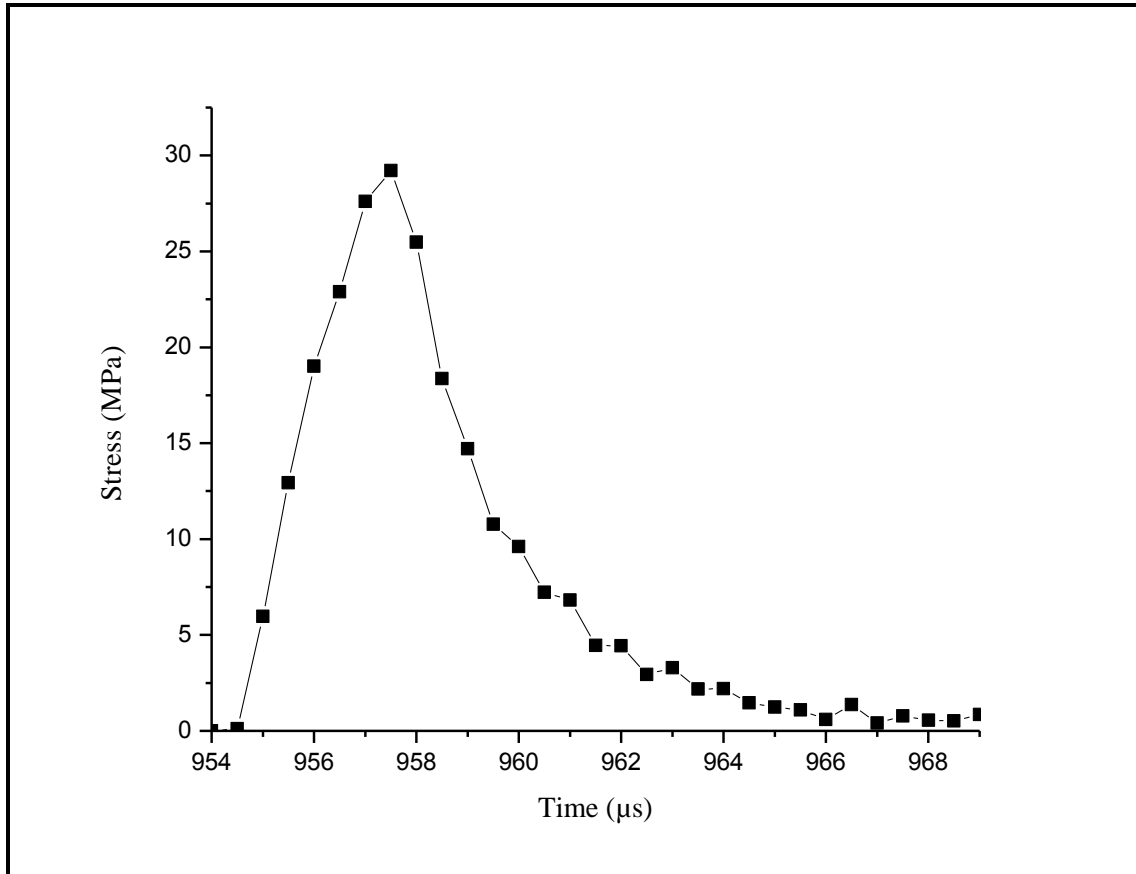


Fig 4.21: Time history curve for stress in element number 562

Element number 562 is the element present at almost the middlemost position in the meshed sample. This element is also present along the loading diameter. 14m/s velocity has been given to the striker bar and the effects for stress has been noted here. The graphical representation for time history of stress has done and represented in Fig 4.21. It is clear from this curve that the stress value rises in this element and attains a peak of 27 MPa at 957 μs. afterwards the curve recedes in value and reaches a zero point at about 990 μs. This shows that the value of the stress for middle portion is mmuch lower than the values at some other portion.

- (c) The velocity of the striker bar has been changed for this modeling and taken equal 10 m/s. All other necessary properties are adopted as specified earlier in Table 3.1 and Table 3.2.

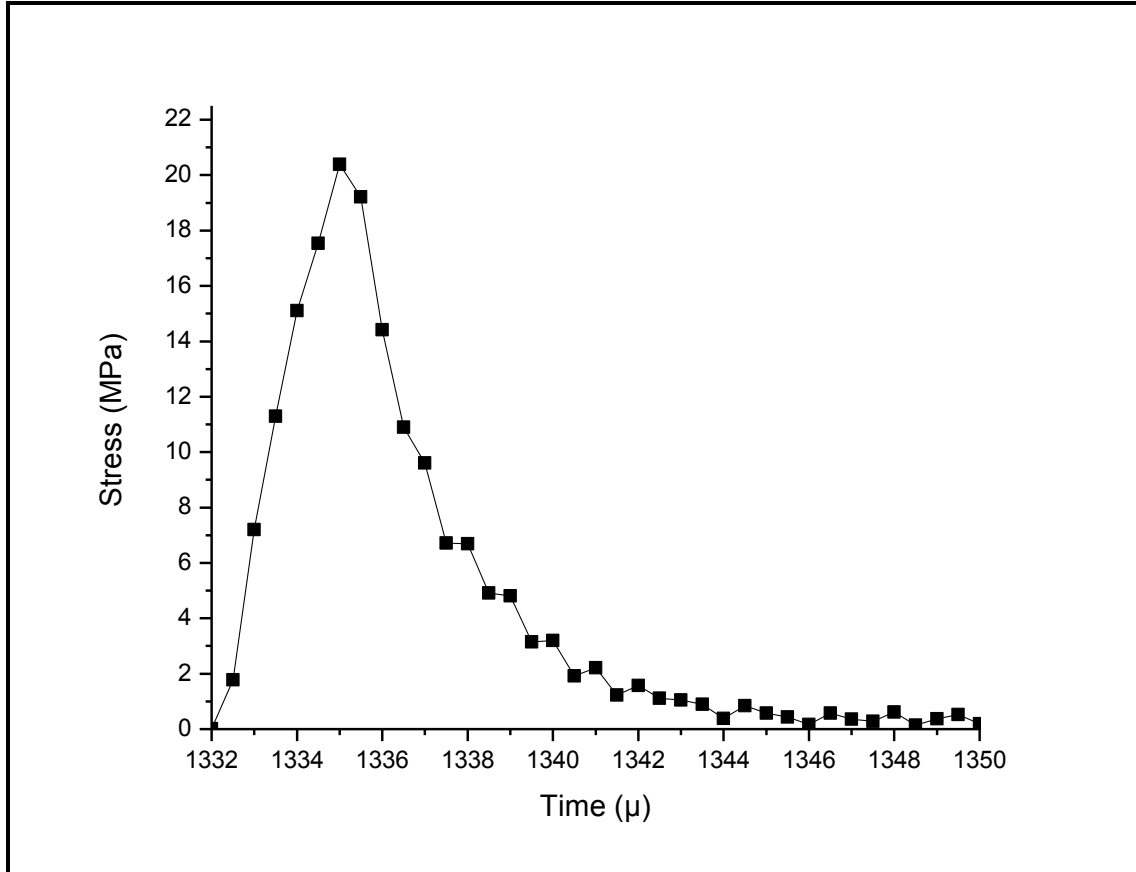


Fig 4.22: Time history curve for stress in element number 1845

Time history curve for stress in the element number 1845 has been plotted for this simulation model and represented here in this section in Fig 4.22. It can be seen in this Figure that the peak value is 20MPa for stress. Peak arises at 1335 μ s of time. As compared to the results obtained for the striker bar velocity of 14 m/s, these results are delayed and are much lesser in magnitude. This shows that the stresses and ultimately the failure in the elements for this model at much lower values in terms of magnitude and time values. This curve ultimately gets unloaded at about 1360 μ s.

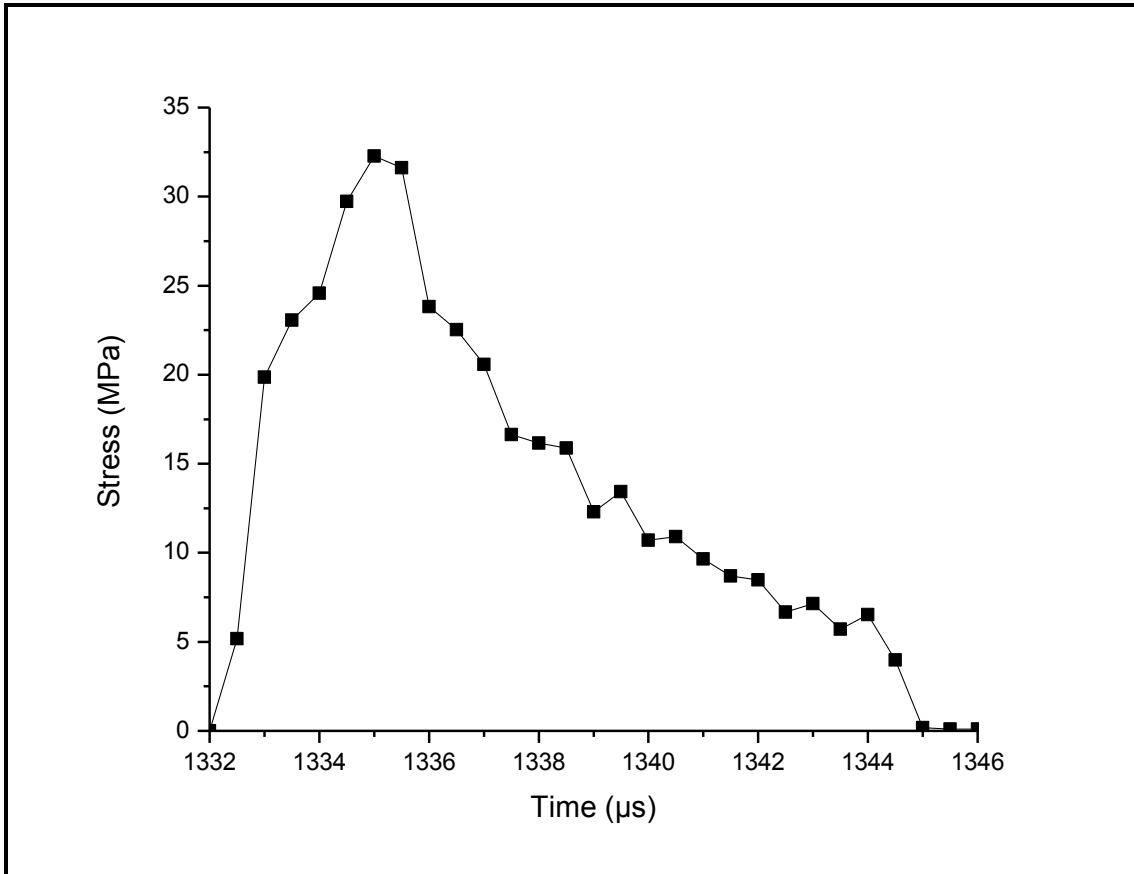


Fig 4.23: Time history curve for stress in element number 1771

Fig 4.23 shows the time history curve for stress in element number 1771. This element is adjacent to transition bar and along the loading diameter of the sample. It attains a maximum value of 32 MPa at about 1335 μ s. Ultimately the curve reaches the zero value at 1345 μ s. As compared to model given in 4.2.1 (b), here the stress value is of lower magnitude and at a delayed time period. The magnitude of stress in the former case was 38 MPa at 955 μ s, while in the latter case this value is 32 MPa at 1335 μ s. So its clear from this comparison that the velocity of the striker bar has significant impact on the results. And when compared to the model given in section 4.2.1 (a), its clear that the magnitude of stress has decreased to a much lower value in this case.

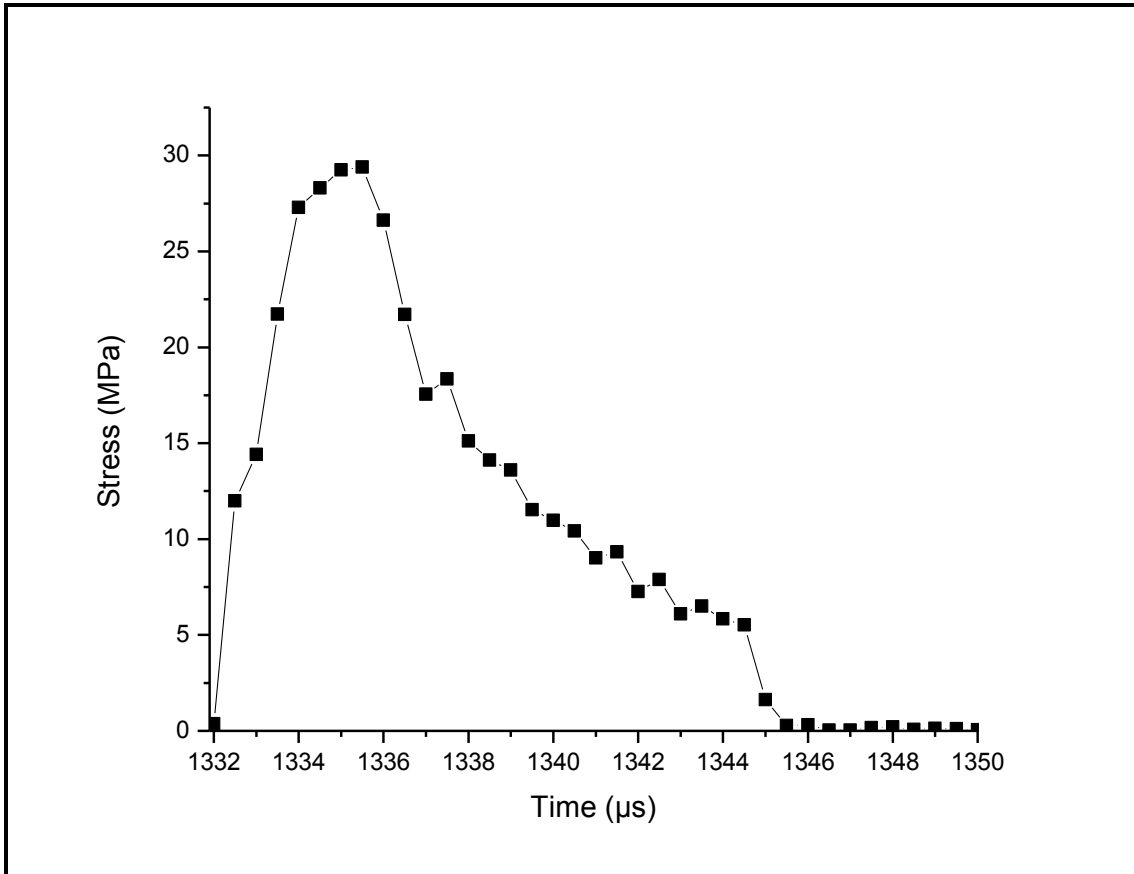


Fig 4.24: Time history curve for stress in element number 719

Here in Fig 4.24 time history curve for stress in element number 719 has been plotted. Element number 719 is the element present in the middle portion of the disc sample. Here the curve rises from 1332 μs and falls back to zero at 1347 μs. The peak value is attained at 1335 μs. This peak value has a magnitude of 28 MPa. Again a lower peak is obtained for extremely short duration. After that it comes to zero value at about 1347μs.

- (d) The velocity of the striker bar has been changed for this case and taken equal to 7m/s. While all other geometrical as well as material properties has been taken from Table 3.1 and Table 3.2.

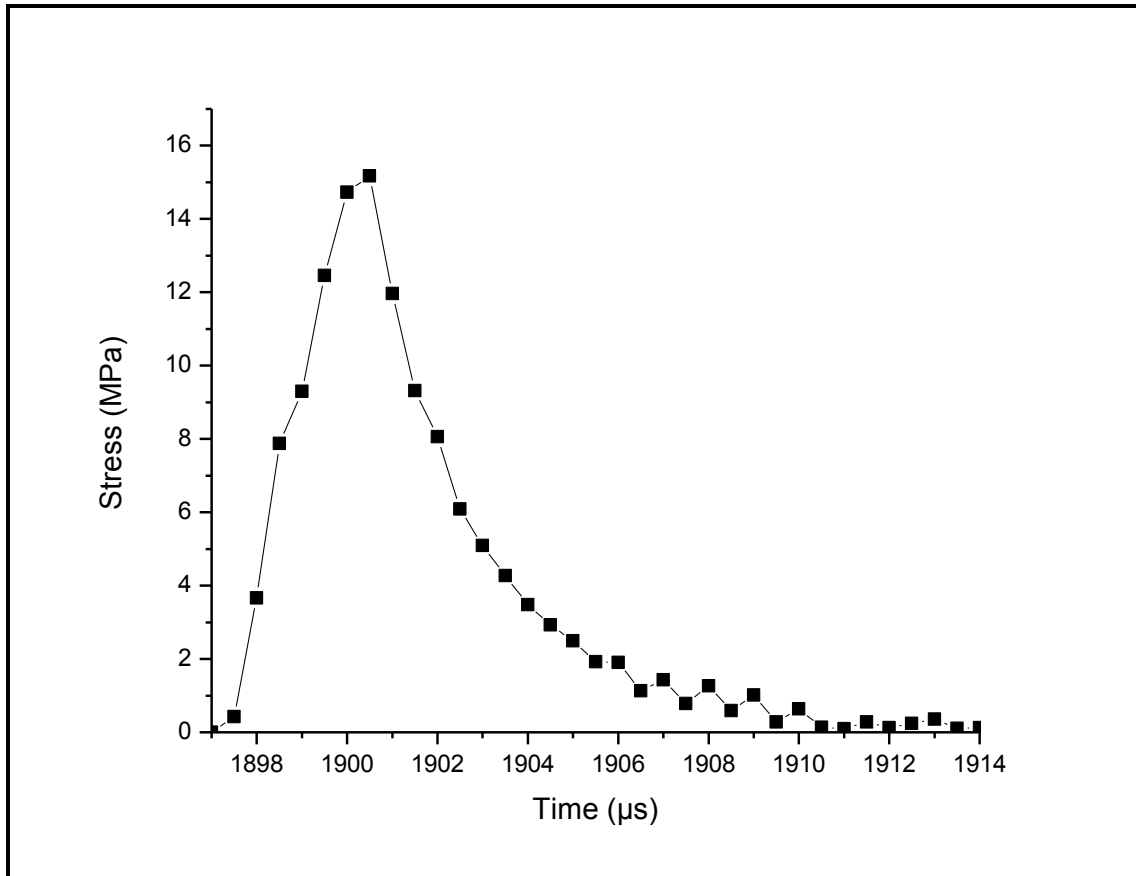


Fig 4.25: Time history curve for stress in element number 4236

Element number 4236 is the element present along the loading diameter. Time history curve for stress has been given in Fig 4.25 for this element number 4236. Here 1897 μ s is the time from where the rising limb of graph appears. This curve then rises upto 15 MPa value. After that point it starts to fall back to zero value. As compared to the earlier models given in 4.2.1 section, values obtained for this model are much lower and at much delayed time period. For this particular case the peak value is obtained at 1901 μ s. This time is a delayed time period as compared to other simulation models.

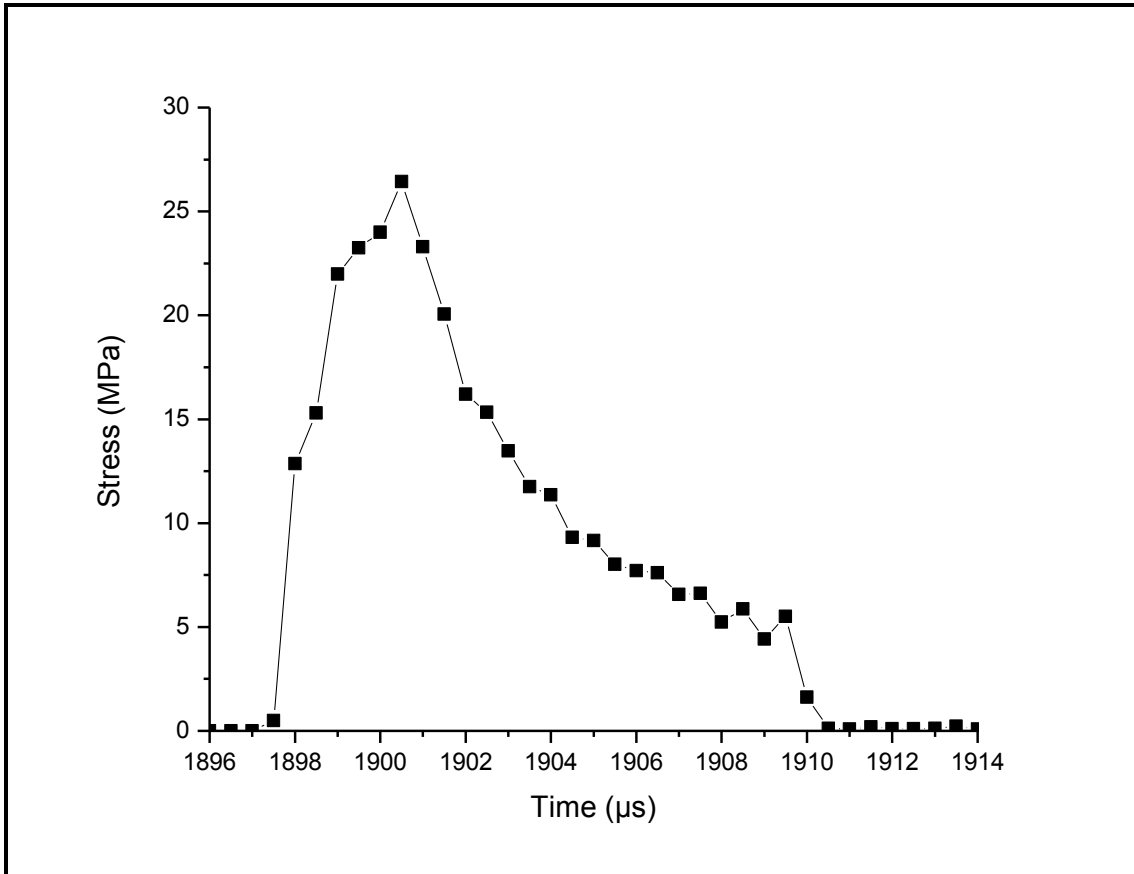


Fig 4.26: Time history curve for stress in element number 1667

Time history curve for stress has been plotted here in Fig 4.26 for element number 1667. This element is along the diameter of the disc sample and at the extreme right corner along the loading diameter, adjacent to incident bar. Peak value of stress is equal to 26 MPa and is obtained at 1900 μs. This magnitude is higher as compared to the middle portion elements while it is lower as compared to higher velocity cases. This curve abruptly rise from zero to maximum value and then falls back to zero value comprising of extremely short duration lower valued peaks.

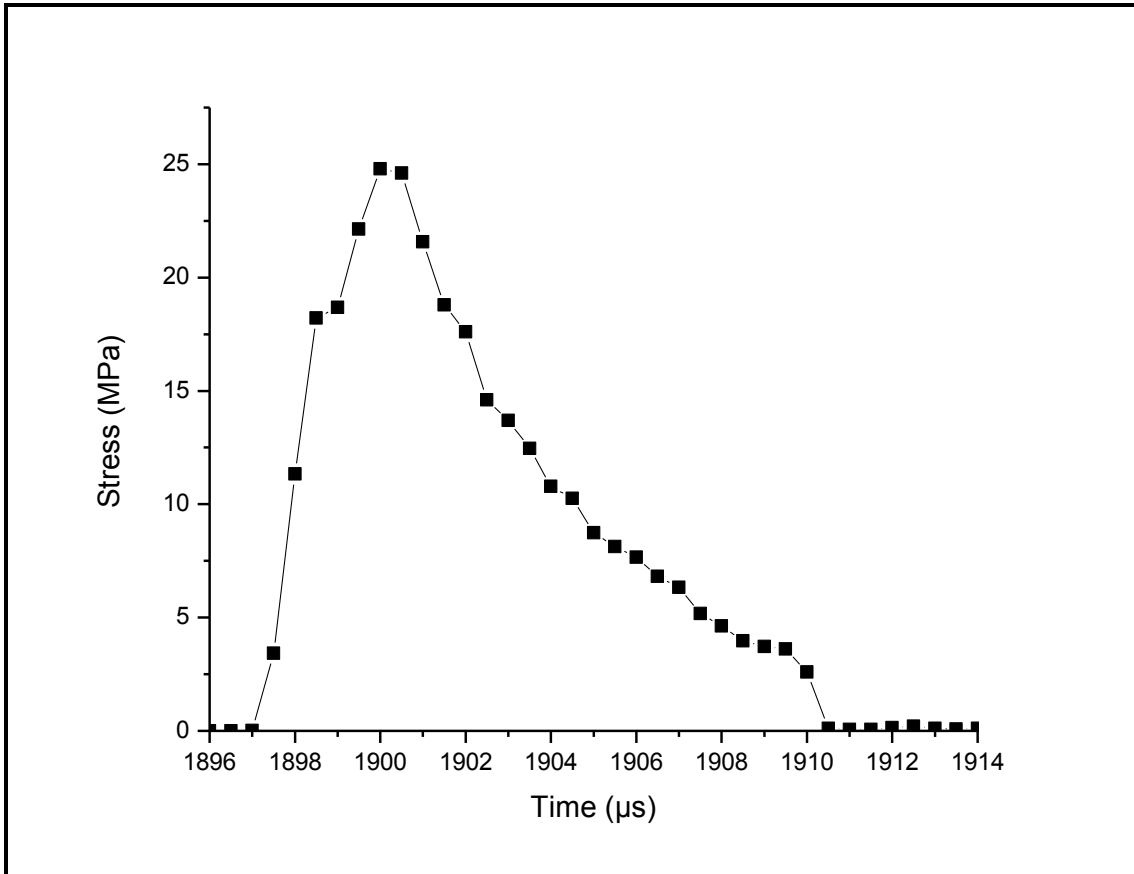


Fig 4.27: Time history curve for stress in element number 482

Stress is plotted against time axis for element number 482 and is shown in Fig 4.27. Element number 482 is the element adjacent to the transition bar and along the loading diameter. Peak value of stress is obtained at 1900 μs with a magnitude of 25 MPa. This shows that as velocity decreases the stress value also decreased in magnitude, while the time is a delayed value.

(e) Time history for strain in different elements have been plotted here in this section for disc sample. Elements have been selected from different portions of the disc sample. The velocity for this case has been taken as 14 m/s, while all other necessary properties to be included have been provided in the tables given in chapter4, i.e. Table 3.1 and Table 3.2.

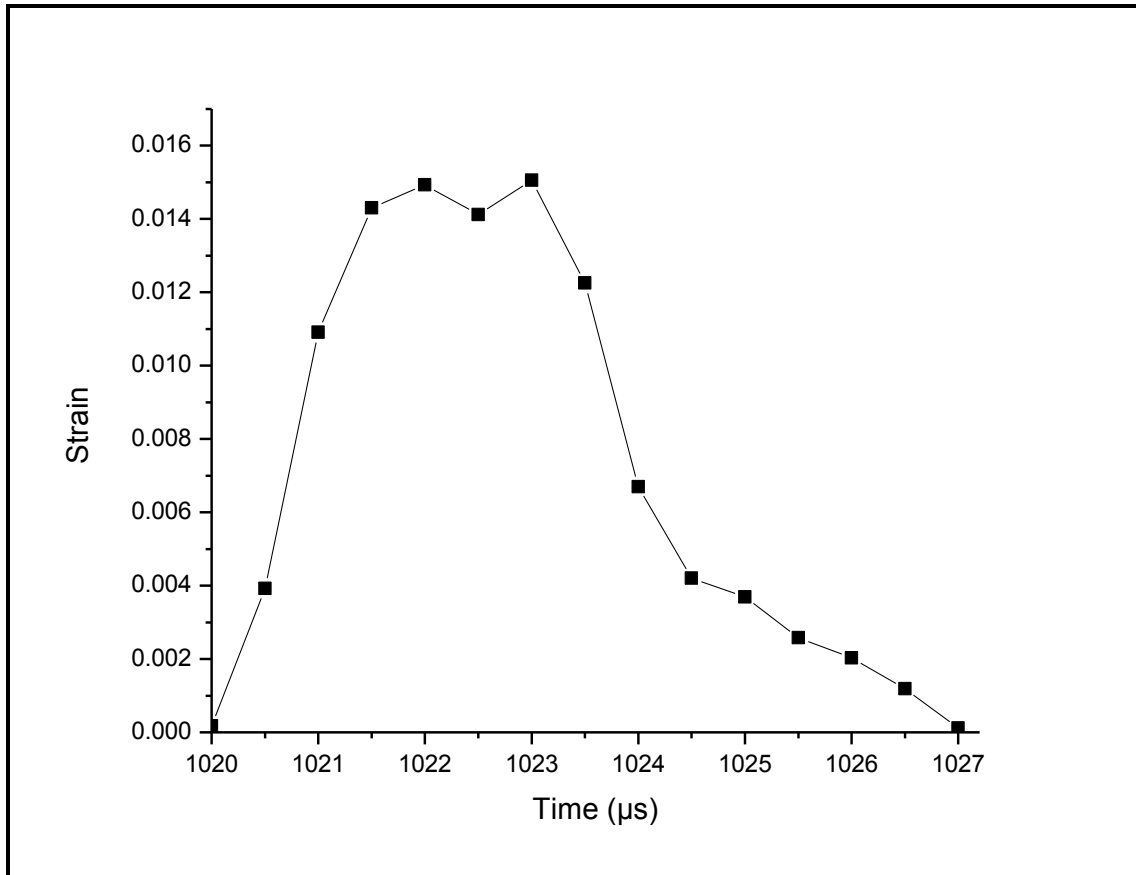


Fig 4.28: Time history curve for strain in element number 2500

Fig 4.28 shows the stress versus time curve for element number 2500 of the disc sample. This element is located along the loading diameter. This curve shows the two peak curve. At 1020 μs the curve starts to rise and attains a maximum strain value of 0.015 at 1022 μs. Again it starts to fall for extremely short duration of time then another peak is obtained at 1023 μs. As compared to the results of the model with 90 GPa elastic modulus the strains obtained are of much lower magnitude.

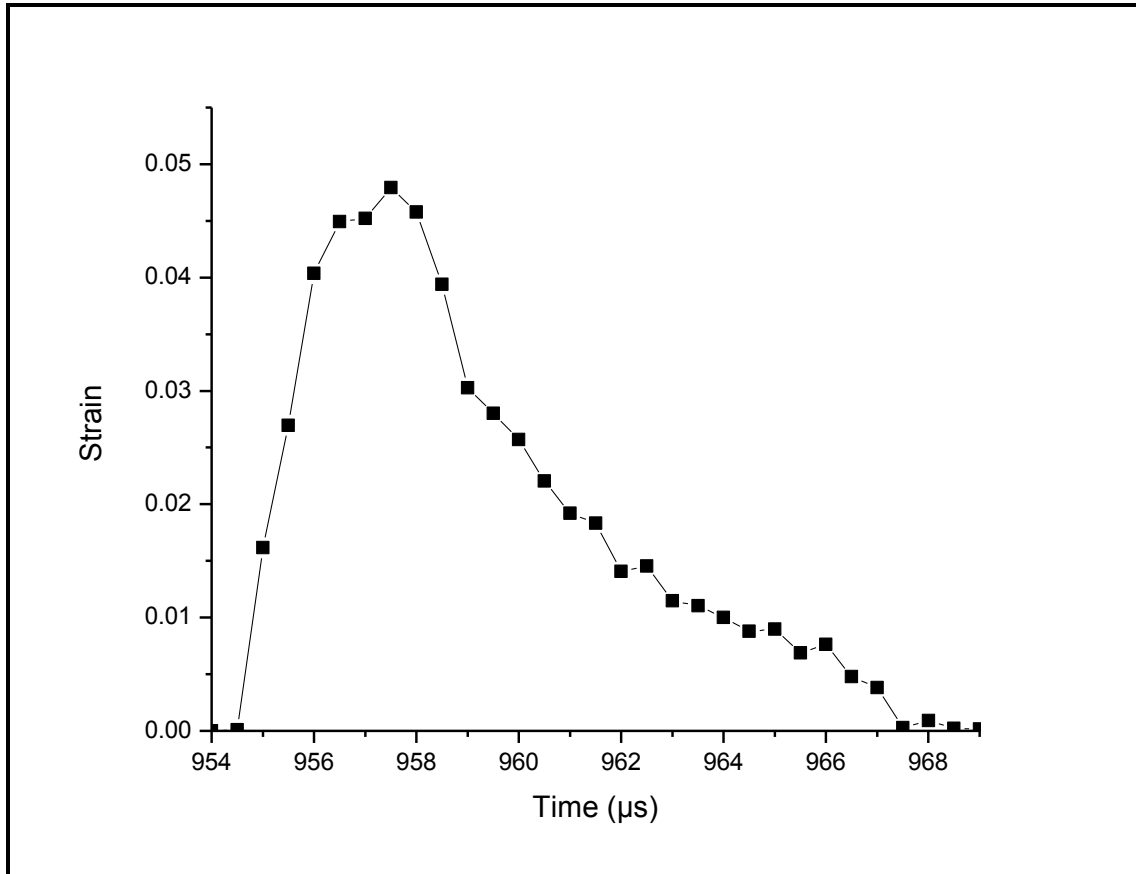


Fig 4.29: Time history curve for strain in element number 1771

Here in the above figure Fig 4.29, time history curve for strain in one of the elements of the sample has been shown. This element is the same as discussed earlier in this article. From the curve it is clear that the peak value of strain for this element is 0.045. This peak arises at 957 μs of time. It also has small peaks at some later times. But ultimately curve reaches a zero point at about 1000 μs of time. The strains developed here are of greater magnitude for the disc sample of steel fibre reinforced concrete.

- (f) Velocity for this model has been taken 10m/s. All other properties are taken from the samples given in tables in chapter 3. Results for different elements are represented graphically here in this part.

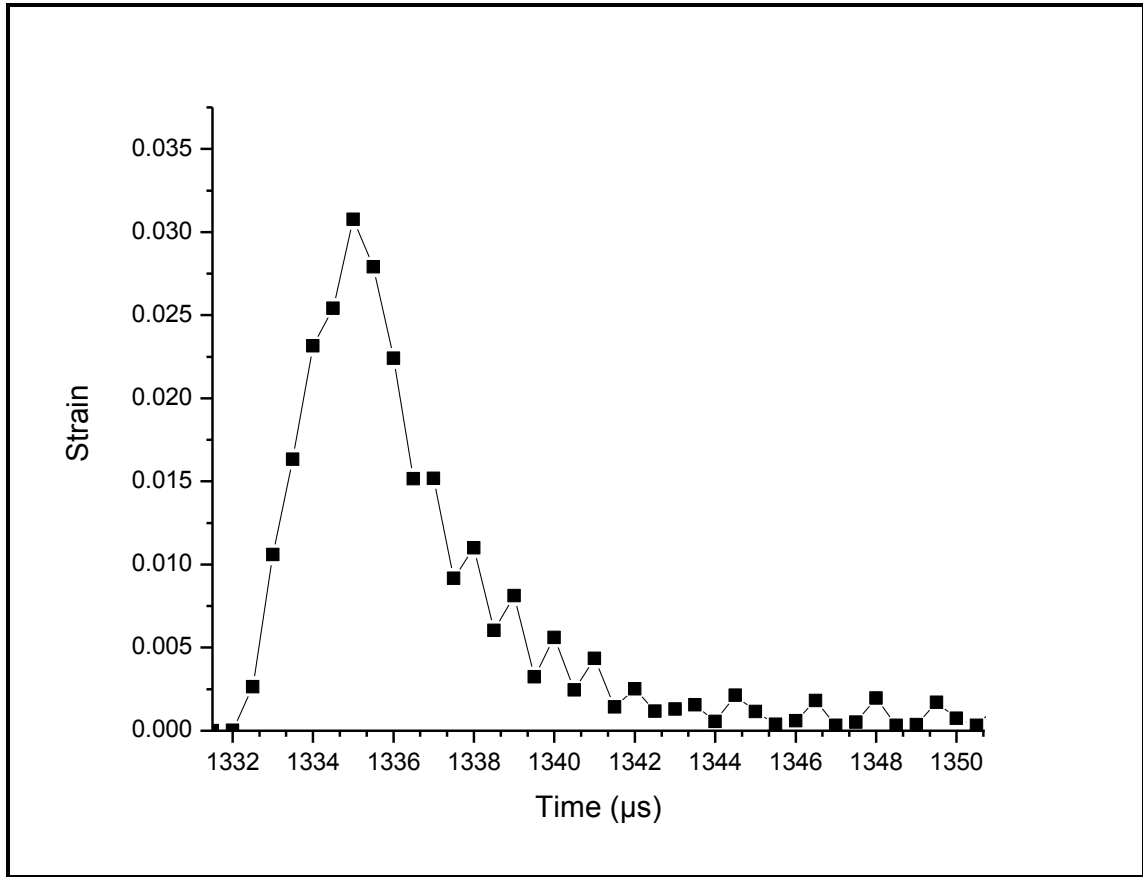


Fig 4.30: Time history curve for strain in element number 4400

The above figure Fig 4.30 represents the stress plotted against time for the most critical sample for this model. It is clear from the Figure that curve attains a maximum of 0.03 of strain for this element under 10 m/s of impact velocity. Curve attains its peak at about 1336 μs of time. Comparing it with other models with higher velocities this value is smaller. While when compared to the model provided in 4.2.1 (a), that has higher elastic modulus this value for strain is higher. This suggests that decreasing the elastic modulus can deform the bodies more under the effect of waves during SHPB test.

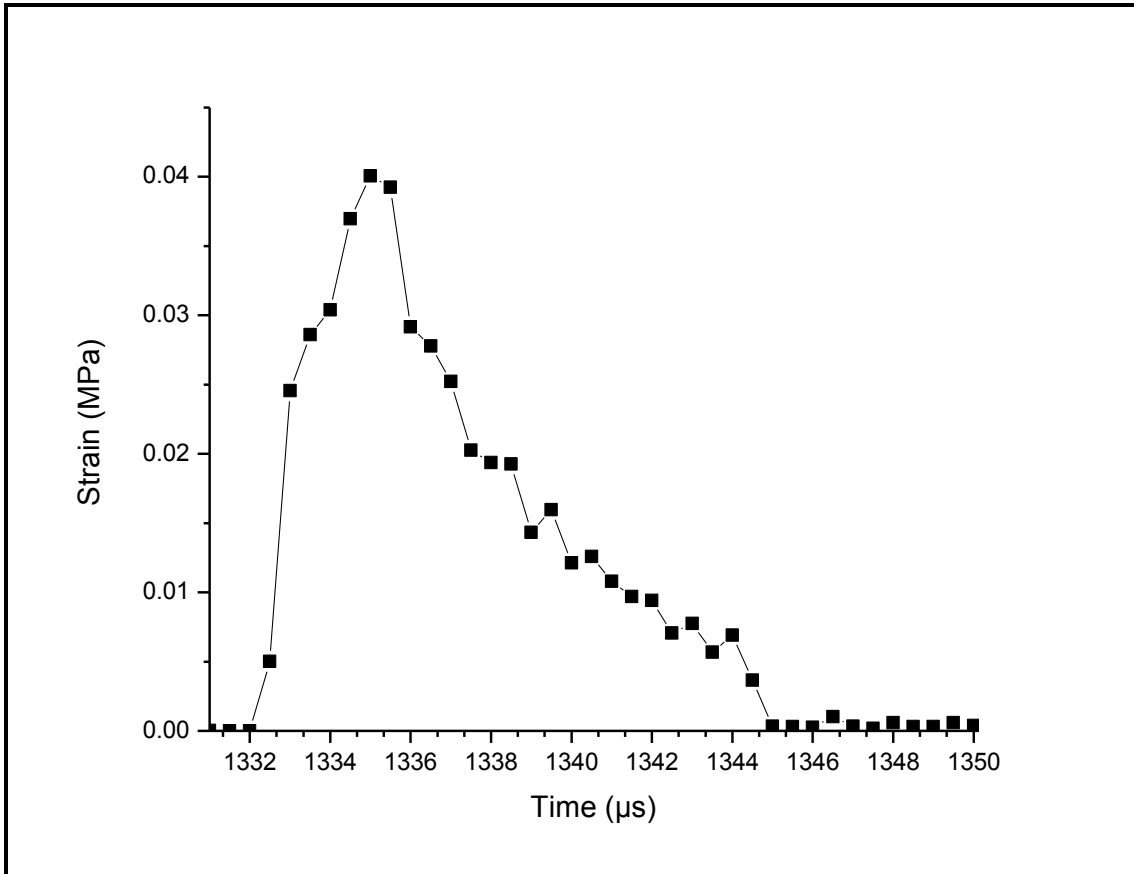


Fig 4.31: Time history curve for strain in element number 1771

This element is the same as discussed in previous part of this section. Fig 4.31 shows the time history curve for strain in element number 1771. From this figure it is clear that the curve rises at 1332 μs of time from zero magnitude. Then reaches a maximum peak magnitude. This maximum value for strain is 0.04 at 1335 μs in this element. Then some lower peaks have also been observed for this curve. Finally the curve falls back to zero magnitude. At time 1345 μs the curve nearly reaches back to zero value. This element seems to be most critical for this case. And the values for strain are also of higher magnitude. Thus more deformation is there in this element as compared to other elements for the same velocity of 10 m/s.

(g) Velocity has been changed to 7 m/s, while all other properties for this model has already been mentioned in chapter 3.

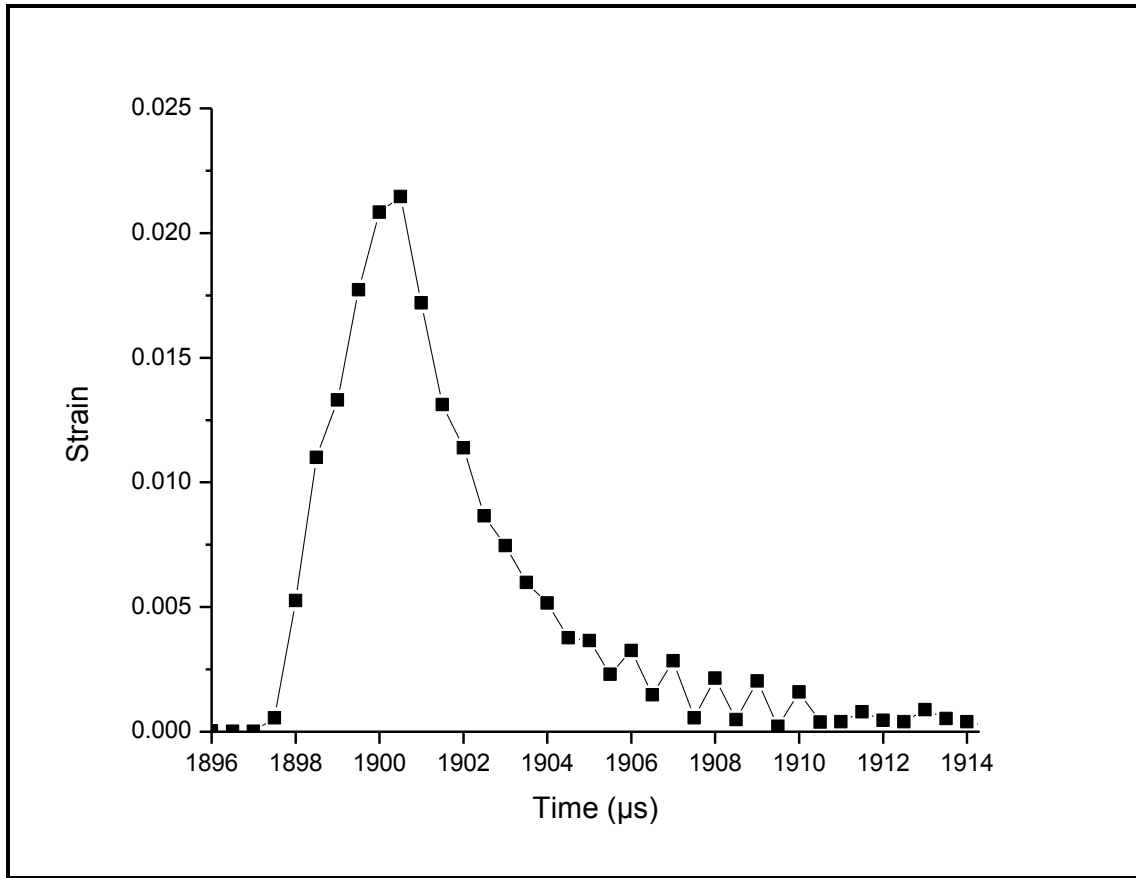


Fig 4.32: Time history curve for strain in element number 4236

Fig 4.32 shows the time history curve for strain in element number 4236. Element number 4236 is the element present at the middle portion of the disc sample. The velocity for the striker has also been changed and decreased thus the peak values obtained are at a lower magnitude. The peak is 0.022 at 1901 μs of time. After the peak point the curve starts to recede and decreases in magnitude for the strain. Then the zero magnitude is obtained at 1911 μs of time.

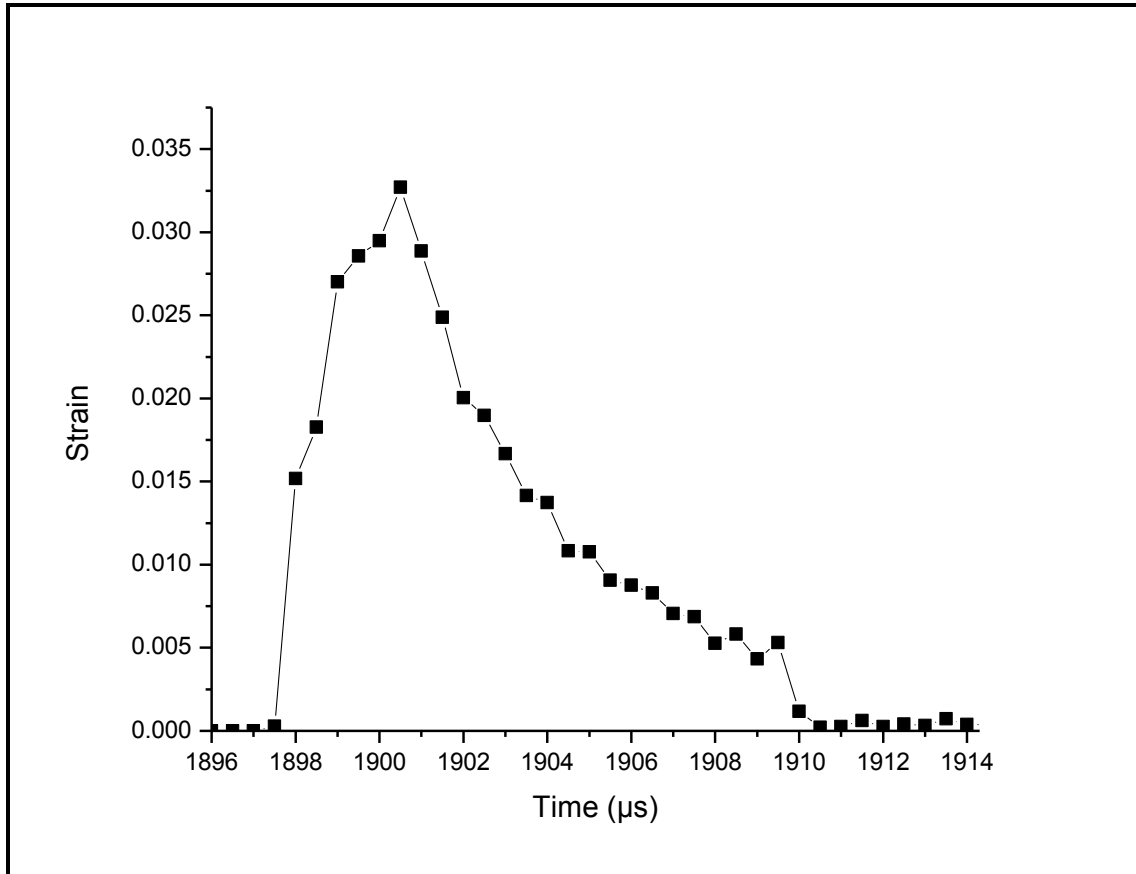


Fig 4.33: Time history curve for strain in element number 1667

This element is the most critical element along the loading diameter. Fig 4.33 represents the time history curve for strain in element number 1667. Maximum value of strain for this case of strain is at 1901 μs and value is 0.032. This magnitude is higher than the previous case of element number 4236. As this element is located near to the incident bar. The effect is more pronounced.

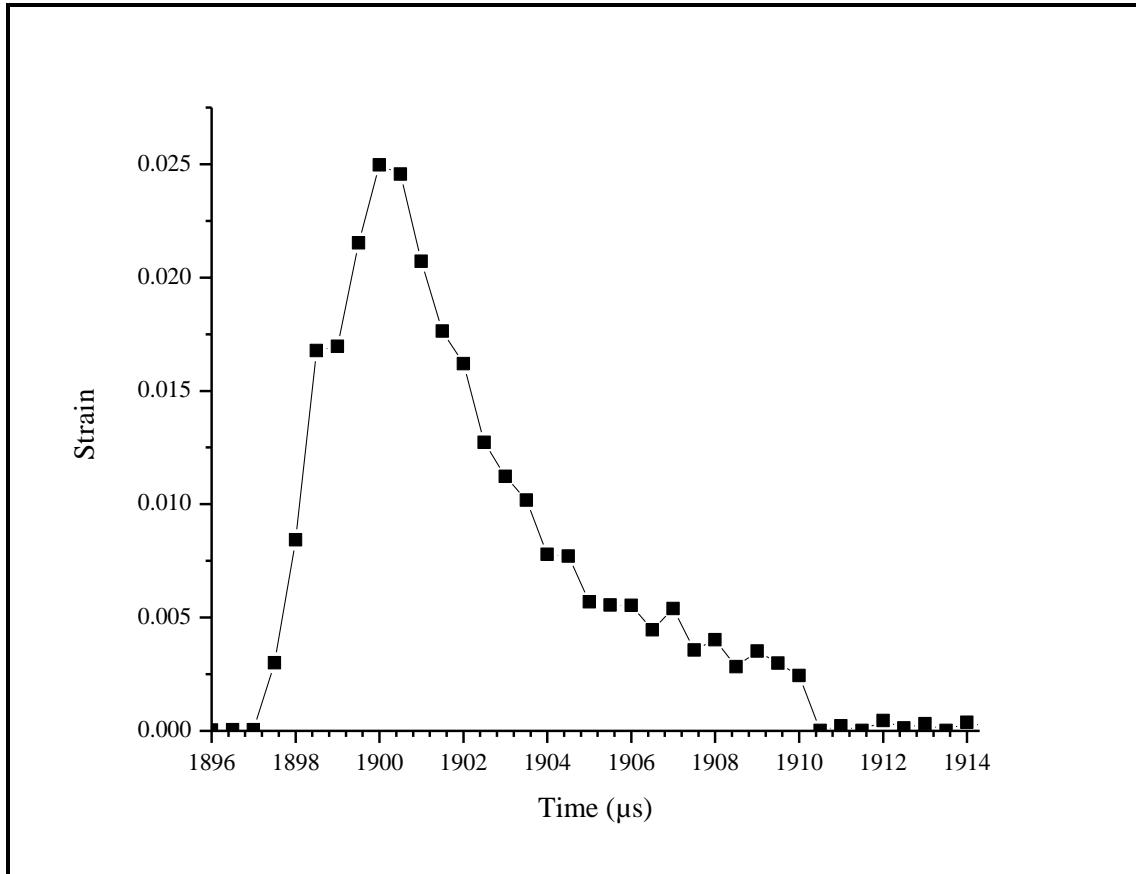


Fig 4.34: Time history curve for strain in element number 482

Fig 4.34 shows the time history curve for strain in element number 482. This is the element present in the opposite corner point of the element number 1667. The peak value here is 0.025 at 1901 μs of time while for the opposite side element this value is 0.032. After achieving the peak magnitude value the curve starts to fall back to zero value after the removal of residual stresses. Thus it can be known easily that this element deforms less than the opposite side element.

- (h) Maximum Principal Stress has been graphically represented here in this section. 14m/s is the velocity adopted for the first case. Three elements are taken for these representations.

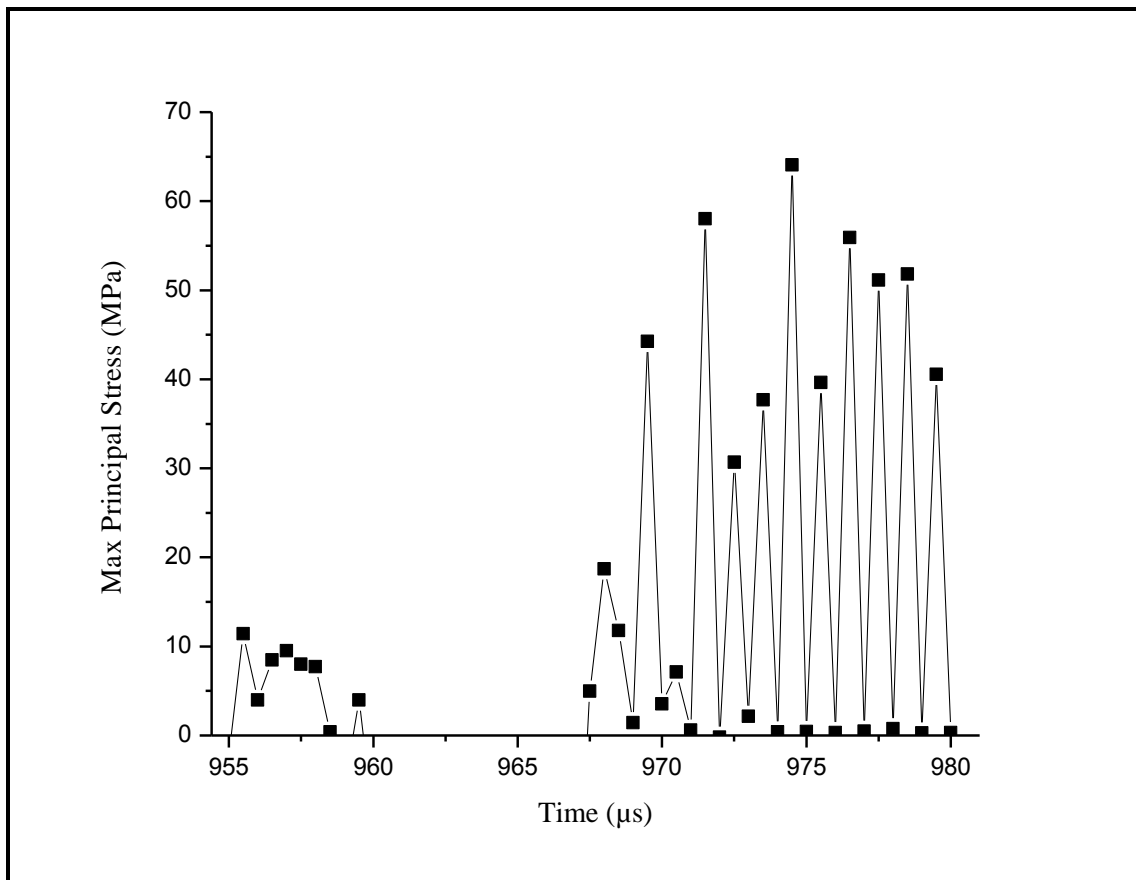


Fig 4.35: Time history curve for maximum principal stress in element number 1845

Element number 1845 is the most critical element for this case. Fig 4.35 shows the time history curve for maximum principal stress in element number 1845. This element is located at the edge point of the sample near the incident bar. Also it is located along the loading diameter. Maximum principal stress has its value as 65 MPa for this case and at a time of 975 μ s. Multiple peak curve can be seen here. These multiple peaks are due to the effect of residual stresses. These stresses act for extremely small period of time, beyond which it falls back to zero value. However the maximum peak magnitude of maximum principal stress for this element i.e. 65 MPa is lower than the value obtained for the curves in section 4.2.1 (a).

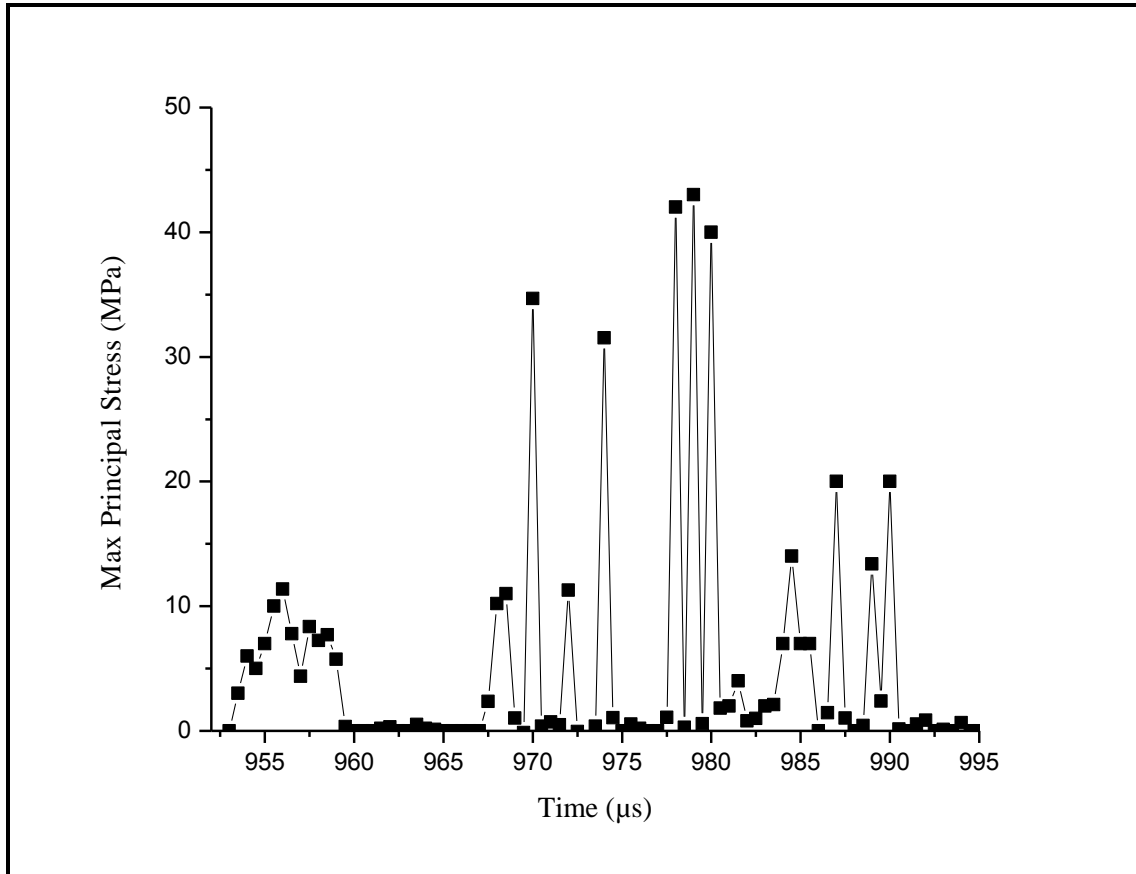


Fig 4.36: Time history curve for maximum principal stress in element number 1771

The element number 1771 has already been defined in previous sections. Fig 4.36 shows the time history curve for maximum principal stress in element number 1771. This element is located at an opposite side along the loading diameter of the sample, and is adjacent to transition bar. The curve shows the maximum principal stress in relation to time. Maximum value from this curve is 45 MPa. Multiple peaks are obtained for this case also. These peaks are the result of residual stresses which remains active for an extremely small period of time. The value becomes zero at 990 μs of time.

- (i) Velocity for this case has been adopted as 10 m/s. All other material and geometrical properties are adopted according to chapter 3.

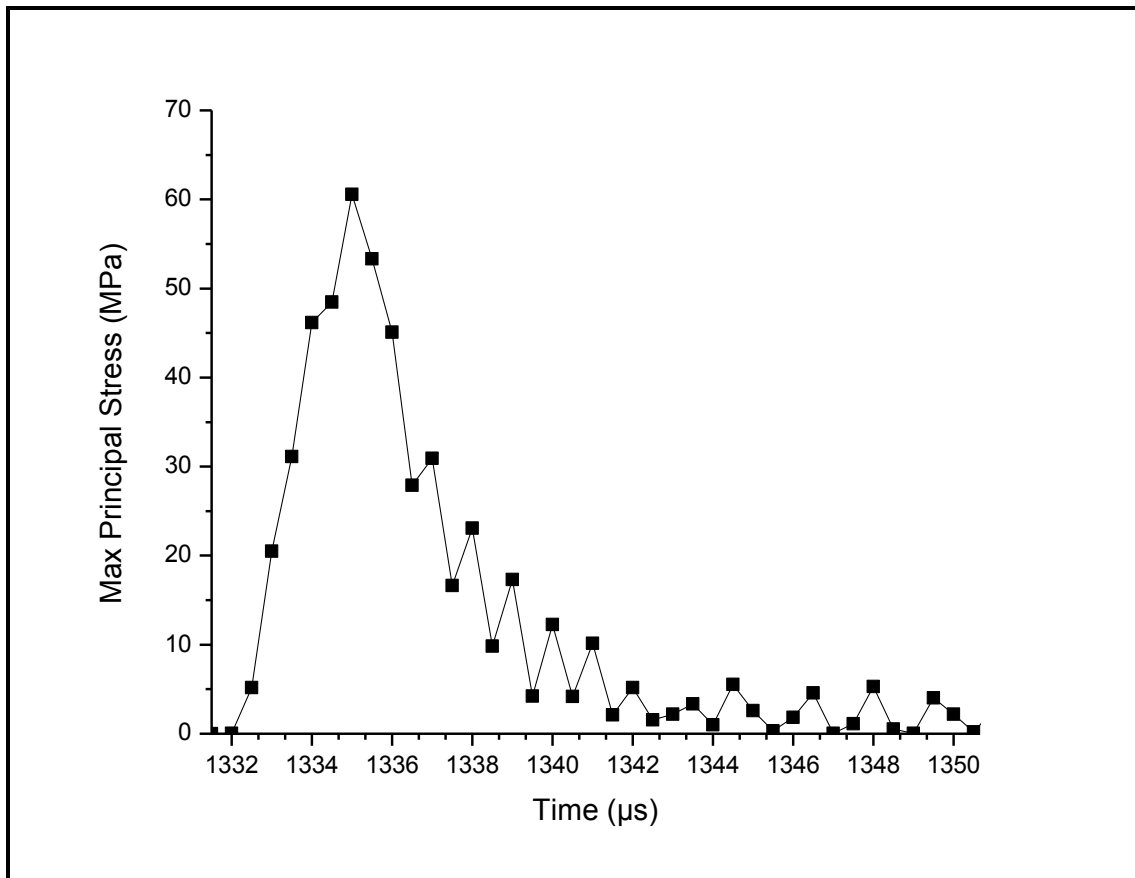


Fig 4.37: Time history curve for maximum principal stress in element number 4400

Fig 4.37 shows the time history for maximum principal stress in element number 4400. Element number 4400 is the element located along the loading diameter of the disc sample and is in contact with incident bar at one face. This element shows the critical behaviour for this case. The highest magnitude of maximum principal stress is obtained for this case only. The highest value reaches 60MPa. The Highest value obtained for the previous case (refer to article 4.2.1(h)) is 65 MPa. Thus a decrease in value can be seen for the maximum principal stress value for this case when compared to the previous case. Also a delay in getting the peak can be seen in two cases. Several multiple peaks are seen in the curve beyond the peak magnitude stresses which arises due to residual stresses. These stresses recede and falls back to zero magnitude at about 1350 μ s of time.

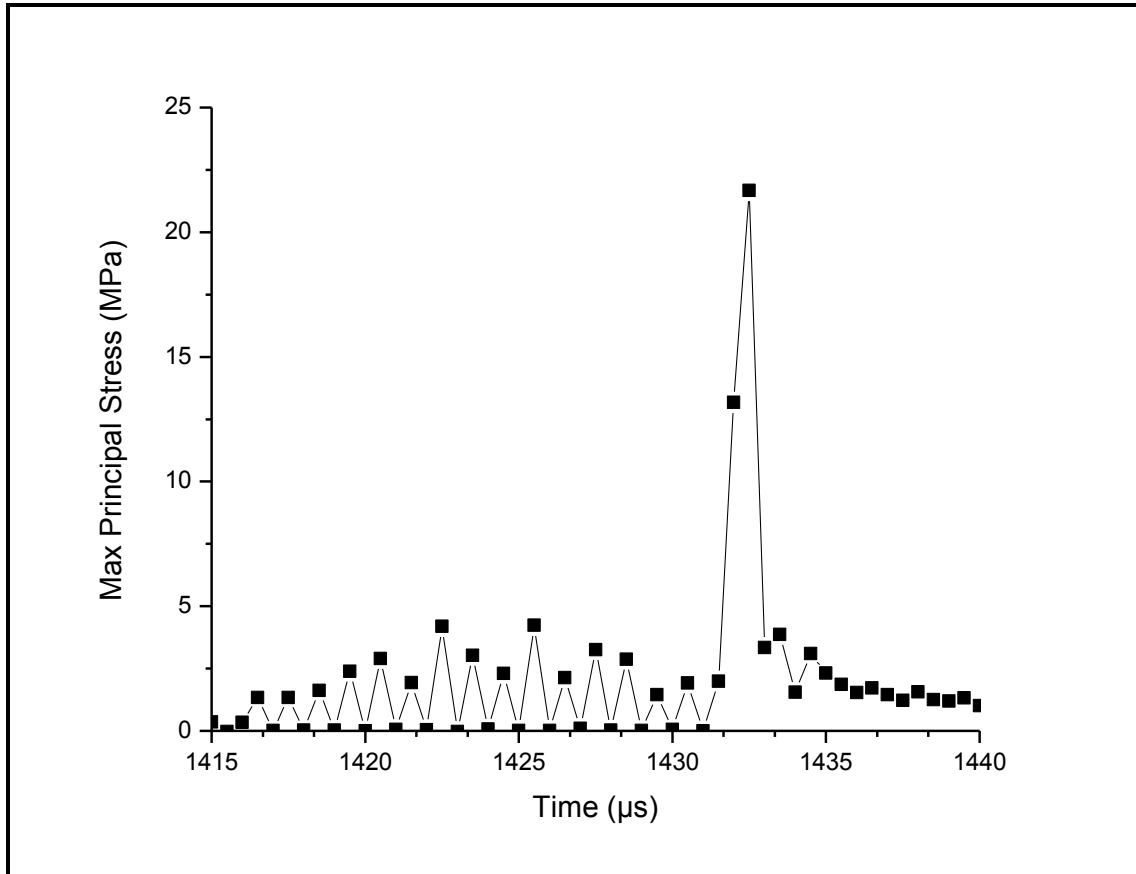


Fig 4.38: Time history curve for maximum principal stress in element number 1771

Time history curve has been obtained for the maximum principal stress in the element number 1771 and shown in Fig 4.38. Here the curve shows multiple peak behaviour. Several small magnitude peaks are obtained here. Maximum peak value is lower as compared to opposite side element number 4400. The maximum magnitude which can be seen from Fig 4.38 above is 22 MPa. However the peak obtained is at a time of 1432 μ s of time. After the maximum peak value has been obtained the curve starts to fall back upto 3 MPa. Beyond this point several multiple peaks are obtained. These peaks are the result of residual stresses. Which ultimately falls back to zero and the curve halts at that point.

- (j) 7m/s velocity has been adopted for this case and all other properties are taken from chapter 4(Table 3.1 and Table 3.2).

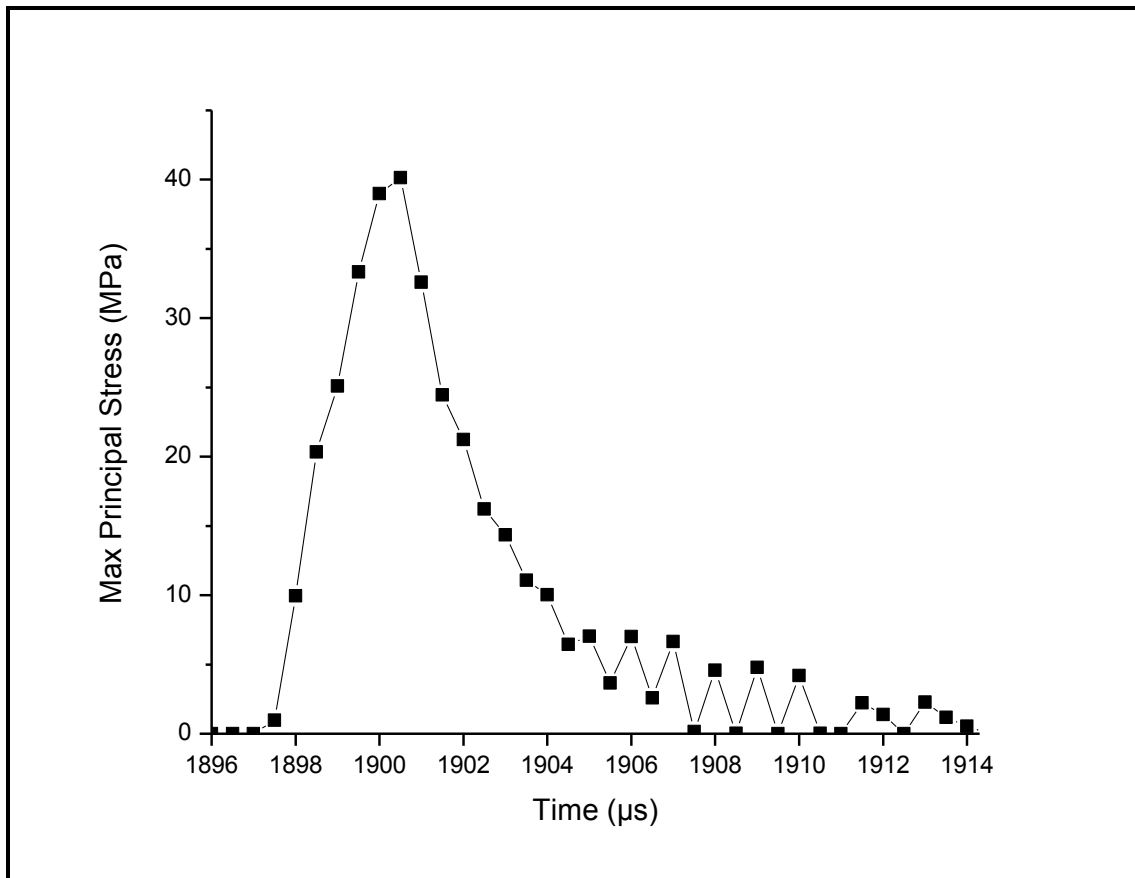


Fig 4.39: Time history curve for maximum principal stress in element number 4236

Fig 4.39 shows the time history curve for maximum principal stress in element number 4236. As the velocity of strike decreases the magnitude of principal stress also have been decreased. The maximum value can be seen from Fig 4.39. Its value is 40 MPa. A decrease can be seen as compared to the previous case. Multiple peaks are obtained here also. However the peak value is obtained at 1901 μ s of time. The smaller magnitude multiple peaks obtained beyond the maximum peak stress are the result of residual stresses. These residual stresses act for an extremely smaller period of time and ultimately reaches a zero value.

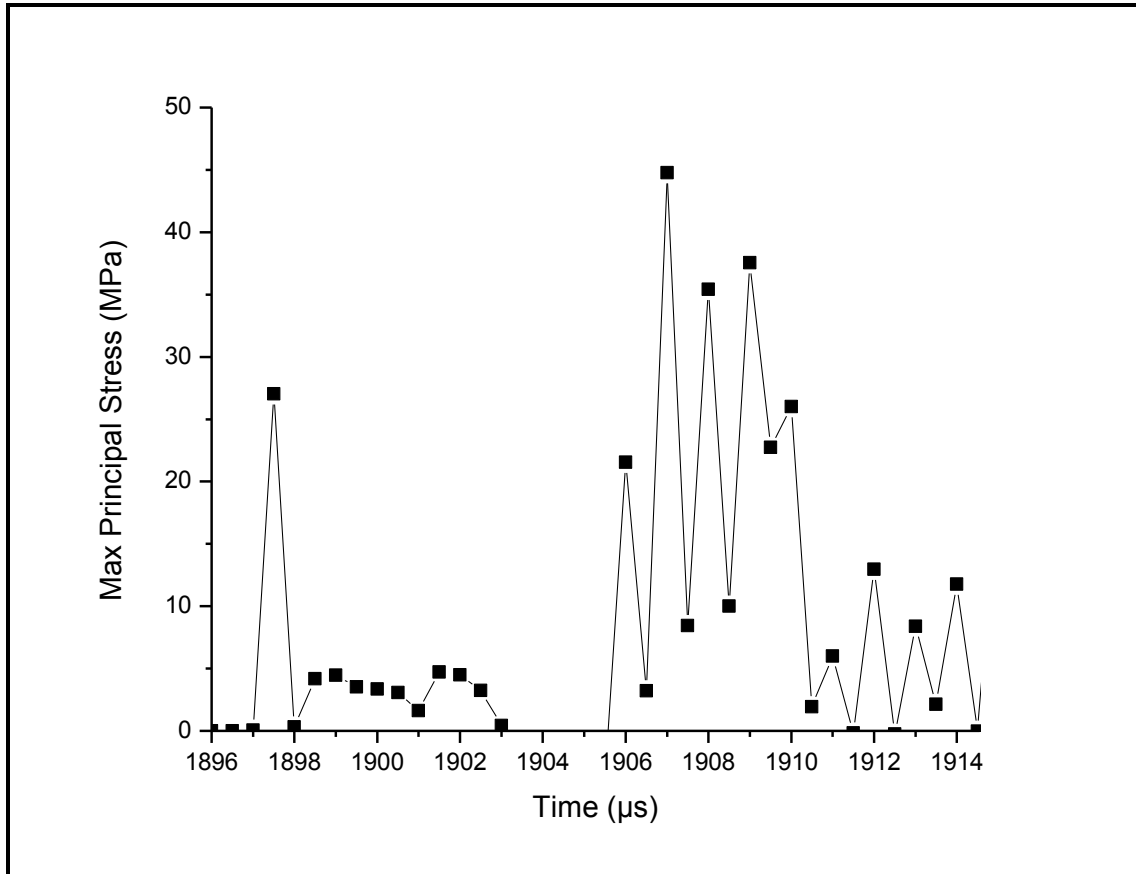


Fig 4.40: Time history curve for maximum principal stress in element number 482

Element number 482 is the middle portion element in the face of disc sample. Fig 4.40 shows the time history curve for maximum principal stress in element number 482. From the curve shown in Fig 4.40 a multiple peak behaviour which is the result of residual stresses can be seen which starts from 1885 μs and ends at 1940 μs . The maximum value for this case has been 45 MPa at 1906 μs . Thus this element seems to be the most critical element for this case. Hence for lower velocities of strike such as 7m/s the stress in the middle portion is more as compared to other portions of disc sample. Thus it is right to say that crack propagates from middle portion to outer edges of the sample at lower velocities of strike for the striker bar.

CHAPTER 5

CONCLUSIONS

5.1 CONCLUSIONS

Steel Fibre Reinforced Concrete is good in taking the stresses as compared to the conventional concrete. The addition of steel fibre can significantly improve its strength, toughness, and resistance to failure. In the cube sample of SFRC the failure pattern starts from edges and proceeds to the middle portion. This behaviour is consistent irrespective of the change in velocity of the striker bar. Thus critical zone is along the edges corner portion. The maximum stresses generated are a little higher in magnitude as expected. However a good consistent relation can be developed with the experimental results known from literature.

Stress distribution in Brazilian disc under dynamic loads is far more complicated. Stress equilibrium should be evaluated at time and space fields simultaneously. Brazilian disc subjected to low impact velocities tends to have good stress equilibrium. The first crack usually initiates at disc centre and propagates along the load direction. Brazilian disc subjected to high impact velocities is hard to get stress equilibrium. At lower velocities when stress reached equilibrium, start-split location appeared at the centre of specimen and cracks propagates along the loading diameter direction. However a complete different behaviour can be seen at higher impact velocity, compressive failure zone was detected at the edge of specimen, and a complete shear failure region arisen at the centre. Stress distribution and failure process simulated by software are coincident with experimental results obtained from literature. As the velocity has been decreased the stress in the elements has also decreased and also the strain values has decreased too. This means that as the impact velocity decreases the deformations has also decreased. However the pattern of crack generation have also changed. Time taken for the failure has been delayed with decrease in impact velocities.

It has also been observed that increasing the elastic modulus improves the stress and strain resistant properties. The samples are able to take more stresses and lesser deformations for higher initial elastic modulus materials. This behaviour is due to plastic hardening of the samples. More the elastic modulus higher will be the resistance to stresses and strains. The simulation model which has higher elastic modulus is able to

withstand higher values of stress and the strains are of smaller magnitude. This means that the deformations are lesser in this case as compared to the one with lower elastic modulus. At the same velocity the model with higher elastic modulus has performed well as compared to model with lower elastic modulus. When the results are compared for cube sample and the disc sample much variation in results have been seen for the same impact velocities and same elastic modulus. The stress in the disc sample are increased and thus the deformations have also increased for the disc sample as compared to the cube sample. Thus disc sample performed well in terms of stress and strain resistance.

5.2 FUTURE SCOPE

The volume of fibres in the specimens can be increased as this will affect the resistance of the concrete against blast or impact loading conditions. These results can be employed in future studies for knowing the impact loading effects for high rate events. The results of the numerical simulations of the SFRC samples can be used to compare the results of the conventional concrete under blast impacts and fibre reinforced concrete under blast loadings. Fibres improves the strength and resistance against the impact and blast loadings. These simulations can be done by changing the properties of the concrete and incorporating the improved properties for new studies. These results can be employed to know the behaviour of structures subjected to blast loads or impact loads. Seismically reinforced structures can be also be modelled and impact of blast loading con this structures can be found, and vice versa can also be done.

REFERENCES

- [1]. Andreou M., Kotsoglou A. & Pantazopoulou S., (2016). "Modeling blast effects on a reinforced concrete bridge" *Advances in Civil Engineering*.
- [2]. Haol H., Hao Y., Li J. & Chen W., (2016). "Review of the current practices in blast resistant analysis and design of concrete structures" *Advances in Structural Engineering*, 19(8).
- [3]. Chen, Xudong & Limei G., (2016). "Dynamic Brazilian test of concrete using split Hopkinson pressure bar" *Materials and Structures*, 50.
- [4]. Ekström J. (2015). "Concrete Structures Subjected to Blast Loading, Fracture due to dynamic response" *Chalmers Civil and Environmental Engineering , structural engineering*.
- [5]. Galhena I. & Galhena A., (2015). "Effects of Blast Loading on Reinforced Concrete Facade Systems" *Doctorate of Philosophy College of Engineering and Science Victoria University*.
- [6]. Kundu, Sumanta, Stroisz, Pradhan A. & Srutarshi, (2015). "A simple Discrete-Element-Model of Brazilian Test" *The European Physical Journal B*. 89.
- [7]. Kye C., (2014). "Effects of blast loading on seismically detailed reinforced concrete columns" *Masters of Applied Science in Civil Engineering Carleton University Ottawa, Ontario*.
- [8]. Morales, Gustavo, Cendón, Gálvez D., Gálvez S. & , Gálvez F., (2013). "Fracture of concrete structural members subjected to blast" *Proceedings of the 8th International Conference on Fracture Mechanics of Concrete and Concrete Structures, FraMCoS* 930-941.
- [9]. Dragani H. & Sigmund V., (2012). " Blast Loading on Structures" *Technicki Vjesnik*, 19(3), 643-562.
- [10]. Islam M. & Wudhipong S. & Liu Z., (2012). "Penetration of Concrete Targets using a MHJC Material Model" *International Journal of Computational Methods*, 9(4), 1250056.

- [11]. Meyer C., (2011). "Development of Geometrical Parameters for Numerical Simulations Using the Holmquist-Johnson-Cook Constitutive Model for Concrete" *Army Research Laboratory-TR*, 5556.
- [12]. Liu Y., Huang F. & Ma A., (2010). "Numerical Simulations Of Oblique Penetration into Reinforcement Concrete Targets" *international journal of impact engineering*, 36(3), 438-446.
- [13]. O'Daniel J., (2010). "Recent ERDC Developments In Computationally Modeling Concrete Under High Rate Events".
- [14]. Wang, Zhiliang, Wu, L.P., J.G., (2010). "A study of constitutive relation and dynamic failure for SFRC in compression" *Construction and Building Materials - CONSTR BUILD MATER*, 24. 1358-1363.
- [15]. Polanco-Loria M., Hopperstad O. and Borvik T., (2007). "Numerical Predictions of Ballistic Limits for Concrete using Modified Version of HJC model" *International journal of Impact Engineering*, 35, 290-303.
- [16]. Ngo T., Mendis P., Gupta A. & Ramsay J., (2007). " Blast Loading and Blast Effects on Structures – An Overview" *Electronic Journal of Structural Engineering*, 7, 76-91.
- [17]. Gram M., Clark¹ A., Hegemier G. & Seible F., (2006). "Laboratory simulation of blast loading on building and bridge structures" *WIT Transactions on State-of-the-Art in Science and Engineering*, 60.
- [18]. Lu Y. & Xu K., (2004). "Modeling of dynamic behaviour of concrete material under blast loading" *International Journal of Solids and Structures*, 14(1), 131-143.
- [19]. IS 4991-1968,(September 1969). "Criteria for blast resistant design of structures for explosions above ground" *Bureau of Indian Standard, Manak Bhavan New Dehli*.
- [20]. Is 875-1967, "Code of Practice for Design Loads (other than Earthquake) for Buildings and Structures" *Bureau of Indian Standard, Manak Bhavan New Dehli*.

APPENDIX A

A.1 Figures representing the visualisations of various results for the Cube Sample

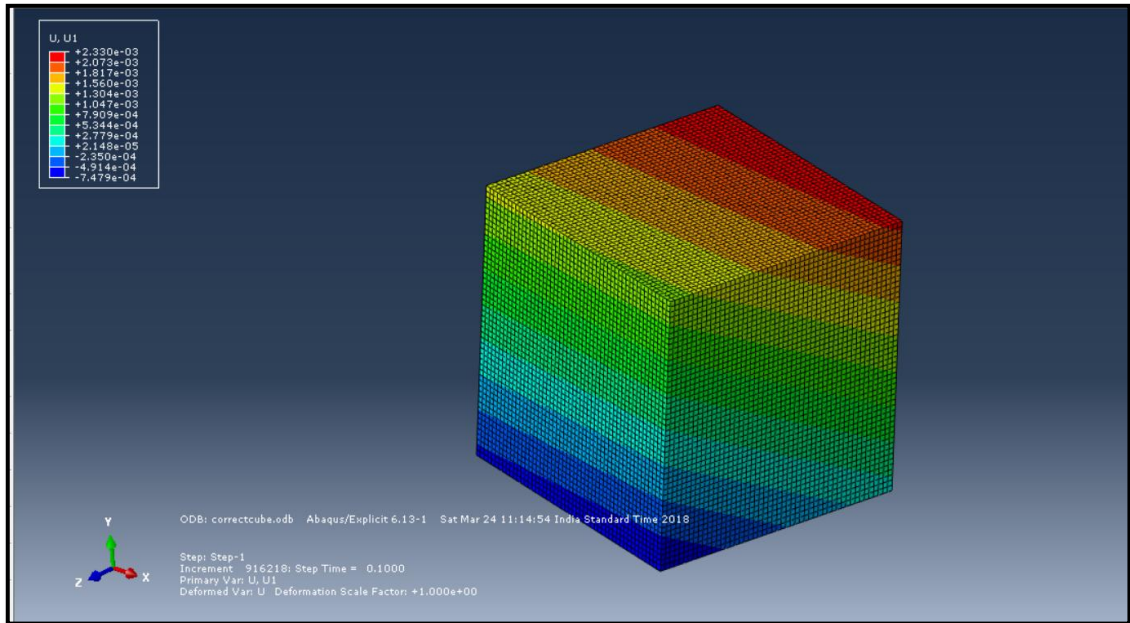


Fig 1: Displacement, U1

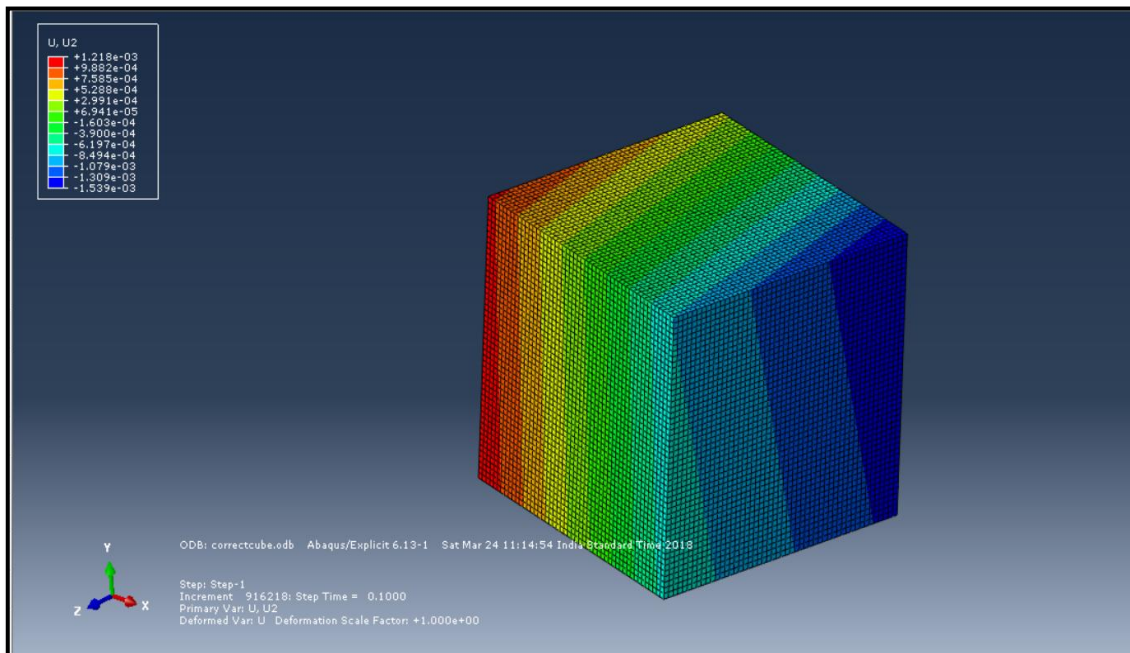


Fig 2: Displacement, U2

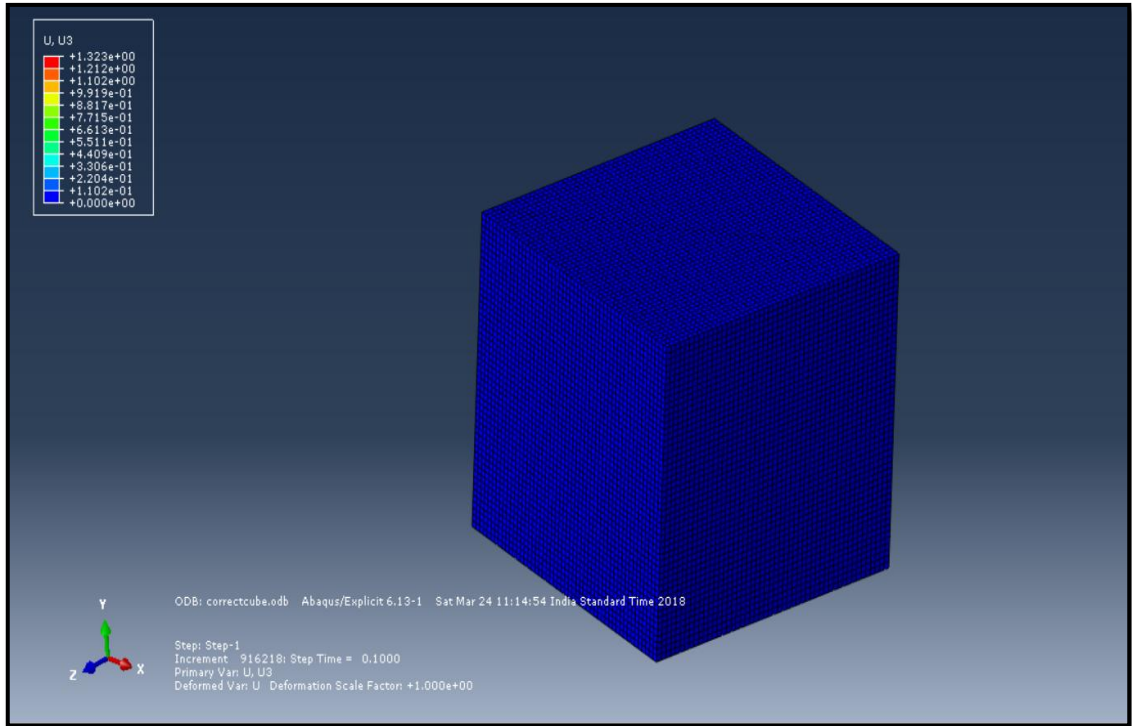


Fig 3: Displacement, U3

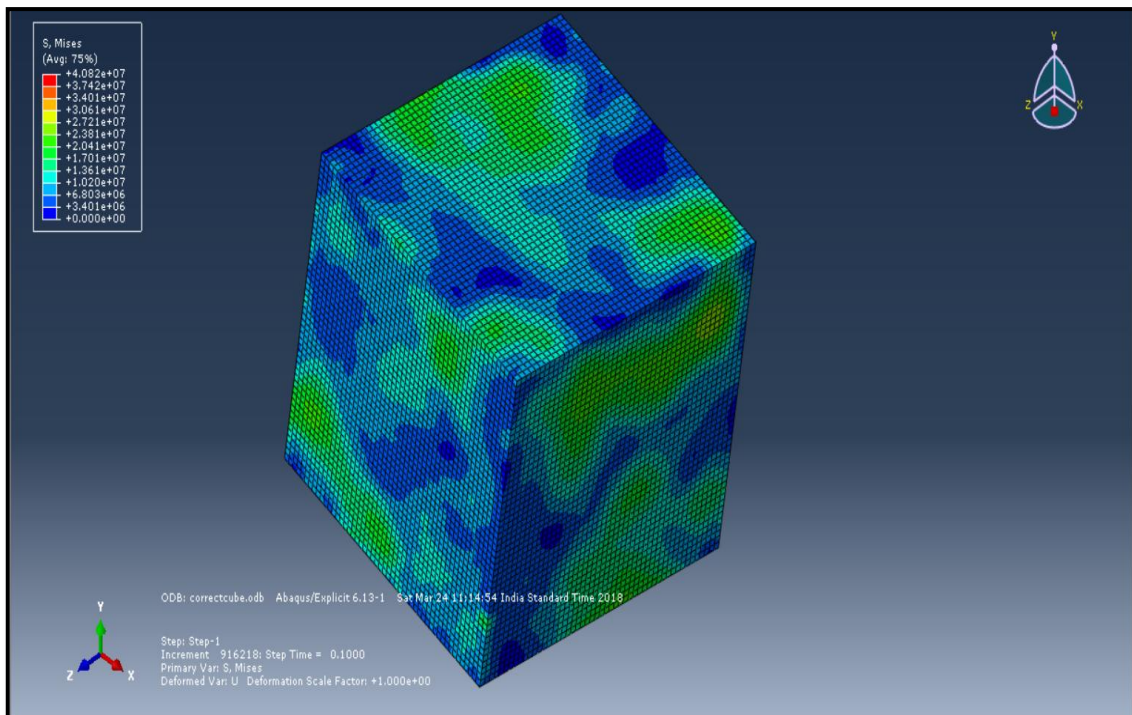


Fig 3: Stress, Von Mises

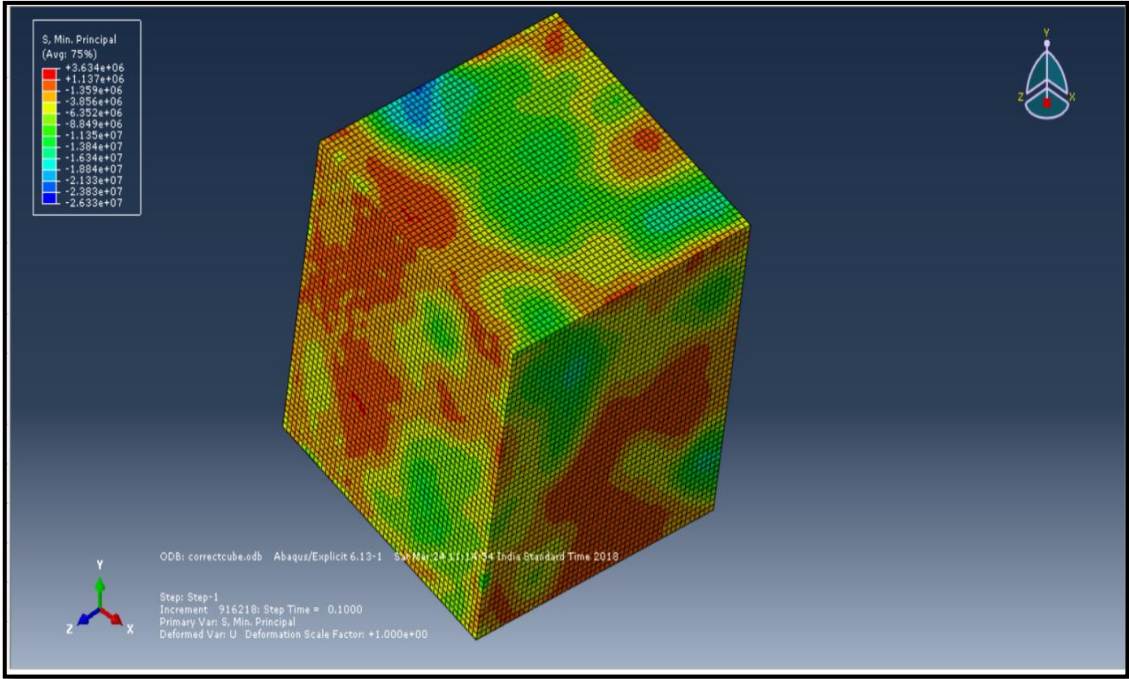


Fig 5: Minimum Principal Stress

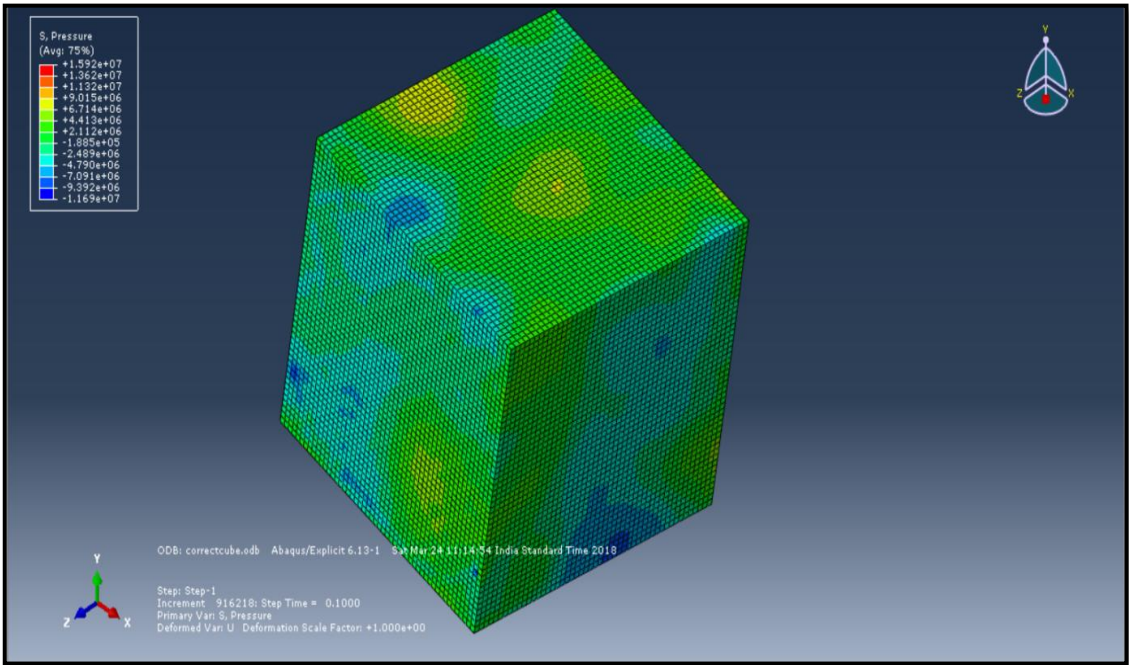


Fig 6: Pressure on the Cube

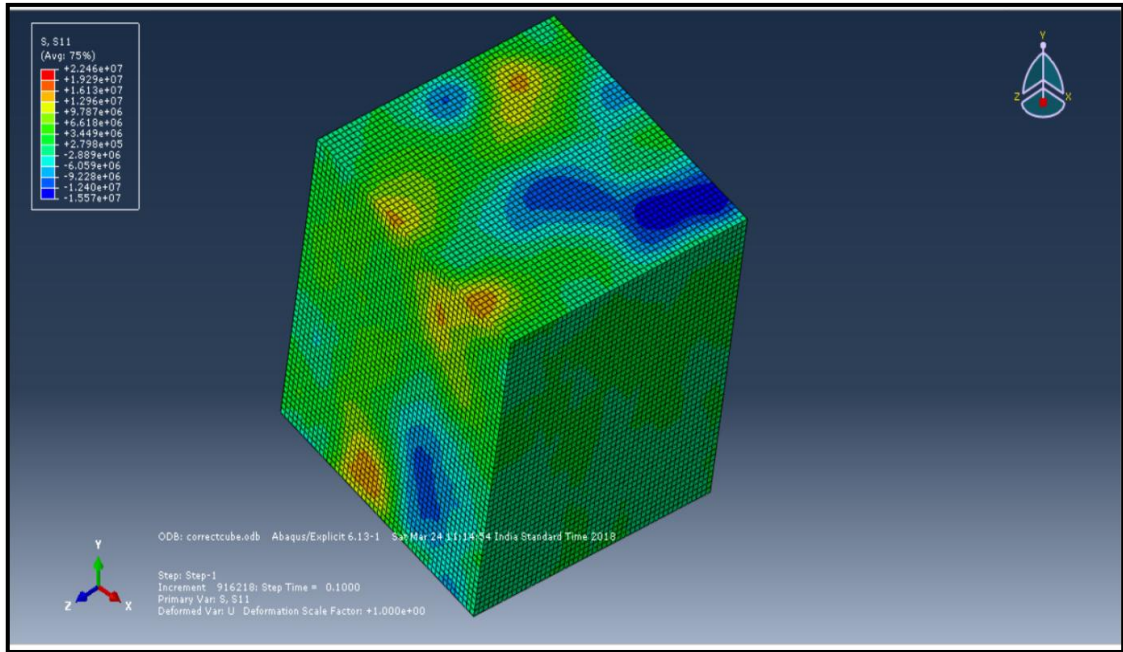


Fig 7: S11 stress

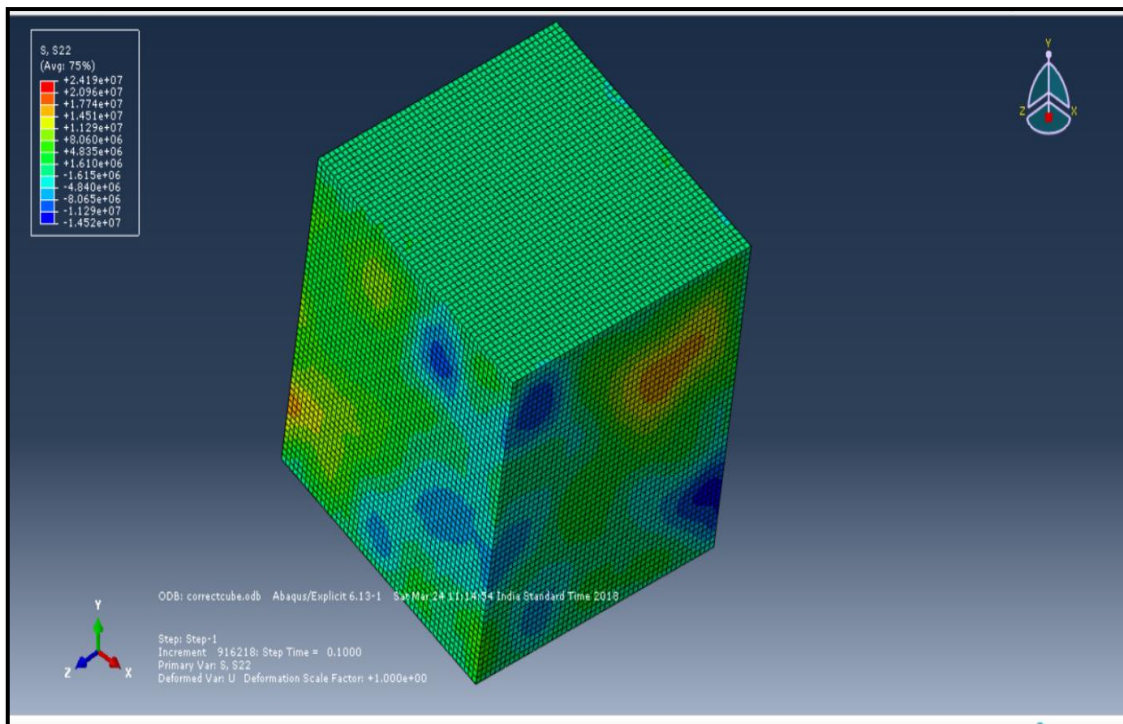


Fig 8: S22 Stress

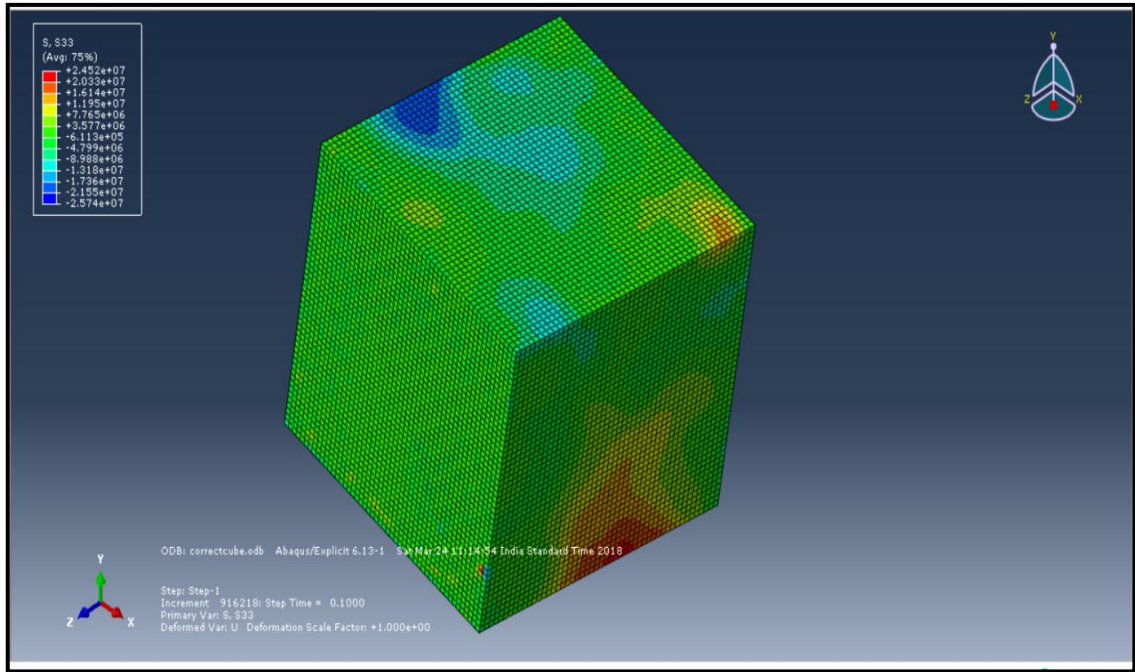


Fig 9: S33 Stress

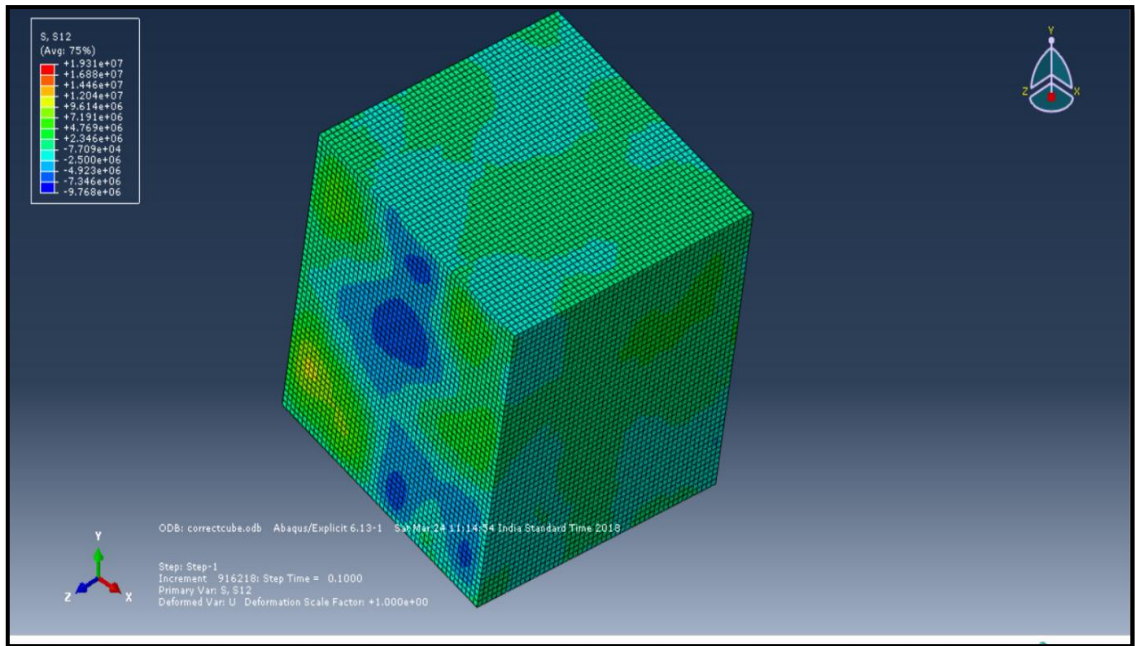


Fig 10: S12 Stress

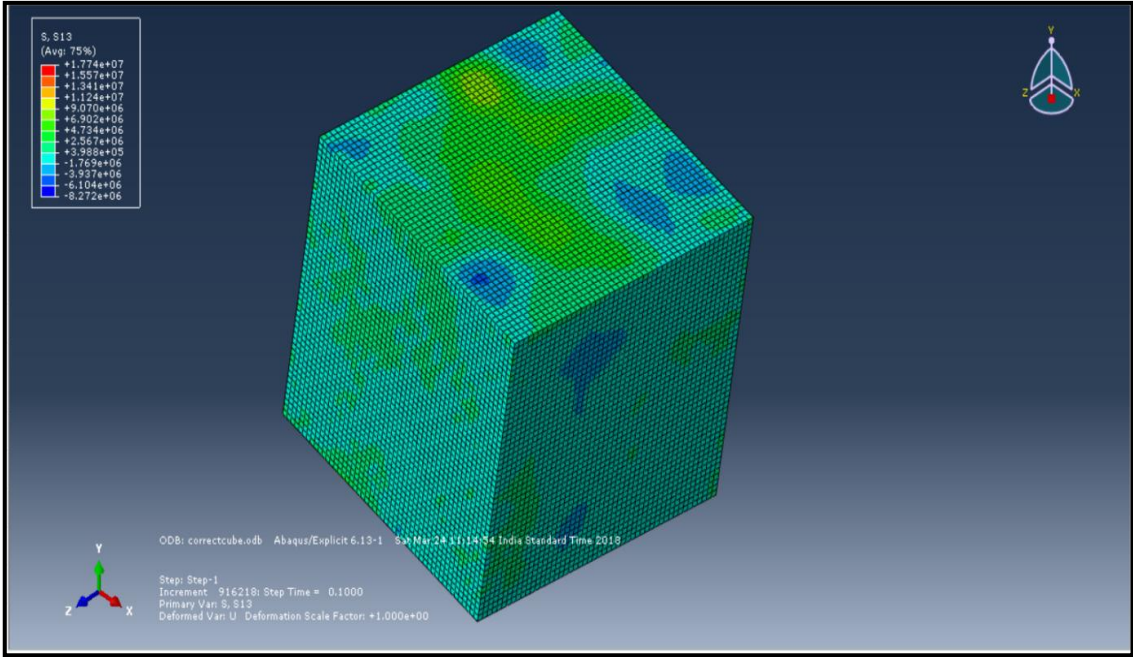


Fig 11: S13 Stress

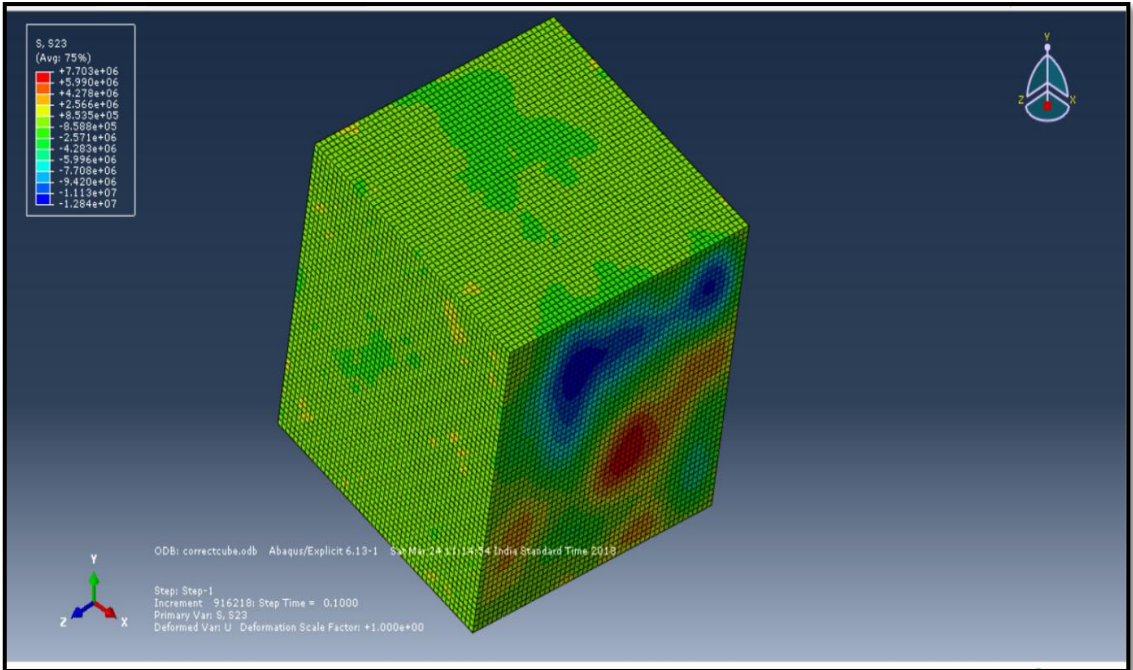


Fig 12: S23 Stress

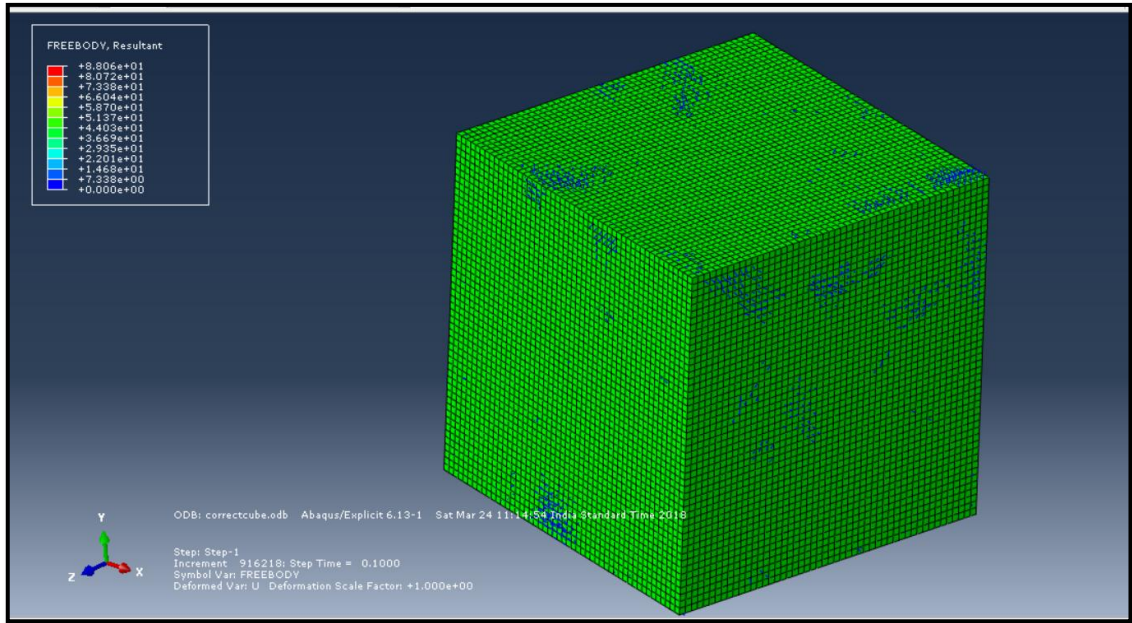


Fig 13: Freebody Resultant

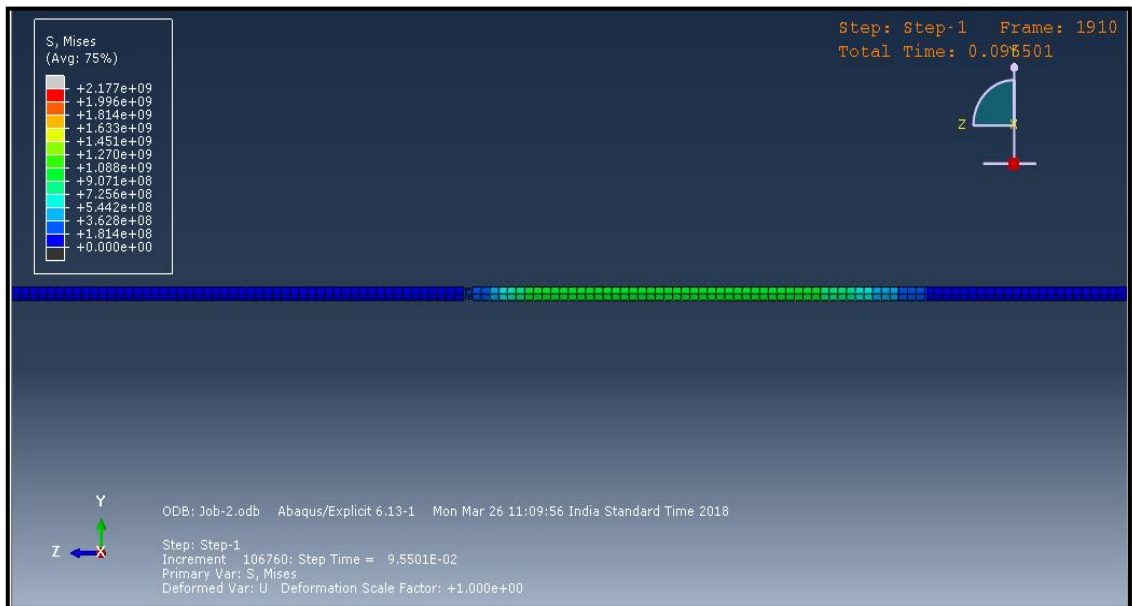


Fig 14: Propagation of the compression wave

APPENDIX B

B.1 Figures representing the visualisations of the results for the disc sample

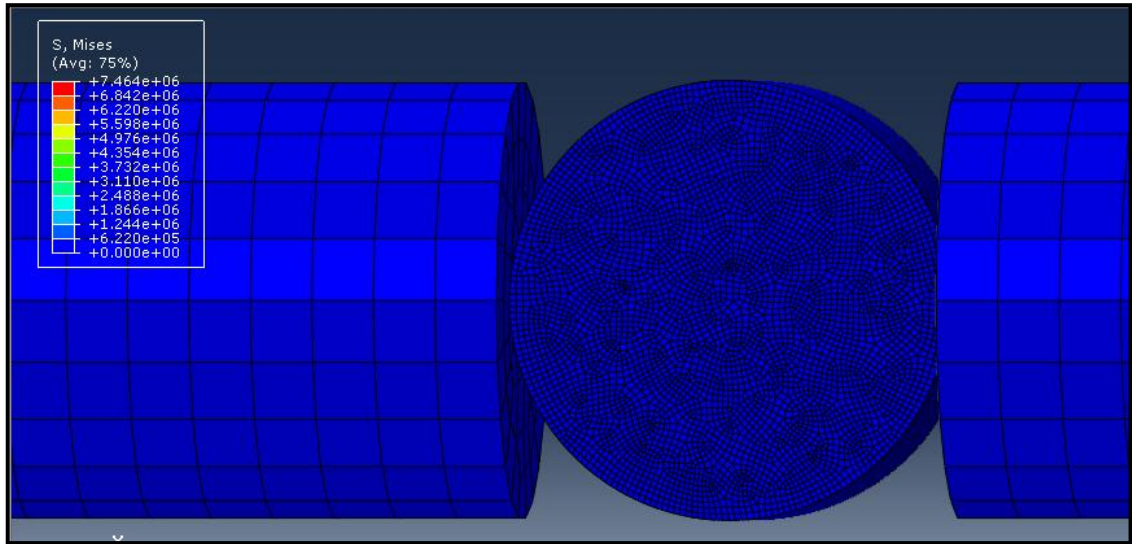


Fig 15: Stress in disc

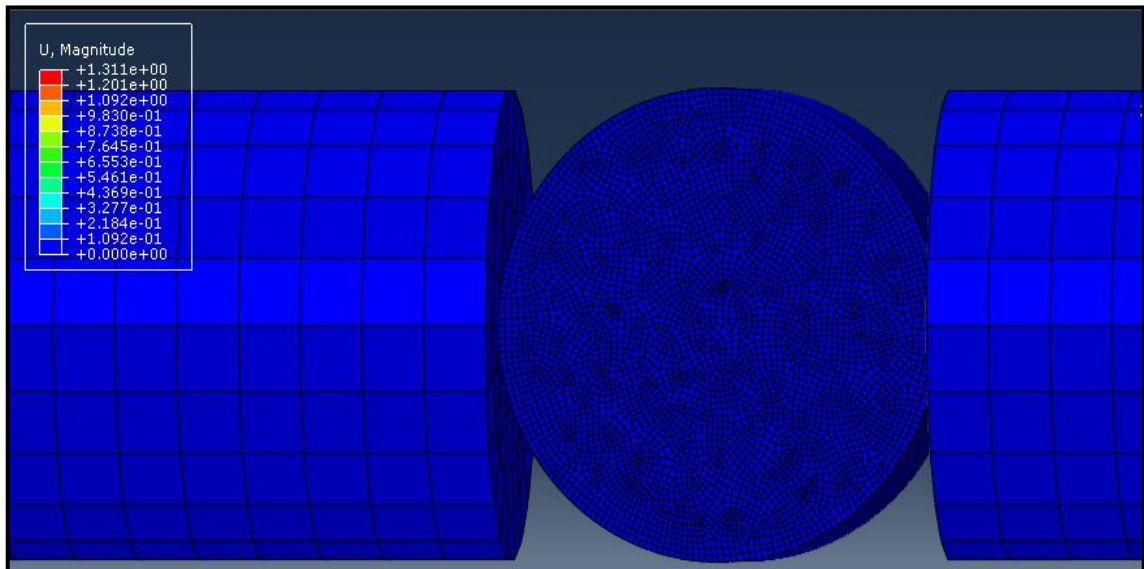


Fig 16: Displacement in disc

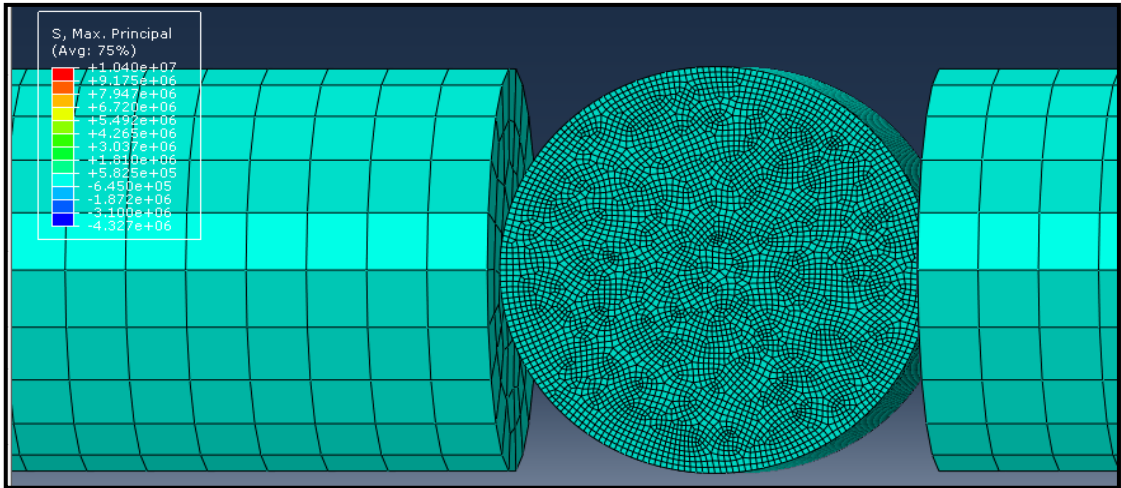


Fig 17: Max Principal Stress

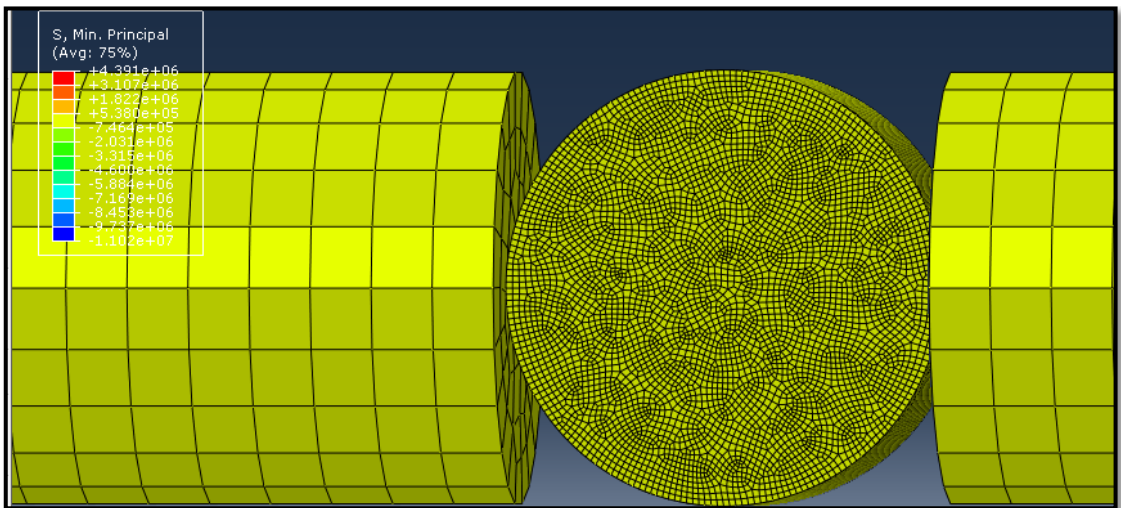


Fig 18: Minimum Principal Stress

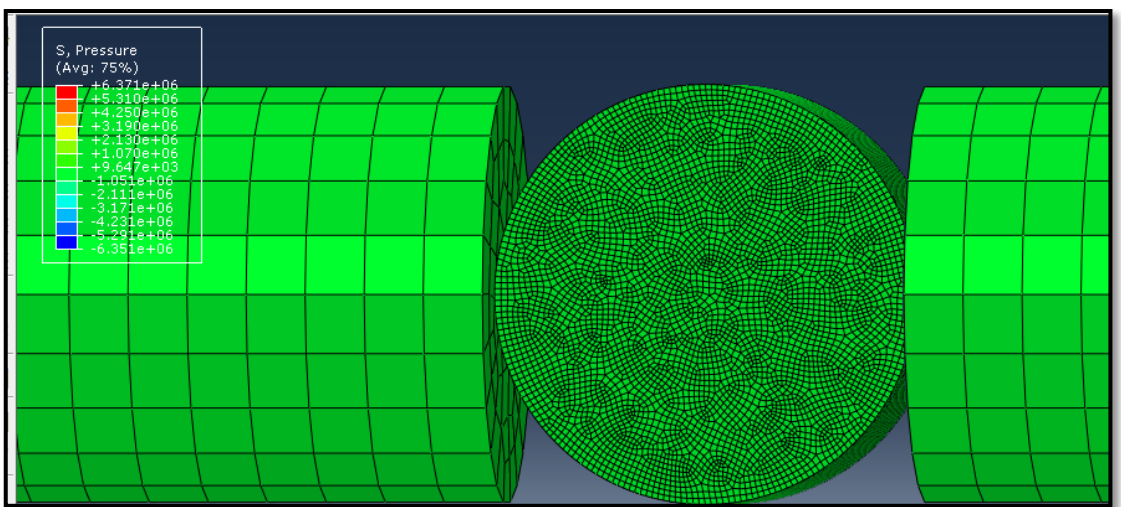


Fig 19: Pressure

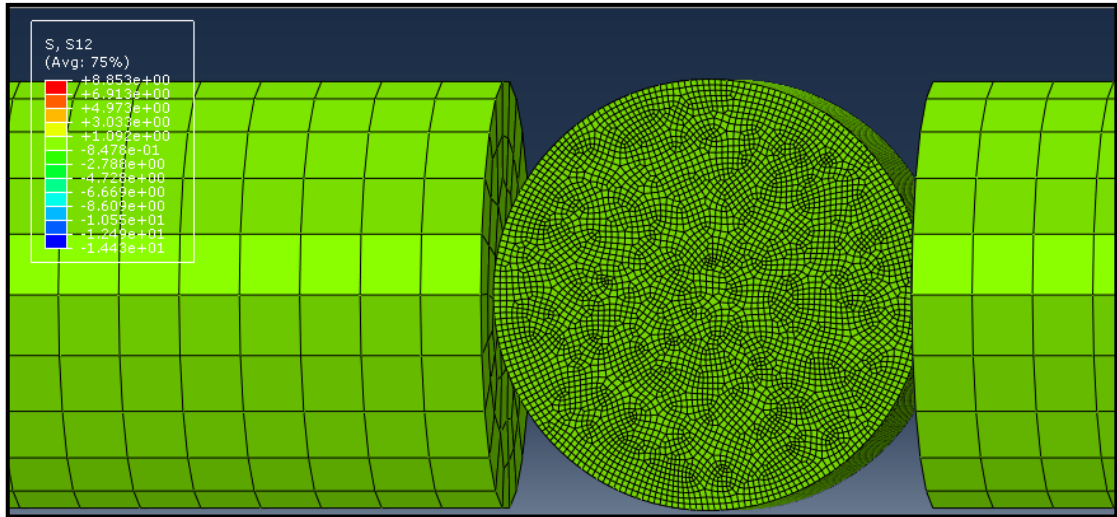


Fig 20: Stress, S12

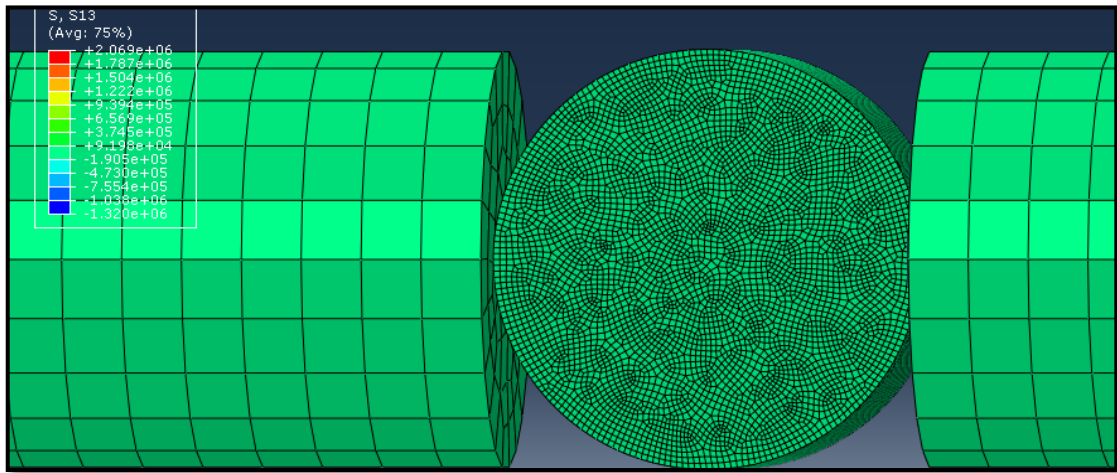


Fig 21: Stress, S13